Characterizing the Function of CSLD Proteins During Plant Cell Wall Deposition in *Arabidopsis*

by

Jiyuan Yang

A dissertation submitted in partial fulfillment
of the requirements for the degree of
Doctor of Philosophy
(Molecular, Cellular and Developmental Biology)
in the University of Michigan
2020

Doctoral Committee:

Associate Professor Erik E. Nielsen, Chair
Professor Steven E. Clark
Associate Professor Ann L. Miller
Associate Professor Yin-Long Qiu
Professor Yanzhuang Wang

Jiyuan Yang

jiyuany@umich.edu

ORCID ID: 0000-0003-0185-1133

Acknowledgements

This thesis covers my major research work in Michigan, which started in the fall of 2013. I would like to offer my sincerest thanks and gratitude to Professor Erik Nielsen, who supervised my entire Ph.D. journey. Erik is a brilliant scientist, and a joyful, kind, patient, and encouraging mentor. I owe all that I have achieved in my academic career to Erik, and cannot adequately express the impact that he had on my development both as a scientist and as an individual. I will always be grateful that I had the chance to know and be mentored by him.

I would like to thank Gwangbae Bak, a former postdoc in Nielsen Lab. Thanks to his hard work on developing the yeast-based protein expression and purification system, the lab can now easily perform *in vitro* assays on multiple interesting proteins.

I would like to thank Fangwei Gu, a former Ph.D. student in the Nielsen Lab. Fangwei is the first MCDB student I knew when joined the department in fall of 2013. He picked me up at the airport. Since he was a senior student when I joined the lab. He taught me most of the basic rules in the lab and helped me get on track with my own research. I greatly appreciate Fangwei's kindness, encouragement, and valuable advice.

I would like to thank the members of my Ph.D. committee, Professor Steven Clark, Professor Ann Miller, Professor Yanzhuang Wang, and Professor Yin-Long Qiu for their support, advice, and helpful insights, as well as their help in revising my thesis.

I acknowledge and thank all current and past members of Nielsen Lab: Jonathon Combs, Pei Li, Xiaolan Zhao, Chaoyang Liu, Jianmei Long, Maha Hamed, Xiaojie Chen, Mikael Dunn, Caroline Lowder, and Emily Frankman.

I acknowledge and thank the staff of the MCDB department. Thanks to Mary Carr, Anna Cihak, Diane Durfy, Jacqueline Glebe, Kimberly Pavuk, and Suzanne Tainter, for their help and support.

I acknowledge and thank Gregg Sobocinski and the imaging core for training me in the use of confocal microscopes, and for his valuable advice on imaging techniques.

I would like to thank all of the lab members from the neighboring plant labs including the Schiefelbein Lab, the MacAlister Lab, the Pichersky Lab, and the Li Lab. The friendly environment in this plant group meant a great deal to me throughout my years as a graduate student.

Finally, I must thank my beloved wife and my parents for all the sacrifices they have made, and for all the confidence, encouragement, and support they have shown me throughout my studies and beyond. I could never have achieved all that I have without them.

Table of Contents

List of Figures

Abstract

As one of the most significant features of plant cells, the cell wall not only defines plant cell shape but also provides strength and rigidity to the plant. During plant development, changes in cell shape are primarily driven by cell expansion, which is controlled by new cell wall deposition and modification. The two major mechanisms that control these changes are called diffuse growth and tip growth. During diffuse expansion, cell wall materials are synthesized and integrated in a polarized fashion along the entire expanding face of the cells. In contrast, during tip growth new cell wall deposition is restricted to a limited plasma membrane domain, leading to the highly polarized cell expansion associated with this directed cell wall construction.

As the major load-bearing component in plant cell walls, cellulose is also the most abundant biopolymer on earth. Unlike many other cell wall polysaccharides, cellulose is synthesized in the plasma membranes by large integral membrane protein complexes called cellulose synthase complexes (CSCs). The catalytic subunits of the CSCs are encoded by members of the *Cellulose Synthase (CESA)* family. Previous research showed that CESA1, CESA3, and CESA6 are required for the formation of active CSCs involved in the synthesis of cellulose in the primary cell wall of cells undergoing diffuse growth in *Arabidopsis*. Interestingly, our laboratory previously demonstrated that CSCs containing CESA3 and CESA6 did not appear to be required for new cellulose synthesis at the apical plasma membranes of root

hair cells undergoing tip growth. Instead, members of a related family of Cellulose Synthase-Like D (CSLD) proteins showed tip-specific localization in these membranes and provided cell wall synthase activity required for maintenance of structural integrity of the cell wall in these tip-growing root hairs. However, while these CSLD cell wall synthases are essential, the nature of the polysaccharides generated by CSLD proteins has remained elusive.

Here, I use genetic and biochemical approaches to characterize the catalytic activity of one member of the *CSLD* family, CSLD3. Genetic complementation of a *cesa6* mutant with a chimeric CESA6 protein containing a CSLD3 catalytic domain demonstrated that the CSLD catalytic domains can successfully generate β-1,4-glucan polymers for cellulose synthesis. Time-lapse fluorescence microscopy demonstrated that these CESA6-CSLD3 chimeric proteins assembled into CSC complexes with similar mobility as CESA6-labeled complexes in hypocotyl cells. Proteoliposomes containing purified, detergent-solubilized CSLD3 and CESA6 proteins could specifically utilize UDP-glucose as an enzymatic substrate and synthesize products that are only sensitive to endo-β-1,4-glucanase. Taken together, these data strongly support the conclusion that CSLD3 represents a UDP-glucose-dependent β-1,4-glucan synthase.

However, whether CSLD proteins require the formation of higher-order complexes to perform β-1,4 glucan synthase activities remained unclear. Here, I used genetic methods to demonstrate that CSLD2 and CSLD3 proteins are functionally interchangeable with each other during root hair elongation and cell plate formation. CSLD5 could partially rescue the root hair elongation defects in *csld3* mutants. However, it plays a unique and essential function during cell plate formation. Proteoliposomes containing CSLD2 and CSLD5 displayed conserved β-1,4 glucan synthases activities similar to those described for CSLD3. Taken together, these results indicate that while all three vegetatively expressed CSLD proteins possess conserved β-1,4

glucan synthases activities, CSLD5 has a more complicated and specialized role during cell plate formation.

To sum up, my dissertation research further supports that CSLD proteins represent a distinct family of cellulose synthase in *Arabidopsis*.

Chapter 1 Introduction: Cell Wall Structure and Synthesis in *Arabidopsis*

The plant cell wall is one of the most characteristic structures that distinguish plant cells from animal cells. It is also the plant cell structure that arguably may have been the earliest described. As early as 1665, Robert Hooke, an English scientist, first observed the structure of plant cells with a microscope of his design, and for the first time called it the "cell" (Hooke, 1665). What he observed was the cell wall, which opened the door to understanding the structure and function of not only plant cells, but was instrumental in the development of the cell theory.

The plant cell wall is a highly dynamic and complicated structural network therefore the regulation and integration of its individual components are likely highly coordinated. The cell wall provides necessary mechanical support for plant cells to resist intracellular turgor pressure (Bruce, 2003; Somerville et al., 2004; Cosgrove, 2005). Changes in plant cell size and shape are physically constrained by the deposition of plant cell walls (Cosgrove, 2005). The cell wall responds to external environmental factors, transports water and nutrients, interacts with symbiotic organisms, and protects plants from pathogens (Showalter, 1993). The cell wall also plays important roles during plant growth and participates in a series of developmental processes such as cell differentiation, disease resistance, cell recognition, and signal transduction

(Malinowski and Filipecki, 2002; Vorwerk et al., 2004; Cosgrove, 2005; Sanchez-Rodriguez et al., 2010; Gilbert et al., 2013; Bacete et al., 2018).

Plant cell walls are the most abundant of renewable energy resource (Pauly and Keegstra, 2008), and have made important contributions to promote the progress of human civilization. Lignocellulose has been used for papermaking for centuries. Cotton and linen fiber have long been used in textiles. Many foods, building materials, and industrial raw materials are derived from plant cell walls. Additionally, when it comes to the application of bio-renewable energy, plant cell walls are considered one of the more promising potential resources for developing the second generation bioethanol, a safe, clean, and renewable energy (Pauly and Keegstra, 2008). This requires gene-editing mediated re-design of plant cell walls to produce more enzymatically accessible lignocellulose, which would be more suitable for conversion to cellulosic ethanol. However, to date, less than 2% of the annual production of cell wall materials is well used by human society (Pauly and Keegstra, 2008).

1.1 Components of the plant cell wall

The plant cell wall is a complex network of cellulose, hemicellulose, pectin, and a wide range of glycoproteins including structural proteins and receptors (Somerville et al., 2004). Plant cell wall contents vary in different species, tissues, cell types, and even in different regions of a single cell. As a result, the structure and composition of plant cell walls are highly complicated and diverse (Burton et al., 2010). In general, plant cell walls can be divided into primary walls and secondary walls. The young cells and tissues in the early stages of growth and development usually only have primary cell walls. The secondary cell walls are a thickened matrix located

between the primary wall and the plasma membrane, which are mainly found in non-growing cells such as plant mechanical tissues (Turner et al., 2007).

1.1.1 Cellulose

Cellulose is the major component in both primary and secondary cell walls. The basic biochemical structure of cellulose is a long, unbranched β-1,4 glucan chain. In plants, cellulose exists in the form of cellulose microfibrils, which are synthesized directly at the plasma membranes by large integral membrane protein complexes called cellulose synthase complexes (CSCs) that were first visualized by early scanning electron microscopy experiments as a six-lobed rosette structures that are often observed at terminal ends of cellulose fibers; hence, CSCs are also often called rosette terminal complexes (Brown, 1996; Kimura et al., 1999). The β-1,4 glucan synthase activity of CSCs was shown to be provided by cellulose synthase (CESA) proteins. There are ten *CESA* genes encoded in the *Arabidopsis thaliana* genome (Richmond and Somerville, 2000). Genetic analysis in the past decades demonstrated that the formation of a functional CSC requires the assembly of at least three different CESA isoforms (Desprez et al., 2007; Persson et al., 2007). In the case of the primary cell walls in *Arabidopsis*, CESA1, CESA3, and CESA6-like (CESA6, CESA2/5/9) isoforms interact to form rosette subunits, and six of these subunits then assemble into CSCs (Arioli et al., 1998; Fagard et al., 2000; Scheible et al., 2001; Desprez et al., 2007; Persson et al., 2007). CESA4, CESA7, and CESA8 participate in the synthesis of the secondary cell walls in *Arabidopsis* (Taylor et al., 1999; Taylor et al., 2000; Taylor et al., 2003; Taylor, 2007). The role of CESA10 remains unclear (Kumar and Turner, 2015). Each CESA isoform in the complex uses the intracellular UDP-Glucose as a substrate and

is thought to be capable of synthesizing one single β-1,4 glucan polymer. Multiple, newly synthesized β-1,4 glucan polymers are extruded into the extracellular space where they then assemble through intermolecular hydrogen bonds to form cellulose microfibrils (Hayashi, 1989; Somerville et al., 2004; Paredez et al., 2006) (Figure 1.1). Due to the application of X-ray diffraction, multiple layers of cellulose microfibrils were observed in both primary and secondary walls. The orientation of these cellulose microfibrils varies in different layers (Xu et al., 2006; Fernandes et al., 2011; Ding et al., 2012). These cellulose microfibrils layers serve as scaffolds and provide mechanical strength and rigidity to resist the intracellular pressure of plant cells (Cosgrove, 2005).

Different approaches have been applied to understand the architecture of CSCs, as well as the structure of cellulose microfibrils. Biophysical studies using dual-axis electron tomography, and atomic force microscopy suggest that there are 18-24 cellulose chains associated to form microfibril with a diameter of 2.9~3.2 nm (Xu et al., 2006; Fernandes et al., 2011; Cosgrove, 2014). A recent modeling study of three possible orientations for the 18-chain microfibril suggest the most probable arrangement of a microfibril is based on 5 layers, in which the cellulose chains are stacked in the form of "34443" model (Kubicki et al., 2018). Analyses of primary cell wall (CESA1, 3, 6) and secondary cell wall (CESA4, 7, 8) CESA stoichiometry using Co-Immunoprecipitation (Co-IP), mass spectrometry (MS), and quantitative immunoblotting demonstrated that each isoform occurs in equimolar amounts with a 1:1:1 stoichiometry (Gonneau et al., 2014; Hill et al., 2014). Taken together, these data suggest a model where each rosette subunit contains three CESA isoforms. Six of these subunits then assemble into CSCs containing 18 CESA isoforms that synthesize 18 cellulose chains to form one microfibril (Figure 1.1). This model is consistent with improved TEM images of CSCs from *Physcomitrella patens*

(Nixon et al., 2016). However, the stoichiometry of CESAs varies in different species (Zhang et al., 2018), and the exact number of CESA subunits per CSC lobe remains an active area of investigation. In addition, during the transition from the synthesis of the primary wall to the secondary wall, CESA7-containing CSCs appeared at the plasma membrane and were found to transiently coexist with CESA6-containing CSCs before their depletion from the plasma membrane (Watanabe et al., 2018). These data suggest the architecture of CSC might change under different circumstances.

The crystal structure of the bacterial cellulose synthase, BcsA-BcsB complex, has recently been solved, which significantly promotes our understanding of the process of cellulose synthesis. This structural analysis reveals the molecular function of a core glycosyltransferase catalytic activity that appears to have been conserved from bacterial cellulose synthases to higher plant cellulose synthases (Richmond and Somerville, 2000; Little et al., 2018) . The QxxRW and FFCGS motifs form a binding site for the terminal disaccharide of the glucan. The TED motif serves as the catalytic motif to form the β-1,4 glycosidic bond (Morgan et al., 2013). The crystal structure also defined the conducting channel for newly synthesized cellulose polymers and proposed the cellulose synthesis-translocation coupling model, which was later confirmed by an *in vitro* reconstituted activity assay (Omadjela et al., 2013). It is now believed that the single glucan polymers are self-assembled into cellulose microfibrils immediately after exit this channel to the extracellular region. Whether this assembly process requires other proteins remains unclear.

The activity of CESA proteins is regulated by a variety of factors. Several studies have shown that the stability of CESA proteins is affected by light and temperature (Jacob-Wilk et al., 2006; Hill et al., 2018). Phosphorylation also plays an important role in regulating CESA protein

activity. The phosphorylation of S180 and S185 residues leads to the degradation of CESA7 (Taylor, 2007). Mutations of CESA1 phosphorylation sites affected the interaction with microtubules and lead to altered microfibril structure (Chen et al., 2010). BIN2 was found as a negative regulator of cellulose synthesis by directly phosphorylating the T157 residue of CESA1 (Sanchez-Rodriguez et al., 2017).

The cellulose synthase complexes (CSCs) are assembled in the Golgi apparatus and delivered to the plasma membrane (Figure 1.2). By regulating CSC assembly and trafficking, plant cells can control the location of the deposition of newly synthesized cellulose along with other cell wall components, and therefore determine the cell expansion process. The trans-Golgi network/early endosome (TGN/EE) compartment played important roles in the process of CSC assembly and sorting. Recent studies identified Golgi-localized proteins, STELLO1 and 2, physically interact with CESAs. In *stl1/2* mutants, the secretion rate of GFP-CESA3 labeled CSCs was highly reduced. Furthermore, the velocities of these complexes within the plasma membrane were reduced as well. This indicated that the activity of CSCs was affected in the absence of STELLO1 and 2 function (Zhang et al., 2016).

The correlation between the alignment of cellulose microfibrils and microtubule arrays was recognized early on (Green, 1962). It has recently been supported by the observation of the mobility of YFP-CESA6 labeled CSCs within the membrane of dark grown hypocotyl tissues. The CSCs moved at constant rates in linear tracks that were aligned and coincident with cortical microtubules. Disruption on the cortical microtubule arrays using depolymerization drugs leads to the disorganization of YFP-CESA6 labeled CSCs (Paredez et al., 2006). These data strongly indicated that the cortical microtubules have a fundamental influence on the distribution and delivery of CSCs in cells undergoing diffuse growth (Figure 1.3). Subsequently, two separate

laboratories identified that the CSCs were delivered to the plasma membrane through the cortical microtubule-associated CESA compartments (MASCs) (Crowell et al., 2009) or small CESA compartments (SmaCCs) (Gutierrez et al., 2009). Movement of these compartments coincides with cortical microtubule depolymerizing ends (Crowell et al., 2009; Gutierrez et al., 2009). Disruption of the cortical microtubule arrays affected the movement of these compartments and resulted in reduced CSC fusion to the plasma membrane (Crowell et al., 2009; Gutierrez et al., 2009).

More support for this "microtubule-microfibril alignment" hypothesis came from the identification of CSI (cellulose synthase-interactive) proteins (Figure 1.2). CSI1 was first identified in a yeast two-hybrid screen for proteins that interacted with the cytosolic localized catalytic domain of CESA6 (Gu et al., 2010). In *csi1* mutants, the hypocotyl tissues displayed similar elongation defects, and a reduced cellulose content to *cesa6* mutants in dark-grown conditions (Gu et al., 2010). Further analysis also showed that the CESA6-labeled CSCs displayed reduced mobility in *csi1* mutants (Gu et al., 2010). Additional proteins are involved in mediating the association between CSCs and cortical microtubules. The cellulose synthase-microtubule uncoupling (CMU) proteins are microtubule-associated proteins that are located as static puncta along cortical microtubules (Liu et al., 2016). These proteins help maintain lateral microtubule array positions at the cortex of plant cells. In *cmu1/2* double mutants, the CSC drags cortical microtubules when moving within the plasma membranes and causes cell twisting defects (Liu et al., 2016). PATROL1 (PTL1), which was initially shown to be involved in the transport of plant H+-ATPases to plasma membranes (Hashimoto-Sugimoto et al., 2013), has been found to interact with CSI1, as well as multiple subunits of exocyst complexes involved in secretion. In *ptl1* mutants, delivery of CESA6-labeled CSC to the plasma membrane was

affected and cellulose synthase defects have been observed. It is believed that CSI1 binds to cortical microtubules as a marker to define the position of secretion while PTL1 mediates the tethering of MASCs/SmaCCs to CSI1 (Zhu et al., 2018).

In addition to the cellulose synthase, other proteins play important roles in cellulose biosynthesis. *KORRIGAN (KOR)* encodes a membrane-localized β-1,4-endoglucanase, that is required for normal cellulose synthesis. Mutants of *KOR* showed a strong reduction in cellulose content (Lane et al., 2001; Sato et al., 2001), and fluorescent fusions of KOR1 co-localized with CESA proteins in CSCs (Vain et al., 2014). It is proposed that KOR1 proteins might be involved in regulating the length of the glucan chains, or they might also function to release tensile strain during cellulose synthesis. Details of the mechanism are still unknown (Figure 1.2) (Ueda, 2014). Sucrose synthase could also affect cellulose synthesis. It positively regulates cellulose production by affecting carbon partitioning, which also alters the cell wall ultrastructure (Coleman et al., 2009).

1.1.2 Callose

Callose is a polysaccharide that contains a β-1,3-glucan backbone with some branches through β-1,6 linkage, and is widespread in higher plants (Chen and Kim, 2009). Callose usually acts as a temporary cell wall material in response to rapid stimuli and can be induced by tissue damage, pathogen infection, and various other physiological stresses (Stone, 1992). Callose accumulation only happens in specialized cell types, or during specific stages of growth and development. Similar to cellulose, callose is also synthesized directly at the plasma membrane by Glucan Synthase Like proteins (GSL) (Richmond and Somerville, 2000; Verma and Hong,

2001). There are 12 *GSL* genes in the *Arabidopsis* genome and most *GSL* genes are expressed in a tissue-specific fashion, consistent with the specific callose distribution (Hong et al., 2001). The GSL proteins also contain multiple transmembrane domains and a large cytoplasmic region, which is considered the catalytic domain (Hong et al., 2001). Callose is enriched at plasmodesmata and plays important roles regulating permeability of plasmodesmata by controlling the size exclusion limit (SEL) (De Storme and Geelen, 2014). β-1,3-glucanases (BGs) also contribute to regulating the homeostasis of plasmodesmatal callose (PDC) (Iglesias and Meins, 2000; Bucher et al., 2001). Along with GSL, these two families of proteins determine the conductivity of plasmodesmata. Both *gsl7 and gsl8* mutants showed a reduced accumulation of callose at the plasmodesmata, and this resulted in enhanced cell-cell transport (Guseman et al., 2010; Xie et al., 2011). Ectopic expression of GSL12 protein during phloem development partially rescues the callose deposition in *gsl7* mutants, indicating that GSL7 and GSL12 are functionally redundant in callose synthesis (Vaten et al., 2011).

Pollen development and cell plate formation are the other two well-studied processes that require callose synthesis and deposition (Meikle et al., 1991; Samuels et al., 1995; Ferguson et al., 1998; Chen and Kim, 2009; Drakakaki, 2015). Multiple GSL proteins contribute to fertility through pollen development. GSL1 and GSL5 are necessary and function redundantly in pollen development and fertility. Pollen grains were collapsed and inviable in the absence of GSL1 and GSL5 (Enns et al., 2005). In *gsl2* mutants, lack of callose altered the exine deposition pattern of microspore and caused male sterility (Dong et al., 2005; Nishikawa et al., 2005). In addition, both GSL8 and GSL10 played essential roles in microspore division, resulting in male gametophyte lethality in *gsl8* and *gsl10* mutants (Toller et al., 2008). Callose also accumulates in cell plates at early stages of cell division (Samuels et al., 1995). GSL6 displayed a specific cell

plate localization in dividing cells (Hong et al., 2001). Severe cytokinesis defects were observed in *gsl8* mutants (Chen and Kim, 2009), suggesting both GSL6 and GSL8 are required for cell plate formation during cell division. Callose deposition on the cell plate is rapidly followed by the deposition of cellulose and other cell wall materials. The callose will then be broken down by β-1,3-glucanases (BGs) (Chen and Kim, 2009).

1.1.3 Hemicelluloses

Exhibiting the second-highest content of the plant cell wall components, hemicelluloses are comprised of a series of polysaccharides that have β-1,4-linked backbones. It is present along with cellulose in almost all terrestrial plant cell walls (Scheller and Ulvskov, 2010). Hemicellulose polysaccharides generally have shorter backbone chains with 500~3000 sugar units as opposed to 7000~15,000 glucose molecules per polymer present in cellulose. In addition, hemicellulose backbone polymers are generally decorated with additional sugar sidechains, while cellulose is unbranched (Gibson, 2012). It is proposed that hemicellulose functions to link individual cellulose microfibrils together, forming a cellulose-xyloglucan network in plant cell walls (Veytsman and Cosgrove, 1998). Based on the structural differences of backbone residues, as well as the side branches, hemicelluloses can be characterized into different classes including xyloglucan, xylan, mannan, and glucomannan (Scheller and Ulvskov, 2010). The contents of hemicellulose vary widely in different developmental stages, tissues or organs, and cell types (Scheller and Ulvskov, 2010).

In *Arabidopsis* primary cell walls, xyloglucan is the most abundant class of hemicelluloses (Liepman et al., 2010). Similar to cellulose, xyloglucan also contains a β-1,4-glucan backbone.

However, most of these glucosyl residues (G) are substituted with a β-1,6 linked xylose (X), which are then further decorated with galactose (L) and fucose (F) residues. This branching is believed to increase the solubility of xyloglucan (Liepman et al., 2010; Scheller and Ulvskov, 2010). The structure and patterns of these xyloglucan sidechains varies in different species and often are used as references in evolutionary studies in plants and algae (Del Bem and Vincentz, 2010). Based on the number and patterns of substituted glucosyl residues, most xyloglucans are classified as "XXXG-type", where β-1,6 linked xyloses (X) are found in the first three glucosyl residues (G), or "XXGG-type", where only the first two glucosyl residues are xylosylated (Fry et al., 1993). In *Arabidopsis*, the major sidechain pattern of xyloglucan is XXXG-type including XXXG, XLXG, XXFG, XLLG, and XLFG subunits (Fry et al., 1993). In the *Poaeceae* and *Solanaceae*, the xylose residues are usually decorated with arabinose (A) instead of galactose (L) residues (Zabotina et al., 2012). Due to the structural complexity of these xyloglucan side chains, xyloglucan biosynthesis requires at least four distinct enzyme classes for the synthesis of β-1,4-linked glucan backbone and the successive addition of xylosyl, galactosyl, and fucosyl residues (Liepman et al., 2010; Zabotina et al., 2012).

The *CSLC (Cellulose Synthase Like-C)* family members are thought to be responsible for the synthesis of the glucan backbone of xyloglucan. *CSLC* family belongs to a larger superfamily of genes known as the *CELLULOSE SYNTHASE-LIKE (CSL)* family, whose members are predicted as glycosyltransferases (GTs) (Richmond and Somerville, 2000) (Figure 1.4). Cells heterologously expressing AtCSLC4 proteins displayed β-1,4-glucan synthase activity in isolated Golgi membranes (Cocuron et al., 2007). Xyloglucan xylosyltransferases (XXT1, XXT2, and XXT5) are responsible for xylosylation of the β-1,4-glucan xyloglucan backbone (Faik et al., 2002; Cavalier and Keegstra, 2006, Alan et al., 2016). They initiate side-chain extensions by

transferring the xylosyl group from UDP-xylose to certain residues on the backbone of xyloglucan (Cavalier and Keegstra, 2006). MUR3 (Murus 3) and XLT2 (xyloglucan l-side chain galactosyltransferase position 2) are responsible for galactosyl modification by adding galactosyl residues to specific xylosyl residues (Madson et al., 2003; Schultink et al., 2013). FUT1 (fucosyltransferase 1) is responsible for fucosyl modification (Perrin et al., 1999; Vanzin et al., 2002). Recent studies discovered that XUT1 (xyloglucan specific galacturonosyltransferase 1) catalyzes the formation of the galactosyluronic acid-(1,2)-α-D-xylopyranosyl linkage. This novel galacturonic acid containing xyloglucan is essential for root hair formation and elongation in *Arabidopsis* (Pena et al., 2012). Recent studies have shown that XXT1, XXT2, MUR3, FUT1, and CSLC4 could form protein complexes in the Golgi, which further supports their roles in xyloglucan synthesis (Chou et al., 2012, 2014).

Xylan is made up of β-1,4 linked xylosyl residues with side branches of α-arabinofuranose and α-glucuronic acids (Scheller and Ulvskov, 2010). Xylans contain α-1,2-linked glucuronosyl and 4-O-methyl glucuronosyl residues also known as glucuroxylans. They are the major component of the secondary wall of dicots (Scheller and Ulvskov, 2010). Xylan contributes to the cross-linking of cellulose microfibrils and lignin through ferulic acid residues (de O. Buanafina, 2009). In monocots, α-arabinofuranose residues are usually found attached to xylan backbones known as arabioxylans and glucuronoarabinoxylans (GAXs) (Scheller and Ulvskov, 2010). These types of xylans are the major noncellulosic polysaccharide of the primary cell wall (~20%) of monocots, although they are less abundant in dicots (Scheller and Ulvskov, 2010). Due to the structural similarity of the xylan backbone to xyloglucan backbone, it has been widely assumed that the xylan synthases were likely also members of the *CELLULOSE SYNTHASE-LIKE (CSL)* families. However, characterization of xylan-deficient *irx9*, *irx14*, and

irx10 mutants indicated that the backbone of xylans is synthesized by members of glycosyltransferase family 43, encoded by *IRX9* and *IRX14*, and members of glycosyltransferase family 47, *IRX10* and *IRX10-like* (Brown et al., 2007; Brown et al., 2009). Unlike CSL proteins, these xylan synthases are type II membrane proteins that contain only one transmembrane domain, and the molecular mechanism by which they synthesize the backbone of xylan is not yet clear (Brown et al., 2009).

Mannan is a set of hemicellulosic polysaccharides formed by the β-1,4 linkage of mannose (Man) (Scheller and Ulvskov, 2010). In some species, galactose and glucose residues are found mixed in the backbone of mannose, and these polysaccharides are called galactomannan and glucomannan, respectively (Rodriguez-Gacio Mdel et al., 2012). Similar to other hemicelluloses, mannan backbones also contain side branches substituted with α-1,6-linked galactose (Gal). The Man:Gal ratio influences the solubility and viscosity of mannans, and interactions with other cell wall polysaccharides (Rodriguez-Gacio Mdel et al., 2012). Glucomannan is the major component of the secondary cell wall of coniferous and monocotyledonous plants (Benova-Kakosova et al., 2006; Stone, 2006). Glucomannan is also enriched in seeds as structural or storage components (Antoni Femenia, 1999). It has been shown that the CSLA proteins from the *CELLULOSE SYNTHASE-LIKE (CSL)* family are responsible for the synthesis of mannan or glucomannan backbone (Dhugga et al., 2004). When lacking the major mannan synthase in seeds, CSLA7, the embryos displayed a slower development rate, resulting in lethality in *Arabidopsis* (Goubet et al., 2003). *In vitro* activity analysis confirmed that these CSLA proteins could use both GDP-mannose and GDP-glucose as substrates (Liepman et al., 2005). Overexpressed CSLA9 could functionally rescue the embryo-lethal defects in *csla7* mutants, indicating that the CSLA proteins are functionally interchangeable (Goubet et al., 2009).

Most hemicelluloses were found with different degrees of *O*-acetylation, which has an important influence on their chemical properties and interactions with cellulose microfibrils (Laura L. Kiefer, 1989; Scheller and Ulvskov, 2010). The degree of *O*-acetylation changes in various plant tissues and during plant development, indicate an important role of this modification (Obel et al., 2009). Due to the complexity of *O*-acetylation, the enzymes involved in this biochemical reaction are not well characterized (Gille et al., 2011). It has been shown that nearly 20~35% reduction of xyloglucan *O*-acetylation was observed in *axy4* mutants, thus the AXY4/AXY4L proteins were proposed as xyloglucan-specific *O*-acetyltransferases (Gille et al., 2011). In addition, reduced levels of *O*-acetylated cell wall polysaccharides were observed in *rwa2* mutants (Manabe et al., 2011).

1.1.4 Pectin

The pectic polysaccharides contain high acidic glycosyl residue content, such as galacturonic and glucuronic acids. According to the composition and structural characteristics, pectic polysaccharides can be divided into rhamnogalacturonan I (RG I), rhamnogalacturonan II (RG II), and homogalacturonan (HG) (Mohnen, 2008; Liepman et al., 2010). Unlike cellulose and xyloglucan that contain β-1,4-linked glucan backbones, homogalacturonan (HG) is mainly formed by a linear backbone of α-1,4 linked galacturonic acid residues (Mohnen, 2008). HG is the most abundant pectic polysaccharide which comprises 65% of total pectins (Mohnen, 2008). β-1,3 xylosyl residue substitution could be found in some side chains of HG and is also called xylogalacturonan (XGA), which has been reported to be specifically present in reproductive tissues (Zandleven et al. 2006). Like hemicelluloses, pectin polysaccharides are synthesized in

the Golgi apparatus, and are then secreted to the plasma membrane by vesicle trafficking (Mohnen, 2008). Due to the structural complexity of pectic polysaccharide side chains, at least 67 different transferases including glycosyl-, methyl-, and acetyltransferases are estimated to be involved in pectin biosynthesis (Mohnen, 2008). However, very limited enzyme function has been identified. Studies have shown that GAUT1 (Galacturonosyltransferase 1) and GAUT7 (Galacturonosyltransferase 7), two Golgi-localized type II membrane proteins, form a heterodimer and this complex is thought to be responsible for the synthesis of HG (Sterling et al., 2006; Atmodjo et al., 2011). Significant reduction of galacturonic acid levels is exhibited in *gaut8* and *gaut12* mutants perhaps indicating that GAUT8 and GAUT12 might be involved in HG biosynthesis (Biswal et al., 2015). XGD1 (xylogalacturonan deficient 1) is a β-1,3-xylosyltransferase that is responsible for synthesizing the xylosyl branch in XGA (Jensen et al., 2008).

Rhamnogalacturonan II (RG II) shared the same α-1,4 linked homogalacturonic acid backbone as HG. Mainly found in dimers, RG II has the most complicated sidechain structures, although amazingly this complex structure is widely conserved in different plant species (Matsunaga et al., 2004). It remains unclear whether the GAUTs are also responsible for synthesizing the RG II backbones (Funakawa and Miwa, 2015). Nevertheless, progress has been made in characterizing the synthases of RG II side chains. 30% reduction in 2-*O*-methyl xylose residues are exhibited in the *mgp4* mutants, indicated MGP4 (Male Gametophyte Defective 4) is responsible for adding the xylose residues to RG II (Liu et al., 2011). In addition, two Golgi-localized α-1,3-D-xylosyltransferases, RGXT1 (Rhamnogalacturonan xylosyltransferase 1) and RGXT2 (Rhamnogalacturonan xylosyltransferase 2), are proposed to participate in RG II side chain synthesis (Egelund et al., 2006). The xylosyltransferase activity was described for both

RGXT1 and RGXT2 proteins that are overexpressed in insect cells, and these proteins utilize UDP-xylose as substrates (Egelund et al., 2006).

In contrast to HG and RG II, Rhamnogalacturonan I (RG I) contains a backbone of the "rhamnose-galacturonic acid" disaccharide repeat linked by α-1,2 and α-1,4 linkages [-α-D-GalpA-1,2-α-L-Rhap-1,4-]$_n$ (James M. Lau, 1985). The RG I backbone also has side chains containing individual, linear, or branched α-L-Ara*f* and β-D-Gal*p* residues (Mohnen, 2008). GATL5 (Galacturonosyltransferase like 5) is proposed to be involved in synthesizing the backbone of RG I (Kong et al., 2013). ARAD1 (arabinan deficient 1) and ARAD2 (arabinan deficient 2) are involved in the synthesis of the branching of arabinose by forming a putative complex (Harholt et al., 2012b). In the *arad1* and *arad2* mutants, the arabinose contents were highly reduced and more unsubstituted arabinan was observed (Harholt et al., 2012b). The direct interaction between ARAD1 and ARAD2 was confirmed by Bimolecular Fluorescence Complementation (BiFC) and Förster Resonance Energy Transfer (FRET) (Harholt et al., 2012b). In addition, the β-1,4-linked galactan branches of RG I was reduced in the *gals1* mutants. When overexpressing GALS1 (Galactan Synthase 1), a 50% increase of β-1,4-linked galactan branch contents was exhibited, indicating the GALS1 catalyzes branching galactans elongation (Liwanag et al., 2012).

Modification of pectin polysaccharides plays important roles in regulating the functions of pectins. They affect various plant development processes, such as cell wall expansion, cellular adhesion, and separation (Mohnen, 2008). For example, most HG are highly methylated. The balance between pectin methylesterase (PME) and its inhibitor (PMEI) controls the overall methylation level of pectic polysaccharides (Jolie et al., 2010). More evidence has shown that the backbones of pectic polysaccharides are covalently linked with each other, and also associated

with cellulose and hemicellulose (Mohnen, 2008; Scheller and Ulvskov, 2010). The cross-linked pectin polysaccharides are proposed to help facilitate microfibril slippage during cell expansion (Cosgrove, 2005).

1.1.5 Lignin

Lignin is a mixed polymer formed by phenolic monomers including coniferyl alcohol (G unit), sinapyl alcohol (S unit), and p-coumaryl alcohol (H unit), which are connected by ether linkages (Vanholme et al., 2010). These three units are all synthesized from Phenylalanine (Phe) through general phenylpropanoid and monolignol-specific pathways (Rippert et al., 2009). CINNAMATE 4-HYDROXYLASE (C4H), *p*-COUMARATE 3-HYDROXYLASE (C3H), and FERULATE 5-HYDROXYLASE (F5H) are endoplasmic reticulum (ER) membrane-localized cytochrome P450 enzymes involved in the lignin biosynthetic pathway, which are thought to be active at the cytosolic side of the endoplasmic reticulum (ER), with these lignin subunits then secreted across the plasma membrane by as yet unidentified transporters (Ro et al., 2001). Unlike other cell wall polysaccharides linked by glycosidic bonds, lignin polymerization requires a very complicated process containing three steps of reactions. Firstly, the monolignol phenol subunits are oxidized and dehydrogenated. Two subunits containing monomer radicals then couple to form a covalent bond and become a dimer, which will soon be dehydrogenated to be ready for the next subunit (Vanholme et al., 2010). It is believed that extracellular peroxidases and laccases are involved in monolignol dehydrogenation. Due to the gene redundancy, it has been difficult to identify the particular enzymes involved these processes (McCaig et al., 2005). Lignin, along with cellulose microfibrils and various hemicellulose polysaccharides, forms

complicated networks in wood (Chonlong Chio, 2019). The lignin composition varies in different species and shows diversity in evolution. In general, softwood lignin from gymnosperms is mainly made of coniferyl alcohol (G unit) with low content of p-coumaryl alcohol (H unit), while hardwood lignin from angiosperms contains a blend of coniferyl alcohol (G unit) and sinapyl alcohol (S unit). The lignin of gramineous plants contains a mixture of all three coniferyl alcohol (G unit), sinapyl alcohol (S unit), and p-coumaryl alcohol (H unit) subunits (Zakzeski et al., 2010; Li et al., 2014). As the most abundant form of biomass in nature, lignocellulosic materials are considered as a major potential resource for bioethanol generation, and an alternative source for various aromatic polymer and biomaterials production. Thus, the degradation of lignin and converting lignin to other valuable products are of great interest for future investigation (Chonlong Chio, 2019).

1.1.6 Cell wall structural proteins

In addition to cellulose, hemicellulose, pectin, and other polysaccharides, the plant cell wall also contains numerous structural proteins, which are involved in controlling cell expansion, regulating polysaccharide assembly, and sensing cell wall integrity (Jamet et al., 2006). Cell wall structural proteins are mainly hydroxy-proline-rich glycoproteins (HRGPs) including extensin, arabinogalactan protein (AGPs), proline/hydroxy-proline-rich proteins (P/HRGPs), and solanaceous lectins (Sommer-Knudsen et al., 1998). Evidence has shown that HRGPs could act as impenetrable physical barriers against pathogen ingress and that they immobilize the pathogens by binding to their negatively charged surfaces (Leach et al. 1982; Mazau et al. 1987; Cassab and Varner 1988). P/HRGPs and extensins are known to be insoluble proteins whereas

AGPs are soluble (Basavaraju et al., 2009). Twenty *EXTENSIN* genes have been identified in *Arabidopsis* genome (Cannon et al., 2008). Proline residues in extensin are usually hydroxylated by prolyl-4-OH hydroxylases and then further decoration with arabinose residues (Velasquez et al., 2011; Ogawa-Ohnishi et al., 2013). Hydroxyproline *O*-arabinosyltransferases (HPATs) are responsible for addition of the first arabinose residue linked to hydroxyproline (Ogawa-Ohnishi et al., 2013). The second and third arabinose residues are added by RRA3 (Reduced Residual Arabinose 3) and XEG113 (Xyloglucanse 113), respectively (Velasquez et al., 2011). It was reported that extensin has the ability to self-assemble and form positively charged scaffolds during the formation of the cell plate at the end of cytokinesis (Cannon et al., 2008). Extensin then reacts with negatively charged pectin to form an extensin pectate matrix that would guide the following deposition of newly synthesized cell wall components (Cannon et al., 2008). Evidence has been presented that disruption of O-arabinosylation results in defective cell walls in multiple tissues (Cannon et al., 2008; Velasquez et al., 2011; Ogawa-Ohnishi et al., 2013).

Proline/hydroxyproline-rich proteins (PRPs), another types of HRGPs also contribute to cell wall structure (Sommer-Knudsen et al., 1998). Four *PRP* genes are characterized in *Arabidopsis* (Fowler et al., 1999). Among these, *AtPRP1* and *AtPRP3* encode proteins containing an N-terminal PRP-like domain, while *AtPRP2* and *AtPRP4* represent a novel group of PRP genes that encode proteins containing a C-terminal PRP-like domain (Fowler et al., 1999). *PRP1* and *PRP3* are exclusively expressed in root tissues, and the expression levels of PRP3 is positively correlated root hair elongation (Fowler et al., 1999). However, no morphological defect of root hairs was observed in the *prp3* mutants (Larson et al., 2014). This might be due to gene redundancy, but the exact functions of PRPs remain unclear.

Arabinogalactan protein (AGPs) are highly glycosylated HRGPs (Sommer-Knudsen et al., 1998). Based on the amino acid sequences, molecular sizes, and potential domains, eighty-five *AGPs* genes have been identified in the *Arabidopsis* genome (Showalter et al., 2010). Similar to extensins, most proline residues in AGPs are also modified to hydroxyproline, which could be further glycosylated with β-1,3-galactan side chains. Progress has been made on the identification of enzymes that are involved in AGP side chain biosynthesis (Qu et al., 2008; Basu et al., 2013; Liang et al., 2013; Tan et al., 2013; Nguema-Ona et al., 2014). In general, the individual AG chain may consist of up to 120-150 sugar residues (Tan et al., 2013). The glycosylation of AGPs is essential for their function (Nguema-Ona et al., 2014). One study showed that APAP1 (Arabinoxylan Pectin Arabinogalactan Protein 1) can be found covalently linked to hemicellulose and pectin polysaccharides (Tan et al., 2013). This suggests a potential cross-linking role for AGPs in cell wall assembly.

Another well-studied cell wall protein is the expansin family, which function to loosen plant cell walls and promote cell expansion by physically separating cellulose microfibrils (Sampedro and Cosgrove, 2005). Recent studies have shown the crystal structures of bacterial expansin (EXLX1) complexed with cellulose-like oligosaccharides, which clarifies the target of expansin (Georgelis et al., 2012). Based on sequence similarity, the *EXPANSIN* gene family is divided into four distinct subgroups: *α-expansins (EXPA)*, *β-expansins (EXPB)*, *expansin-like A (EXLA)*, and *expansin-like B (EXLB)* (Sampedro and Cosgrove, 2005). In *Arabidopsis*, downregulation of *EXPA10* caused smaller malformed leaves, while upregulation of *EXPA10* increased the diameter of rosette leaf clusters (Cho and Cosgrove, 2000). Studies in other species have confirmed the cell wall loosening activities for both EXPA and EXPB proteins, while the roles of EXLA and EXLB remain unclear (Sampedro and Cosgrove, 2005).

1.2 Structural organization of the cell wall

Although the biochemical structures of major cell wall polysaccharides have been well established, much remains unknown regarding how these different cell wall polysaccharides and cell wall proteins interact to form a functional network with certain rigidity as well as flexibility for potential expansion (Park et al., 2012). The tethered network model is one of the more representative and the most widely accepted depictions of the structure of the primary cell wall (Veytsman and Cosgrove, 1998). The main point of this model is that the cellulose microfibrils serve as the major load-bearing skeleton component, while hemicellulose – xyloglucan, in particular – functions to link individual microfibrils together forming a cellulose-xyloglucan network. Pectin polysaccharides, which are much more hydrophilic due to the presence of acidic glycans, bind water and cations and serve to fill the spaces between elements of the cellulose-xyloglucan network. However, this model is based on several indirect observations on the binding behaviors of xyloglucan (Hayashi and Maclachlan, 1984; Hayashi et al., 1987; McCann et al., 1990; Pauly et al., 1999) therefore its validity was called into question by a double mutant in *Arabidopsis*, *xxt1/xxt2*. These mutants are completely lacking in xyloglucan, yet displayed only minor growth defects (Cavalier et al., 2008). Recent studies using biophysical methods (2D, 3D high-resolution magic-angle-spinning solid-state NMR) demonstrated that nearly 25-50% of the cellulose microfibrils exhibit close contact with pectins (Wang et al., 2012). The biochemical structure analysis of ARABINOXYLAN PECTIN ARABINOGALACTAN PROTEIN1 (APAP1) also adds new evidence for a modified model where both pectins and hemicelluloses are tightly bound to cellulose microfibrils (Tan et al., 2013). As for the secondary wall, lignin is

believed to fill most of the gaps between the cellulose microfibrils and provide additional mechanical strength to these structures (Vanholme et al., 2013). The detailed structure of the cell wall network remains to be further studied and revealed.

1.3 Regulation of cell wall synthesis

Plant hormones play important roles in regulating the composition and structure of cell walls. Studies have shown that mutations in several key genes for plant hormone synthesis and signal transduction lead to the downregulation of cell wall-related gene expression. The expression of xyloglucan endotransglucosylase-hydrolase (XTH) in the hypocotyl of *Arabidopsis* was induced by gibberellin (Liu et al., 2007). The mRNA level of *KORRIGAN (KOR)* in brassinosteroid (BR) synthetic mutants (*det2*) was also down-regulated (Nicol et al., 1998). These results indicated that plant hormones could influence plant growth and development through shaping cell wall biosynthesis and deposition (Didi et al., 2015; Majda and Robert, 2018).

prc1 (procuste 1) is a null mutant of CESA6, which displayed a dwarf hypocotyl defect under dark grown condition. By screening for suppressors of *prc1*, a member of *Catharanthus roseus* ReceptorLikeKinase1-like (CrRLK1L) family, THE1 (THESEUS 1), was identified (Hématy et al., 2007). The hypocotyl elongation defects were partially rescued in the *the1/cesa6* double mutants, even though the cellulose content in this double mutant was unchanged and remained much lower than in wild type plants. These results suggested that *THESEUS1* might act as a sensor for cell wall integrity (Hematy et al., 2007). *FER (FERONIA)* and *HERK1 (HERCULES 1)*, both of which are induced by brassinosteroid (BR) signaling, are also members

of the CrRLK1L family and closely related to *THE1*. Genetic studies have shown that BR may be correlated with the cell elongation signaling pathways regulated by these three receptor-like kinases (Guo et al., 2009). *FER* has been demonstrated to function as the surface regulator for RAC/ROP signaling pathway that is important for root hair elongation (Duan et al., 2010). Recent studies have shown that *FER* is also involved in plant immunity. By binding to RALF23 as the signal ligand, FER could phosphorylate MYC2, the transcription factor in the JA signaling pathway, to induce its degradation (Guo et al., 2018). The double mutant of two LRR-RLK proteins, FEI1 and FEI2, demonstrated altered cell expansion in root tissues, reduction in cellulose content, and lignin ectopic deposition. Yeast two-hybrid experiments showed that both FEI1 and FEI2 could interact with ACC synthase, suggesting that the signal pathway mediated by FEI1/2 might be related to ethylene synthesis (Xu et al., 2008).

1.4 Current study on CSLD proteins

In *Arabidopsis*, there are seven *CSL (Cellulose Synthase-Like)* families including *CESA, CSLA, CSLB, CSLC, CSLD, CSLE,* and *CSLG*, among which the *CSLD* family shares the highest protein sequential similarity to *CESA* family (Richmond and Somerville, 2000) (Figure 1.4). There are six *CSLD* genes in *Arabidopsis* genome, although *CSLD6* is thought to be a pseudogene and does not appear to be expressed (Bernal et al., 2008). *CSLD1* and *CSLD4* were highly expressed in pollen tubes, and plants display male sterility in the absence of *CSLD1* and *CSLD4* (Bernal et al., 2008). *CSLD2, CSLD3,* and *CSLD5* are broadly expressed in various vegetative tissues (Bernal et al., 2008). In *csld3* mutants, root hair elongation terminates soon after initiation of tip-restricted expansion, resulting in cell rupture and a hairless phenotype

(Favery et al., 2001). Shorter and deformed root hairs were observed in *csld2* mutants, indicating that both CSLD2 and CSLD3 are involved in the root hair elongation processes (Bernal et al., 2008). Despite their broad expression, *csld2*, *csld3*, and *csld2/3* double mutant plants were largely normal in other tissues and organs, suggesting non-essential activities in tissues and organs that develop primarily through diffuse growth and not tip-growth. However, *csld5* mutants did not affect root hair elongation, although they did display a moderate reduction in overall plant size (Bernal et al., 2007), which suggests a potential role of *CSLD5* in vegetative tissue development.

Although the phenotypes of *csld* mutants have been well studied, the function of the CSLD proteins has remained controversial. CSLD proteins were first identified to be highly expressed in pollen tubes of *Nicotiana alata* (Doblin et al., 2001). Due to the high degrees of sequence similarity to CESA proteins, CSLD proteins were initially proposed to synthesize cellulose in tip-growing pollen tubes (Doblin et al., 2001). Further studies confirmed the important roles of CSLD1 and CSLD4 in pollen, as *csld1* and *csld4* mutants are male sterile, presumably due to defects in pollen tube growth (Favery et al., 2001; Wang et al., 2001; Bernal et al., 2008). CSLD2 and CSLD3 also displayed essential roles for root hair elongation (Favery et al., 2001; Bernal et al., 2008). A recent study demonstrated that CSLD2, CSLD3, and CSLD5 all contributes to cell plate formation during plant cytokinesis (Gu et al., 2016). CSLD5 displays cell-cycle specific accumulation in dividing cells (Yoshikawa et al., 2013; Gu et al., 2016; Yang et al., 2016), while CSLD2 and CSLD3 protein levels are stable (Gu et al., 2016). Several different biosynthetic activities have been suggested for members of the *CSLD* family. Less xylan accumulation has been reported in the *csld5* mutants, which also displayed reduced pectin (homogalacturonan, HG) production and reduced growth in the absence of CSLD5 protein

(Bernal et al., 2007). Altered organization of xyloglucan and cellulose in root hairs has been reported in a weak mutant allele of *CSLD3*, in *rhd7* mutants (Galway et al., 2011). Recently, biochemical activities were described for CSLD2, CSLD3, and CSLD5 proteins expressed in isolated microsomal membranes from tobacco. It was reported that these CSLD proteins specifically utilized GDP-Mannose as substrates to form β-1,4-mannan polymers and displayed elevated mannan synthase activity (Verhertbruggen et al., 2011; Yin et al., 2011). On the other hand, previous research in our laboratory showed that a functional chimeric CSLD3 protein containing the catalytic domain of CESA6 could fully rescue the hairless defects in *csld3* mutants, indicating CSLD3 might provide a UDP-glucose-dependent β-1,4-glucan synthase activity (Park et al., 2011).

1.5 Statement of questions and attribution

With conflicting results about the nature of the polysaccharides synthesized by CSLD proteins, the initial goal of my thesis research was to develop genetic and biochemical approaches to definitively establish the catalytic activity of CSLD3. In addition, a second goal was to characterize to what extent the biochemical activities of other CSLD family members were conserved with those of CSLD3.

Chapter two describes the genetic and biochemical experiments carried out to establish whether a member of the CSLD family, CSLD3, is involved in the synthesis of β-1,4-mannan or β-1,4-glucan polysaccharides. I generated all the data presented in this chapter, which was used as the main body for a recent manuscript that has been published in *The Plant Cell*. I am listed as the co-first author in the primary position on this paper. In addition to the experiments I

performed, Gwangbae Bak, as the other co-first author, developed the *in vitro* protein expression, purification, and activity analysis system. This system provided us with the opportunity to perform additional *in vitro* experiments. He also provided essential data indicating the substrate preference of CSLD proteins, as well as the structural information about purified CSLD3 and CESA6 protein complexes. Tucker Burgin, one of the second authors, provided the computational modeling analysis of CSLD3 protein for the publication.

Chapter three describes experiments focused on determining the functional relationship between different CSLD proteins during cell wall synthesis. I generated all the data shown in this chapter. Several transgenic lines used in this chapter were constructed by a former Ph.D. student in the laboratory, Fangwei Gu. This chapter will form an individual publication to *Plant Physiology* where I will be listed as the first author, and Fangwei Gu will be listed as the second author.

The appendix chapter describes experiments studying the potential roles of Cornichon proteins in the trafficking of CSLD3 proteins to the plasma membrane. I performed all the experiments presented in this chapter. The data could potentially become the basis of future work or a publication, in which case I will be listed as an author.

In addition to the data present in this dissertation, I have also been listed as a second author in the following publication: [Gu, F., Bringmann, M., Combs, J.R., **Yang, J.**, Bergmann, D.C. and Nielsen, E., 2016. Arabidopsis CSLD5 functions in cell plate formation in a cell cycle-dependent manner. The Plant Cell, 28(7), pp.1722-1737]. I provided the split-ubiquitin based yeast two-hybrid analysis in this article, which indicates that CSLD5 could specifically interact with CCS52A2, while CESA3 and CSLA9 do not.

A

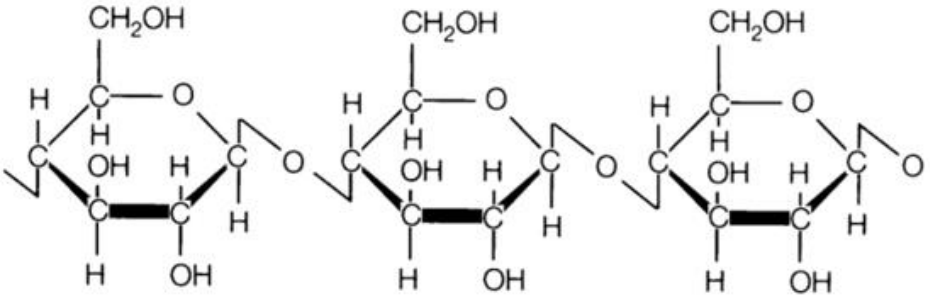

β-1,4-glucan chain

B

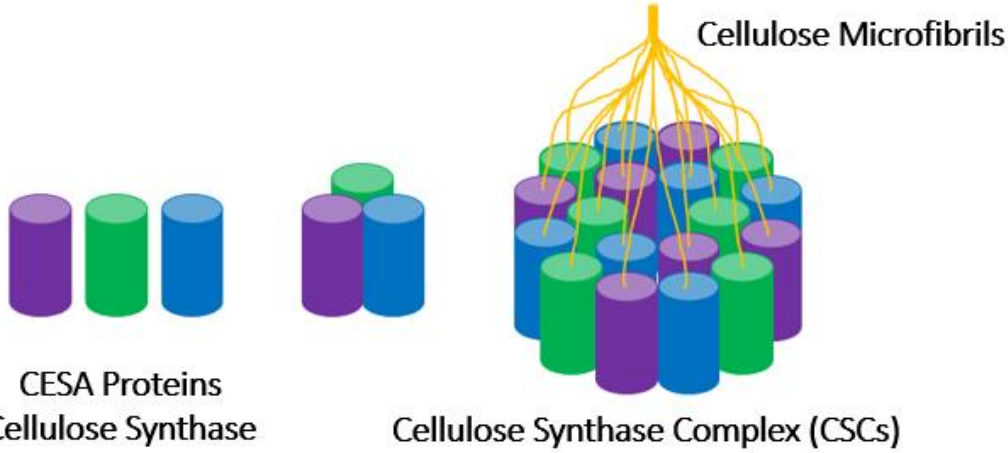

Figure 1.1. Schematic representations of the basic structure of Cellulose Synthase Complex (CSCs) and the formation of cellulose microfibrils.

(A) The basic chemical structure of a single β-1,4-glucan chain. (**B)** A simplified model representing the formation of a Cellulose Synthase complex (CSCs). Three different CESA isoforms (CESA1 in purple, CESA3 in green, and CESA6 in blue) are represented in different colors. The different isoforms of CESA proteins are associated together and form the subunit of one lobe within a six lobed rosette structure that makes up the higher-order CSC complex. 18 β-1,4-glucan chains synthesized in one complex will then associate through hydrogen bonds to form cellulose microfibrils (shown in yellow lines).

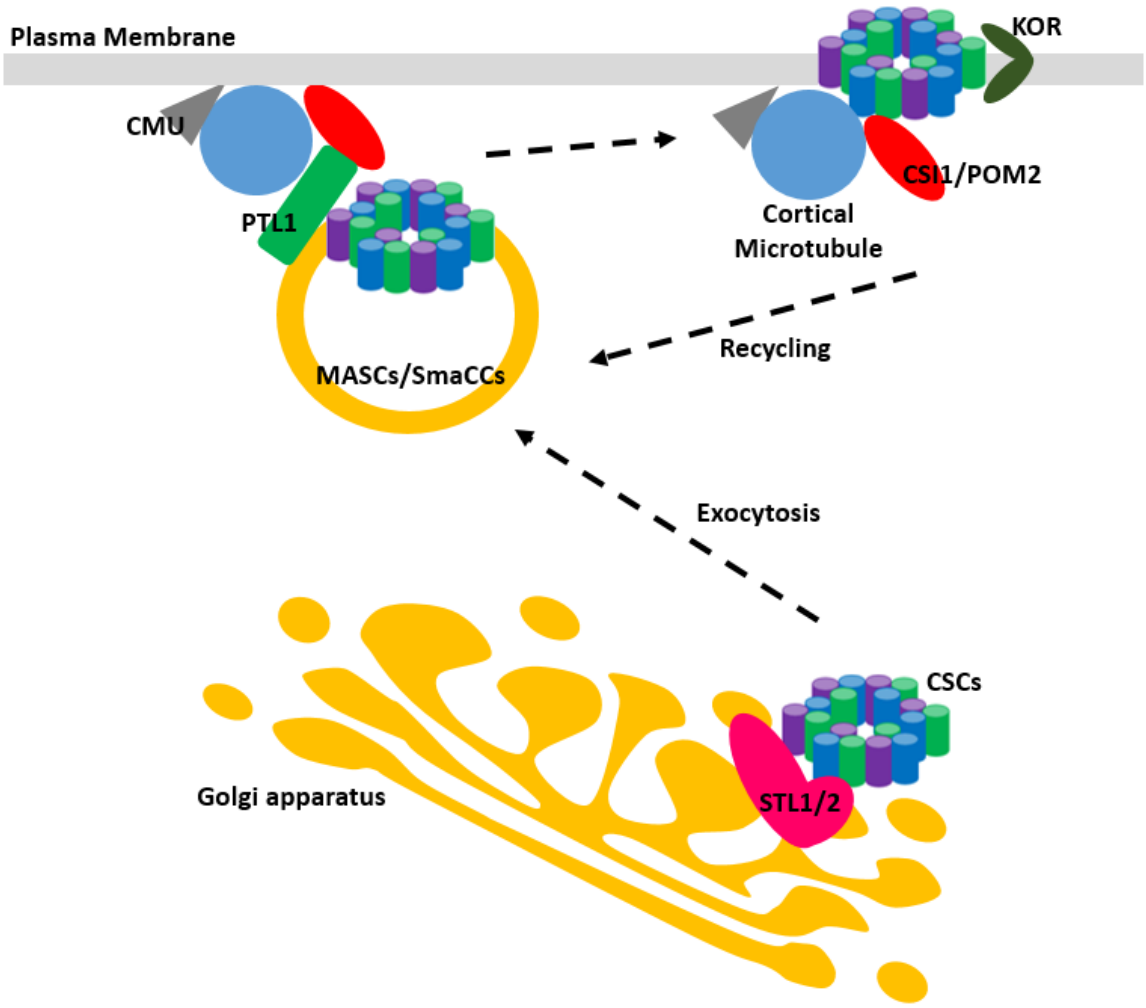
Plasma Membrane
KOR
CMU
CSI1/POM2
PTL1
Cortical
Microtubule
Recycling
MASCs/SmaCCs
Exocytosis
CSCs
Golgi apparatus
STL1/2

Figure 1.2. Model of CSC trafficking.

CSCs are assembled in the Golgi apparatus with the help of STL1/2. MASCs/SmaCCs are membrane trafficking compartments responsible for CSC delivery. CMU (grey triangle) functions to stabilize cortical microtubule (blue circle) attachment to the plasma membrane. CSI1 (red oval) binds to the microtubules as a marker to define the position of secretion. PTL1 (green rectangle) mediates the tethering of MASCs/SmaCCs to CSI1. STL1/2, STELLO1 and STELLO2. MASCs/SmaCCs, cortical microtubule-associated CESA compartments/small CESA compartments. CMU, cellulose synthase-microtubule uncouplings protein. CSI1, cellulose synthase-interactive protein 1. PTL1, PATROL1.

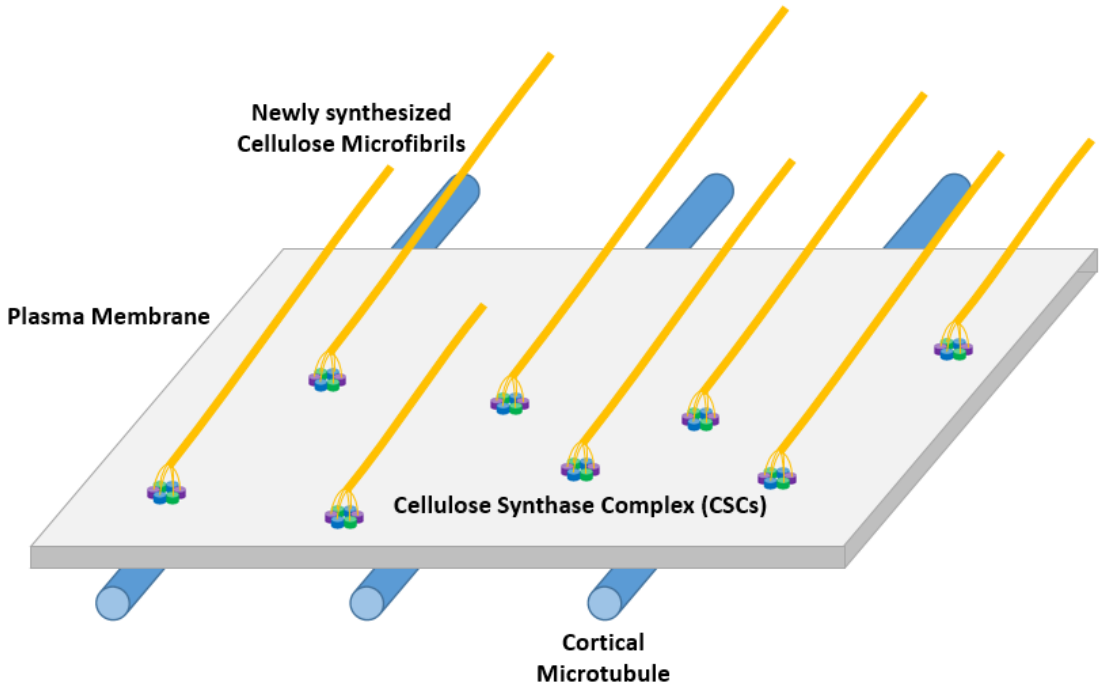

Figure 1.3. Polarized cell expansion during diffuse growth is controlled by the orientation of newly synthesized cellulose microfibril deposition.

Individual β-1,4-glucan polymers synthesized by individual CESA components of integral membrane CSC complexes in the plasma membrane assemble into cellulose microfibrils (yellow lines). The orientation of cellulose microfibrils is controlled by the interaction of CSCs with cortical microtubule arrays at the cytoplasmic face of the plasma membrane. Plant cells control cell expansion direction by regulating the orientation of the cortical microtubule arrays.

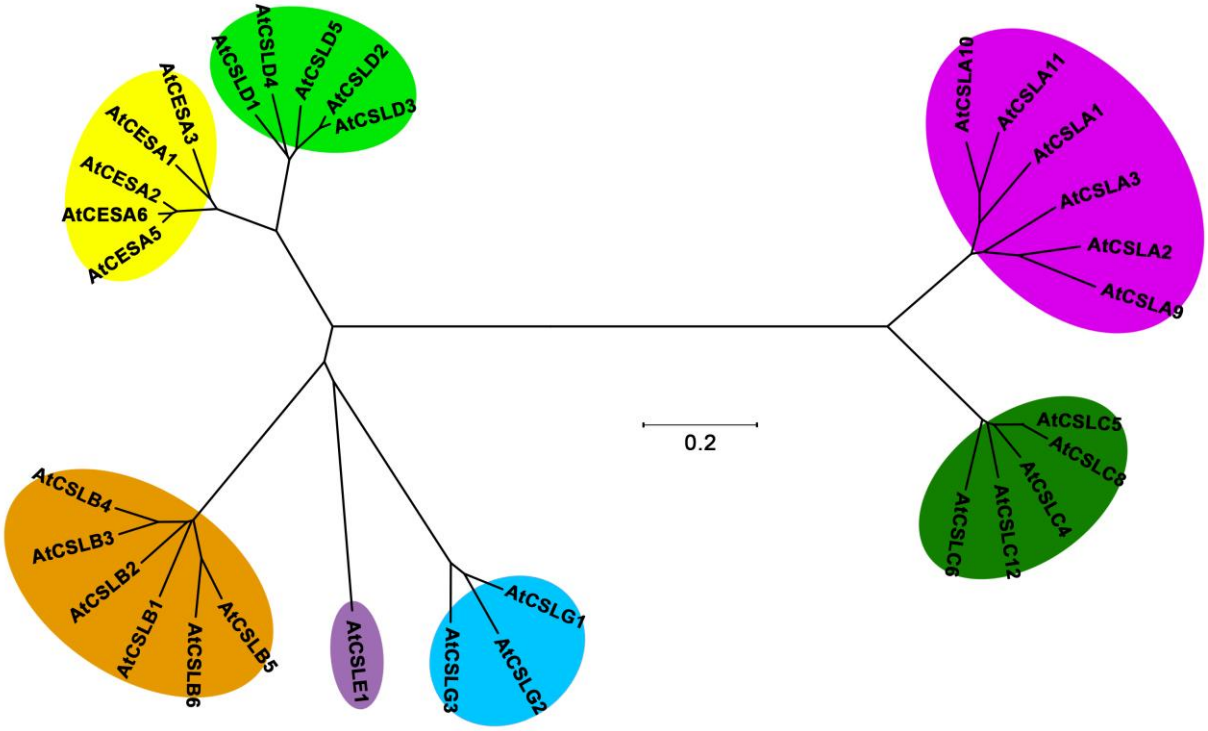
AtCSLD4
AtCSLD1
AtCSLD5
AtCSLD2
AtCSLD3
AtCESA3
AtCESA1
AtCESA2
AtCESA6
AtCESA5
AtCSLA10
AtCSLA11
AtCSLA1
AtCSLA3
AtCSLA2
AtCSLA9
0.2
AtCSLC5
AtCSLC8
AtCSLC4
AtCSLC12
AtCSLC6
AtCSLB4
AtCSLB3
AtCSLB2
AtCSLB1
AtCSLB6
AtCSLB5
AtCSLE1
AtCSLG1
AtCSLG2
AtCSLG3

Figure 1.4. The phylogenetic tree of *CSL* superfamily in *Arabidopsis*.

Unrooted, bootstrapped (n = 1000 trials) neighbor-joining tree of the *Arabidopsis CSL* superfamily was constructed using MEGA7 (Kumar et al., 2016). Bootstrap values above 600 are indicated next to the relevant node. The scale bar represents the number of amino acid substitutions per site. CSL genes in the *Arabidopsis* genome are grouped into seven subfamilies based on the alignment of full-length protein sequences. *CESA (cellulose synthase), CSLA, CSLB, CSLC, CSLD, CSLE*, and *CSLG* subfamilies are boxed with different background colors. Based on the branches of this phylogenetic tree, the sequences of CSLD proteins are more similar to CESAs, not CSLAs. At, *Arabidopsis*.

Chapter 2 Biochemical and Genetic Analysis Identify CSLD3 as a β-1,4-glucan Synthase that Functions during Plant Cell Wall Synthesis

2.1 ABSTRACT

Plant cell walls are mainly composed of cellulose, hemicellulose, and pectin. The synthesis and deposition of these polysaccharides constrain plant cell expansion and ultimately define the size and shape of plant cells. Cellulose microfibrils are considered to be the major load-bearing components in plant cell walls. During diffuse growth, ordered arrays of cellulose microfibrils are directly synthesized by plasma membrane-localized CESA proteins. These CESA proteins are organized into multimeric complexes called cellulose synthase complexes (CSCs), which are integral to controlling the directionality of cell expansion. However, during tip-growth, occurring in root hairs and pollen tubes, or *de novo* formation of cell plates during plant cytokinesis, newly synthesized cell wall polysaccharides are only deposited in a restricted region. Members of cellulose synthase-like D (CSLD) protein family specifically localize to apically-localized plasma membranes in these cells and synthesize polysaccharides at the growing tips. However, while these CSLD cell wall synthases are essential, the nature of the

polysaccharides generated by CSLD proteins has remained elusive. Here we use genetic and biochemical approaches to characterize the catalytic activity of one member of the CSLD family, CSLD3. Genetic complementation of a *cesa6* mutant with a chimeric CESA6 protein containing a CSLD3 catalytic domain demonstrated that the CSLD catalytic domains can successfully generate β-1,4-glucan polymers for cellulose synthesis. Time-lapse fluorescence microscopy demonstrated that these CESA6-CSLD3 chimeric proteins assembled into CSC complexes with similar mobility as CESA6-labeled complexes in hypocotyl cells. Proteoliposomes containing purified, detergent-solubilized CSLD3 and CESA6 proteins could specifically utilize UDP-glucose as enzymatic substrates and synthesize products that are only sensitive to endo-β-1,4-glucanase. Taken together, these data strongly support the conclusion that CSLD3 represents a UDP-glucose-dependent β-1,4-glucan synthase.

2.2 INTRODUCTION

Cellulose is one of the most abundant organic polymers in nature and is the principal component of the plant cell wall, providing most of its tensile strength (Baskin, 2005; Cosgrove, 2005). Cellulose microfibrils contain multiple β-1,4-glucan chains that associate via intermolecular hydrogen bonds and are synthesized by large, membrane-localized complexes called "rosette complexes" (Baskin, 2005; Cosgrove, 2005). In *Arabidopsis*, CESA proteins interact to form rosette subunits, and six of these subunits then assemble into multimeric rosette complexes, often referred to as cellulose synthase complexes (CSCs) (Kimura et al., 1999). CSCs contain several CESA subunits, each thought to be capable of synthesizing β-1,4-glucan polysaccharides. *Arabidopsis* contains ten *CESA* genes of which the proteins encoded by at least

three (CESA1, CESA3, and CESA6) are required for cellulose-synthesis during primary cell wall formation (Arioli et al., 1998; Fagard et al., 2000; Scheible and Pauly, 2004). While earlier models suggested each rosette subunit may contain six CESA proteins, recent studies combining ultrastructural analysis and computer-modeling of plant CESAs using bacterial cellulose synthase structures have proposed rosette subunits may contain as few as three CESAs each (Nixon et al., 2016; Vandavasi et al., 2016). Furthermore, *in vitro* reconstitution of cellulose synthase activity was observed in proteoliposomes containing only *Pp*CESA8 (Purushotham et al., 2016; Cho et al., 2017) highlighting that our understanding of the composition of functional cellulose synthase rosette complexes remains incomplete.

In addition to cellulose and pectin, primary cell walls of terrestrial plants also contain hemicellulosic polysaccharides, such as xyloglucan and β-1,4-mannans (Baskin, 2005; Cosgrove, 2005). Members of the *Cellulose Synthase-Like (CSL)* family are family 2 glycosyltransferases (GT2s) that synthesize glycan backbones of cellulose and most hemicellulosic polysaccharides, with the exception of β-1,4-xylan (Scheible and Pauly, 2004; Liepman et al., 2010; Smith et al., 2017). Members of the CESA superfamily have been resolved into 6 lineages in *Arabidopsis*, including the CESAs and six cellulose synthase-like (CSL) clades: CSLA, CSLB, CSLC, CSLD, CSLE, and CSLG (Richmond and Somerville, 2000). *CSLA*s were shown to encode proteins that synthesize β-1,4-mannans, catalyzing the formation of β-1,4-mannan and glucomannan *in vitro* when heterologously expressed in insect cells (Dhugga et al., 2004; Liepman et al., 2005). At least one member of the *CSLC* family has been implicated in the synthesis of the β-1,4-glucan backbone of xyloglucan in the Golgi (Cocuron et al., 2007), and other CSLCs have been localized to the plasma membrane, where they may synthesize non-crystalline β-1,4-glucan (Dwivany et al., 2009). Members of the *CSLF*, *CSLH and CSLJ* families, which are largely

present only in cereals and grasses, predominantly synthesize mixed-linkage (1,3;1,4)-β-glucans (Burton et al., 2006; Doblin et al., 2009; Little et al., 2018). Recently, two members of the *CSLF* family from *Hordeum vulgare* (*Hv*CSLF3 and *Hv*CSLF10) have been shown to synthesize a novel β-1,4-linked glucoxylan polymer, indicating that a single CSL family can possess multiple, not single, carbohydrate synthetic activities (Little et al., 2019). However, the functions of *CSLDs* and the other *CSL* families (CSLB, CSLE, CSLG) remain poorly characterized (Scheible and Pauly, 2004).

CSLD proteins were initially proposed to synthesize cellulose in tip-growing pollen tubes, consistent with the high degrees of sequence similarity and overall domain organization CSLDs share with CESAs (Doblin et al., 2001). Confirming an important role in tip-restricted cell expansion, *Arabidopsis CSLD2* and *CSLD3* genes are required for proper root hair growth, and *csld1* and *csld4* mutants are male sterile, presumably due to defects in pollen tube growth (Favery et al., 2001; Wang et al., 2001; Bernal et al., 2008). The functional roles of CSLD enzymes are not restricted solely to cells undergoing tip-restricted expansion, with CSLD2, CSLD3, and CSLD5 all participating in the construction of newly-forming cell walls during plant cytokinesis (Gu et al., 2016), and CSLD5 also displays cell-cycle specific accumulation in dividing cells (Yoshikawa et al., 2013; Gu et al., 2016; Yang et al., 2016). Cellulose polysaccharide epitopes have been observed in tip-growing root hairs and pollen tubes (Park et al., 2011; Chebli et al., 2012), and in newly-forming cell plates (Miart et al., 2014), although the predominant cell wall polysaccharide in pollen and cell plates has been generally thought to be the β-1,3-glucan callose (Meikle et al., 1991; Samuels et al., 1995; Ferguson et al., 1998; Chen and Kim, 2009; Drakakaki, 2015). Several different biosynthetic activities have been suggested for members of the CSLD family. In *Arabidopsis*, CSLD5 insertional mutants accumulated less

xylan in stems and had reduced pectin (Bernal et al., 2007). In a weak mutant allele of CSLD3, *rhd7*, the organization of xyloglucan and cellulose was altered in root hairs (Galway et al., 2011). Microsomal membranes isolated from tobacco over-expressing *A. thaliana* CSLD2, CSLD3, and CSLD5 proteins were shown to contain elevated mannan synthase activity, specifically utilizing GDP-mannose as an activated nucleotide-sugar donor (Verhertbruggen et al., 2011; Yin et al., 2011). Further, examination of cell wall epitopes in newly-forming cell plates in shoot apical meristems in *csld5* mutants displayed altered β-1,4-mannan accumulation (Yang et al., 2016). Alternatively, a functional YFP-CSLD3 fusion protein localized to apical plasma membranes in the tips of growing *Arabidopsis* root hairs, and genetic chimeras where the CSLD3 catalytic region (residues 340–921) was replaced with the corresponding CESA6 catalytic domain rescued root hair defects in *csld3* mutant plants, supporting a UDP-glucose dependent cellulose synthase-like activity for CSLD3 (Park et al., 2011).

Here we show, using a combination of genetic, biochemical and cell biology approaches, that a Citrine-CESA6 chimeric fusion protein containing the catalytic domain of CSLD3 integrates into plasma membrane-localized CSCs and can fully rescue both the hypocotyl elongation and cellulose accumulation defects in the *prc1-1* (cesa6 null) mutant. In addition, we show that proteoliposomes containing purified CESA6 and CSLD3 utilize UDP-glucose to synthesize cellulose. Our results reveal that CSLD3 functions as a β-1,4-glucan synthase in plant cell wall synthesis.

2.3 RESULTS

2.3.1 A genetic chimeric CESA6 protein containing the CSLD3 catalytic domain quantitatively restores hypocotyl elongation defects observed in *cesa6* mutants

CESA and CSLD proteins share overall membrane topology and maintain high degrees of sequence identity, especially in the central domain where critical catalytic residues are absolutely conserved (Figure 2.1A; (Morgan et al., 2013; Sethaphong et al., 2013; Slabaugh et al., 2014)). Previous research in the laboratory demonstrated that a fluorescently-tagged chimeric fusion protein in which the CSLD3 catalytic region was replaced with the corresponding CESA6 catalytic domain was able to quantitatively rescue *kjk-2* (*csld3* null) root hair defects (Park et al., 2011). While these results indicated that the catalytic domain of CESA6 could functionally replace CSLD3 domain in root hair cells during tip growth, it's unclear whether CSLD proteins have the ability to organize into higher-order complex and synthesize β-1,4-glucan chains what further assemble into cellulose microfibrils as CESA proteins. To address this, I constructed a Citrine-tagged CESA6 chimeric protein containing the CSLD3 catalytic domain (Citrine-CESA6:D3CD) under the endogenous CESA6 promoter sequences (Figure 2.1A). The dramatic hypocotyls and root expansion defects observed in *cesa6* (*prc1-1*) mutant plants (Figure 2.1B, C) indicated that the cells are unable to support the rapid diffuse growth in the absence of CESA6 protein. In the *cesa6* (*prc1-1*) mutant plants expressing the Citrine-CESA6:D3CD protein, both dark-grown hypocotyl elongation defects (Figure 2.1B, D) and root elongation defects were quantitatively restored either in the dark (Figure 2.1B,D) or in light (Figure 2.1C, E), indicating CSLD3 catalytic domain sequences could functionally replace CESA6 catalytic domain sequences in the CESA6 primary cell wall cellulose synthase protein. This result suggests that

the nature of polysaccharides synthesized by the CSLD is the same as the ones found in cellulose microfibrils.

I also generated stably transformed *Arabidopsis* lines expressing Citrine-CESA6:D3CD chimeric protein under the cauliflower mosaic virus promoter (*CaMV 35S*), a constitutively expressed promoter. Interestingly, the transgenic plant lines displayed a tissue-specific restoration. The root elongation defects observed in *prc1-1* mutant under both dark (Figure 2.2A, C) and light (Figure 2.2B, D) grown conditions were partially rescued, while no significant difference was detected in hypocotyl tissues compared to *prc1-1* mutant (Figure 2.2C, D). These results indicated the *35S* promoter might not maintain a consistent expression level in root and hypocotyl tissues. To test this hypothesis, the distribution pattern of Citrine-CESA6:D3CD proteins was recorded by spinning-disk confocal microscopy using three-day-old, dark-grown seedlings. Fluorescent Citrine-CESA6:D3CD signals were observed at high levels mainly in the root tissues, while they displayed much lower levels of fluorescence in hypocotyl tissues, consistent with the degrees of rescue earlier observed for hypocotyl and root elongation (Figure 2.3A). The expression level differences were further confirmed using RT-PCR analysis. The relative expression level of CESA6:D3CD was qualitatively much higher in root tissues than those in hypocotyl tissues (Figure 2.3B). Taken together, these results suggest that the degree of defects rescue is dependent on the levels of expression and accumulation of these chimeric constructs in the root and hypocotyl tissues.

2.3.2 Citrine-CESA6:D3CD chimeric proteins integrate into CSC complexes with other CESA proteins and display similar mobility as CSCs containing YFP-CESA6

In plants, CESAs organize into multimeric CSCs that can be visualized as discrete fluorescent particles that display linear motility within the plasma membrane (Paredez et al., 2006; Desprez et al., 2007). To determine whether Citrine-CESA6:D3CD chimeric proteins were present in motile CSCs, we performed time-lapse laser-confocal microscopy and investigated CSC motility in time-averaged projections in plants stably expressing either YFP-CESA6 (Figure 2.4A-C) or Citrine-CESA6:D3CD (Figure 2.4D-F). CSC complexes trajectories were observed for both YFP-CESA6 (Figure 2.4C; blue lines in right panel) and Citrine-CESA6:D3CD chimera proteins (Figure 2.4F; red lines in right panel). Speeds calculated for YFP-CESA6 containing CSCs (Figure 2.4G, blue bars; 10 cells, 7 seedlings, 419 particles) were virtually indistinguishable from Citrine-CESA6:D3CD containing CSCs (Figure 2.4D, red bars; 11 cells, 6 seedlings, 408 particles) at 356.2 +/- 49.8 nm/min and 368.4 +/- 45.5 nm/min, respectively. While these velocities are somewhat faster than the speeds of ~250–300 nm/min reported in several previous studies (DeBolt et al., 2007; Vain et al., 2014; Watanabe et al., 2018), others have reported higher particle velocities of ~350–400 nm/min (Paredez et al., 2006; Gutierrez et al., 2009; Li et al., 2012; Lei et al., 2014), which are consistent with the velocities we detected. These results indicate that Citrine-CESA6:D3CD chimera proteins are capable of integrating into primary cell wall CSCs, and based on their similar speeds, display similar cell wall biosynthesis characteristics.

Earlier genetic studies indicated that at least three distinct CESA proteins are required for cellulose synthesis during primary cell wall formation, and therefore CSCs involved in primary cell wall cellulose synthesis are thought to assemble with both essential cellulose synthases,

CESA1 and CESA3, and at least one of either CESA6 or CESA2/5/9 (Arioli et al., 1998; Fagard et al., 2000; Scheible and Pauly, 2004). To test whether motile CSCs containing Citrine-CESA6 and Citrine-CESA6:D3CD also contain other CESAs implicated in cellulose synthesis in primary cell walls, transgenic *Arabidopsis* expressing these fluorescent CESA6 fusions as well as GFP-CESA3 (Desprez et al., 2007) were generated and analyzed by laser-scanning confocal microscopy. Fluorescence signals specific for either Citrine/YFP or GFP (Figure 2.6) were collected simultaneously from plants expressing GFP-CESA3 and either YFP-CESA6 (Figure 2.5A) or Citrine-CESA6:D3CD (Figure 2.5C). Significant overlap of GFP-CESA3 (Figure 2.5A, C; green), and either YFP-CESA6 (Figure 2.5A; magenta) or Citrine-CESA6:D3CD (Figure 2.5C; magenta) signals were observed. When relative fluorescence intensity values for individual CSC complexes were examined, significant coincident fluorescence could be observed for GFP-CESA3 (Figure 2.5B, D; green) and either YFP-CESA6 (Figure 2.5B; magenta) or Citrine-CESA6:D3CD (Figure 2.5D; magenta), indicating that both fluorescently-tagged CESA6 and CESA6:D3CD proteins occur in multimeric CSCs with other CESA proteins.

2.3.3 The quantitative rescue of *cesa6* defects requires the catalytic activity of YFP-CESA6 and Citrine-CESA6:D3CD chimeric protein

While these results supported the integration of Citrine-CESA6:D3CD chimeras into CSCs and rescue of *prc1-1* mutant phenotypes, they did not directly address whether the Citrine-CESA6:D3CD chimera was catalytically active, or simply allowed for assembly of complexes with non-functional subunits. To address this directly, we mutated a conserved TED motif responsible for formation of β-1,4-glucosidic bonds in the extending glucan polymers (Morgan et

al., 2013; Morgan et al., 2016), replacing both aspartic acid and glutamic acid with alanine residues. Neither stably transformed Citrine-CESA6-TAA, nor Citrine-CESA6:D3CD-TAA plants were able to fully rescue dark-grown hypocotyl and root elongation defects (Figure 2.7A, B, and Figure 2.8). Interestingly, while Citrine-CESA6:D3CD-TAA expressing plants were indistinguishable from *prc1-1* mutants, we did observe a small, statistically significant increase in dark-grown hypocotyl length in seedlings expressing the Citrine-CESA6-TAA protein (~15%; Figure 2.7A, B). Quantification of crystalline cellulose in these seedlings using the Updegraff method confirmed that expression of both YFP-CESA6 and Citrine-CESA6:D3CD restored crystalline cellulose content to wild-type levels (Figure 2.7C), while cellulose content of Citrine-CESA6:D3CD-TAA seedlings was indistinguishable from that of the *prc1-1* mutant background. Interestingly, consistent with earlier phenotypic analysis (Figure 2.7A, B), we also observed a small, statistically-relevant increase in crystalline cellulose content in the Citrine-CESA6-TAA expressing seedlings (Figure 2.7C). Taken together, these results strongly support the interpretation that the quantitative rescue of *prc1-1* mutant phenotypes and chemotypes observed in seedlings expressing YFP-CESA6 and Citrine-CESA6:D3CD chimeras requires the catalytic function of a β-1,4-glucan synthase.

While the introduction of point mutations in both Citrine-CESA6-TAA and Citrine-CESA6:D3CD-TAA mutants are unlikely to affect overall folding of these proteins, we wanted to address whether these mutant proteins also associated into CSCs in these transgenic seedlings and whether these "catalytically dead" constructs displayed any differences in either CSC trafficking or dynamics in these plants. As with their wild-type counterparts, both Citrine-CESA6-TAA (Figure 2.10A-C) and Citrine-CESA6:D3CD-TAA (Figure 2.10D-F) proteins were incorporated into discrete CSC complexes in the plasma membrane of *Arabidopsis* hypocotyl

cells at generally similar densities as observed for catalytically active versions of these proteins (Figure 2.9 and Figure 2.10). To assess whether either the presence of a CSLD3 catalytic domain in chimeric proteins, or TAA point mutations affecting the assembly and delivery of CESA6-containing CSCs to plasma membranes, we examined rates at which fluorescently-labeled CSCs appeared in a photobleached plasma membrane region for CSC complexes containing YFP-CESA6, Citrine-CESA6:D3CD, Citrine-CESA6-TAA, and Citrine-CESA6:D3CD-TAA (Figure 2.9A-D; red boxes). For all constructs we observed similar rates of delivery of new, fluorescently-labeled CSCs, indicating that the assembly of CESA6-containing CSCs and their delivery to plasma membranes were not significantly affected (Figure 2.9E-F). However, when we examined CSC motility events, we observed that CSCs tracks containing Citrine-CESA6-TAA were markedly shorter than those containing YFP-CESA6 (Figure 2.10A-C; green lines in 5C right panel), and CSC complexes containing Citrine-CESA6:D3CD-TAA were virtually immobile (Figure 2.10D-F; red lines in 5F right panel). Speeds calculated for CSC motility events for complexes containing TAA point mutations in their catalytic domains were also significantly slower than their catalytically active counterparts, with Citrine-CESA6-TAA particle speed reduced to 207.2 +/- 63.7 nm/min (Figure 2.10G; green bars; 6 cells, 6 seedlings, 283 particles), and Citrine-CESA6:D3CD-TAA to 142.3 +/-87.5 nm/min (Figure 2.10G; red bars; 6 cells, 6 seedlings, 253 particles). All together, these results confirm that "catalytically-dead" Citrine-CESA6-TAA and Citrine-CESA6:D3CD-TAA subunits successfully integrated into CSCs and are delivered to plasma membranes in rates largely indistinguishable from their catalytically-active counterparts. However, CSCs containing these TAA mutant subunits show distinctly slower speeds and dramatically shorter trajectories, consistent with the impaired rescue of *prc1-1* phenotypes and cellulose deposition observed earlier (Figure 2.7).

2.3.4 Detection of β-1,4-glucan polysaccharides in proteoliposomes reconstituted with purified His-CSLD3 and His-CESA6.

While the *in vivo* rescue of cell wall defects in the CESA6 mutant *prc1-1* is consistent with a UDP-Glc dependent β-1,4-glucan synthase activity for CSLD proteins, earlier studies of isolated *N. benthamiana* microsomal membranes over-expressing CSLD proteins identified increased GDP-Man dependent β-1,4-mannan synthase activities (Verhertbruggen et al., 2011; Yin et al., 2011). To directly test whether CSLD proteins could utilize UDP-Glc, proteoliposomes containing purified His-CSLD3 were treated with ultrapure UDP-Glc as substrates. During the glycosyltransferase reaction, the UDP is released as side products and can be measured to quantify the enzyme activity. The catalytic activity of CSLD3 was assessed in the presence of 1 mM Mn2+ and 1 mM Mg2+, and UDP-Glc (Figure 2.11A). Saturable UDP-forming activities were observed for CSLD3 protein with an apparent Km value at 65 mM, consistent with values recently reported for reconstituted PttCESA8 (~30 mM; (Purushotham et al., 2016)), and significantly lower than values determined for the bacterial cellulose synthase, RsBCSA (~500 mM; (Omadjela et al., 2013)).

To determine the nature of the polysaccharides synthesized by CESA6, CSLD3, and CSLA9, proteoliposomes containing purified CESA6, CSLD3, CSLA9, and Ni^{2+}-agarose eluted proteins from an empty vector control were incubated with UDP-Glc, Mg^{2+} and Mn^{2+}, and a UDP-[^{3}H]-Glc as a tracer. Time-dependent accumulation of [^{3}H]-Glc containing reaction products were observed for both CESA6 and CSLD3 upon sedimentation and subsequent purification of insoluble reaction products by paper chromatography (Figure 2.11B), but not for

CSLA9 or the empty vector control proteoliposomes (Figure 2.11C). To determine whether *in vitro*-synthesized material represented β-1,4 glucan, these reaction products were incubated with glucanases specifically degrading β-1,3–linked or β-1,4 –linked glucans. Consistent with the formation of cellulose, both CESA6 and CSLD3 reaction products were selectively degraded only by a β-1,4–specific glucanase, and were largely resistant to treatment with a β-1,3-specific glucanase (Figure 2.11C). Although fibrillar structures, structurally similar to cellulose microfibrils, were observed in recent reconstitution experiments with plant CESAs (Purushotham et al., 2016; Cho et al., 2017), we were unable to detect similar fibrils in reconstituted proteoliposome fractions with either CESA6 or CSLD3. Taken together, these results strongly support the conclusion that CSLD3 utilizes UDP-Glc as a substrate and synthesizes β-1,4-glucan.

2.4 DISCUSSION

Plant cells are surrounded by a load-bearing cell wall comprised of cellulose, hemicelluloses, pectins, and a variety of cell wall proteins (Cosgrove, 2005). Cellulose synthases, or CESA proteins, are contained within a larger superfamily of Cellulose Synthase-Like, or CSL proteins (Richmond and Somerville, 2000). While a number of different biosynthetic activities have been proposed for members of the CSLD family of glycan synthases (Doblin et al., 2001; Bernal et al., 2008; Park et al., 2011; Verhertbruggen et al., 2011; Yin et al., 2011), here we present multiple lines of evidence that support the classification of members of the CSLD family as β-1,4-glucan synthases. Using a genetic rescue approach, we demonstrated that a CESA6 protein chimera in which the CESA6 catalytic domain is replaced with CSLD3 catalytic sequences (CESA6:D3CD) fully rescues *cesa6* mutant alleles (Figure 2; Figure 4C). We

had previously reported that a CSLD3 protein chimera containing a CESA6 catalytic domain could rescue *csld3* null mutant phenotypes consistent with CSLD3 being a β-1,4-glucan synthase (Park et al., 2011). However, it remained unclear whether CSLD proteins assembled into higher-order protein complexes, or if β-1,4-glucan polymers generated by CSLD enzymes could produce microfibrillar cellulose. YFP-CESA6 has been observed to organize into punctate structures similar to CSCs (Paredez et al., 2006; Gutierrez et al., 2009), and loss of CESA6 activity in the *prc1* null mutant results in plants that produce less crystalline cellulose (Fagard et al., 2000; MacKinnon et al., 2006). Quantitative genetic rescue of *prc1* mutant phenotypes by Citrine-CESA6:D3CD chimeras (Figure 2.1) and restoration of crystalline cellulose content back to wild-type levels (Figure 2.7C) strongly support the conclusion that the CSLD3 catalytic domain synthesizes β-1,4-glucan. These CESA6:D3CD chimeras integrate into CSCs (Figure 2.4) that also contain GFP-CESA3 (Figure 2.5), migrate along cortical microtubule tracks with similar speeds to YFP-CESA6 containing CSCs (Figure 2.4), and must be catalytically active in order to fully rescue *cesa6* mutant phenotypes (Figures 2.7, 2.8).

The fact that Citrine-CESA6:D3CD chimeras co-localized and appear to be integrated into CSCs and were delivered to plasma membranes at similar rates as YFP-CESA6 (Figure 2.9), indicates that the amino-terminal and transmembrane domains of CESA6 are likely more important for assembly of these proteins into primary cell wall CSCs and their subsequent subcellular targeting. While it is somewhat surprising that wholesale replacement of the ~70 kDa CESA6 cytosolic catalytic domain with CSLD3 sequences does not affect this assembly, this may perhaps be mitigated because the CESA6 position in primary cell wall CSCs may alternatively be occupied by CESA2 and CESA5 (Desprez et al., 2007). The presence of plant-conserved (PCR) and class-specific (CSR) regions has been proposed to play important roles in

the assembly of plant cellulose synthases into primary and secondary cell wall specific CSCs (Vergara and Carpita, 2001; Scavuzzo-Duggan et al., 2018). At least in the case of integration of the Citrine-CESA6:D3CD into primary CSCs, the absence of CESA6-specfic PCR and CSR domains does not appear to interfere with their assembly into CSCs, although the presence of similar PCR and CSR sequences in CSLDs may perhaps indicate the general ability of CSLD proteins to also assemble into higher-order protein complexes. Similarly, the absence of the cytosolic CESA6 catalytic domain does not appear to negatively affect the movement of these CSCs along characteristic linear tracks (Figure 2.4), indicating that replacement with the CSLD3 sequences does not significantly alter the interaction of these CSCs with Cellulose-Microtubule Uncoupling (CMU; (Liu et al., 2016)) and Cellulose-Synthase-Interacting proteins (CSI1/POMPOM2 and CSI3; (Bringmann et al., 2012; Li et al., 2012; Lei et al., 2013; Lei et al., 2014)), which mediate interactions between cortical microtubules and CSCs.

While rescue of hypocotyl growth defects and accumulation of crystalline cellulose required a catalytically active cytosolic domain in either YFP-CESA6 or Citrine-CESA6:D3CD proteins (Figure 2.7), replacement of glutamate and aspartate residues in the catalytic TED motif with alanines (TAA) did not appear to affect the assembly of CSCs or their delivery to the plasma membrane. However, motility of Citrine-CESA6-TAA and Citrine-CESA6:D3CD-TAA containing CSCs along microtubule tracks were significantly affected, with the speed of Citrine-CESA6-TAA containing CSCs reduced by roughly one-third, and Citrine-CESA6:D3CD-TAA CSCs by slightly more (Figure 2.10). These reduced speeds are consistent with the proposal that microtubule-associated motility is primarily driven by biosynthetic activity and the elongation and assembly of β-1,4-glucan polymers into cellulose microfibrils (Paredez et al., 2006), with a loss of catalytic activity in the CESA6 positions resulting in an associated reduction of ~1/3 of

the CSC velocity. Interestingly, in addition to reduced velocities, we also noted a reduction in the overall length of linear tracks in CSCs containing TAA mutant subunits, perhaps indicating that "pausing" caused by catalytically-inactive CESA6 may increase the chance of disengagement with cortical microtubules and/or endocytosis from the plasma membrane.

Based on genetic reconstitution experiments, as well as biochemical reconstitution of CSLD3 activity *in vitro*, the catalytic domain of CSLD3 appears to prefer UDP-Glc. These studies further support the synthesis of β-1,4-glucan polymers that can integrate into crystalline cellulose. Both of these activities are consistent with a β-1,4-glucan synthase activity for CSLD3, which we directly confirmed using *in vitro* reconstitution experiments with purified CESA6, CSLD3, and CSLA9 proteins (Figure 2.11). These results are also consistent with the recent determination that overexpression of a *Gossypium hirsutum* CSLD3 (*Gh*CSLD3) is able to rescue cell expansion and cell wall integrity defects in *Arabidopsis prc1-1* mutants (Hu et al., 2019).

A UDP-Glc substrate specificity for CSLD3 would appear to be inconsistent with recent descriptions of GDP-Man dependent synthesis of β-1,4-mannan by CSLD proteins (Verhertbruggen et al., 2011; Yin et al., 2011). However, it should be noted that mannan synthesis in these studies was assessed in plant membranes overexpressing CSLD proteins that contained endogenous β-1,4-mannan activity, and that the levels of β-mannan synthesis reported were significantly lower than those observed for GDP-Man dependent mannan synthesis described for CSLA proteins (Liepman et al., 2005; Goubet et al., 2009). Both CSLD3 and CESA6 utilized UDP-Glc to synthesize β-1,4-glucan and did not appear to require the presence of either cellobiose or sitosterol-glucose primers (Lai-Kee-Him et al., 2002; Peng et al., 2002), similar to *in vitro* reconstituted cellulose synthase activities recently described for both bacteria

(Omadjela et al., 2013) and plants (Purushotham et al., 2016; Cho et al., 2017). *In vivo*, cellulose synthase activities are thought to require assembly of hetero-oligomeric complexes with at least three distinct plant CESAs (Taylor et al., 2003; Somerville, 2006; Desprez et al., 2007; Persson et al., 2007). However, consistent with earlier *in vitro* reconstitution studies with purified hybrid aspen PttCESA8, or moss (*Physcomitrella patens*) PpCESA8 (Purushotham et al., 2016; Cho et al., 2017), we observed accumulation of β-1,4-glucan in membranes containing only CESA6 proteins, suggesting that at least *in vitro* activities may not require assembly of hetero-oligomers. It should be noted, however, that the specific activity we report in reconstituted CESA6 proteoliposomes is significantly lower than those reported *in vivo* (Reiss et al., 1984).

Why might land plants have evolved two distinct families of β-1,4-glucan synthases that can assemble into higher-order complexes? One of the distinguishing features of cellulose deposition in plant lineages is the organization of cellulose into paracrystalline microfibrils, whose deposition is associated with the orientation of an underlying array of cortical microtubules (Ledbetter and Porter, 1963). Indeed, the delivery (Crowell et al., 2009; Gutierrez et al., 2009), and migration upon cortical microtubules (Paredez et al., 2006; Desprez et al., 2007) appears to be intimately regulated by association of plasma membrane CSCs with a number of microtubule-associated proteins (Bringmann et al., 2012; Li et al., 2012; Lei et al., 2013; Liu et al., 2016). Earlier analysis of the CESA and CSLD gene families revealed that the CSLD genes display more diversity in their intron/exon organization, perhaps indicating that these are the older evolutionary group (Richmond and Somerville, 2001; Hazen et al., 2002; Little et al., 2018). Consistent with this, CSLD gene families are generally larger and more diverse in green algae such as *Coleochaete orbicularis*, and bryophytes including the moss *P. patens*, and the vascular seedless plant *Selaginella moellendorffii* (Harholt et al., 2012a;

Mikkelsen et al., 2014). CSLDs are essential for the protonemal tip-growth that occurs during vegetative growth in *P. patens* (Roberts and Bushoven, 2007). CSLD-dependent cell wall deposition appears to be essential in the apical plasma membranes of tip-growing cells (Doblin et al., 2001; Favery et al., 2001; Wang et al., 2001; Park et al., 2011) and during cell plate deposition in dividing cells (Gu et al., 2016; Yang et al., 2016): two cellular contexts in which plasma membrane-associated cortical microtubules are generally absent (Emons and Ketelaar, 2012). One possibility is that CSLD complexes represent ancestral CSCs that synthesize cellulose microfibrils, but in a manner not as tightly associated with cortical microtubule organization. Evidence for a distinct, randomly distributed fibrillar cell wall element has been described in the apical domain of tip-growing root hairs (Newcomb and Bonnett, 1965; Akkerman et al., 2012; Emons and Ketelaar, 2012). A major unresolved question is whether these CSLD3-containing complexes assemble into similar rosette complex configurations *in vivo*, as with CESA-containing complexes, and whether the β-1,4-glucan polymers synthesized by these oligomeric CSLD complexes assemble into cellulose microfibrils that are similar or distinct in nature to those generated by CSCs containing CESA proteins.

2.5 MATERIALS AND METHODS

Plant material and growth conditions

Arabidopsis thaliana lines used in this study were derived from *Col-0* ecotype. The pCESA6::eYFP-CESA6 expressing line was kindly provided by Chris Somerville, UC-Berkeley (Paredez et al., 2006). Seeds were sterilized with 10% Clorox bleach solution, rinsed five times with distilled water, then stored at 4°C for 2 days before being plated on growth medium

comprised of 0.25X Murashige and Skoog Basal Medium,1% sucrose, and 0.6% phytagel. Plates were placed vertically in a growth chamber at 21°C and grown under long-day conditions (16 hours light (200 uE/m2s)/8 hours dark photoperiod). For dark-grown conditions, plates were wrapped in aluminum foil. Three-day-old dark-grown seedlings were used for microscopy analysis. Five-day-old seedlings were used for morphology analysis. For propagation of mature plants, 14-day old seedlings were transferred to soil and grown in environmental chambers at 21°C under long-day conditions (16 hours light/8 hours dark photoperiod).

Yeast expression plasmid construction and growth conditions

S. cerevisiae (Strain INVSc1, Thermo Fisher, Cat#: C81000) was used for protein expression. Untransformed yeast was cultured in YPD medium. Positive colonies containing pYES2/NT C plasmids (Thermo Fisher, Cat#: V825220), expressing N-terminal His-tagged CESA6, CSLD3, or CSLA9, were selected and cultured overnight at 30°C and 180 rpm in SC-Ura + Glucose medium composed of 1.9 g/L SC-Ura (uracil drop-out) powder, 1.7 g/L yeast nitrogen base without amino acids and ammonium sulfate, 5 g/L ammonium sulfate, and 20 g/L glucose. Yeast cells were harvested, rinsed in sterile water, and used to inoculate 200 ml of SC-Ura + Raffinose medium with the same nitrogenous base composition containing 20 g/L raffinose to an OD600 equal to 0.03. Cultures were grown for 14 to 16 h at 30°C and 180 rpm until the OD600 reached 2.0. Protein expression was induced by addition of 800 ml of SC-Ura + Galactose medium containing 20 g/L galactose, and cells were incubated for an additional 6 h at 30°C and 180 rpm. Yeast cells were harvested, weighed, flash frozen in liquid nitrogen, and stored at -80°C.

Plant expression plasmid construction and plant transformation

The CESA6 promoter was amplified (2251 bp upstream of ATG, primers shown in Supplemental Figure 8) and cloned into a pCAMBIA1301 vector upstream of a Citrine fluorescent protein coding sequence (Griesbeck et al., 2001), replacing the *35S* promoter to generate pCambia1301:pCESA6. To construct the CESA6:D3CD chimeric protein coding sequence, the following three fragments were assembled: a CESA6 N-terminal domain fragment corresponding to CESA6 amino acids 1–321, a CSLD3 catalytic domain fragment corresponding to CSLD3 amino acids 340–921, and a CESA6 C-terminal fragment corresponding to CESA6 amino acids 861–1084. These three DNA fragments were ligated together and integrated into the pCambia1301:pCESA6 vector using the Gibson assembly method (Gibson et al., 2009). Point mutations for CESA6 (E463A, D464A) and the CESA6:D3CD chimera (corresponding to CSLD3 E508A and D509A) coding sequences were generated using PCR (shown in Supplemental Figure 8). Resulting N- and C-terminal fragments of the CESA6 and CESA6:D3CD chimera sequences were ligated together and integrated into the pCambia1301:pCESA6 vector by Gibson assembly. Plasmids were transformed into *Agrobacterium tumefaciens* strain GV3101 and then transferred to *Arabidopsis* using the standard floral dip method (Clough and Bent, 1998).

Hypocotyl and root length morphology analysis

Images of 5-day-old seedlings were recorded using an Epson Perfection 4990 Photo scanner. The lengths of hypocotyl and root regions were measured using Fiji-ImageJ (Schindelin et al., 2012). All transformed lines were grown side by side on the same plate, and at least 15 individuals were measured per line. Three independent biological replicates were performed for each line.

Cellulose content

Ten-day-old dark-grown seedlings (with seed coats attached) were collected and rinsed five times with distilled water to remove sucrose and residual MS medium. Samples were frozen in liquid nitrogen, ground to a fine powder, suspended in 80% (v/v) ethanol, filtered through a 45 mm nylon mesh (Industrial Netting, Cat#: WN0045), and then washed with 80% (v/v) ethanol followed by 100% ethanol. Cell wall residue was resuspended in a solution of chloroform: methanol (1:1) and shaken slowly for 2 h at room temperature. Cell wall residue was collected by filtration through 45 mm nylon mesh, and washed extensively with acetone, yielding AIR (alcohol insoluble residue) for Updegraff analysis to determine cellulose content (Updegraff, 1969). Briefly, 3 ml of acetic/nitric reagent was added to 2 mg of AIR and boiled in a water bath for 30 minutes. Insoluble crystalline cellulose residue was collected by sedimentation in a Sorvall ST 16R centrifuge with TX-400 swinging bucket rotor at 5000 rpm for 5 minutes at room temperature., rinsed with 5 ml distilled water, resuspended in 1 ml of 67% sulfuric acid, and incubated for 1 h at room temperature. 5 mg of pure cellulose (Sigma, Cat#: C0806) was dried at 105°C for 6 h and dissolved in 1 ml of 67% sulfuric acid, and then 50 ml distilled water was added to generate 100 mg/ml cellulose-sulfuric acid solution stock. The cellulose content was

quantified by the anthrone assay with a standard curve containing 0, 4, 10, 20, 30 mg/ml cellulose-sulfuric acid solution diluted from the 100 mg/ml cellulose-sulfuric acid solution stock.

Fluorescent imaging, FRAP analysis, and co-localization analysis

Images were acquired using a Leica confocal laser scanning microscope SP8 using a 100X oil lens (Type F Immersion oil, NA=1.518) and processed with the Leica Application Suite X (LAS X) Life Science Microscope software. YFP and citrine fluorescence were excited at 514 nm and visualized from 519 nm to 650 nm. CSC complexes movements were collected at 10 second intervals. Raw images were enlarged from 256*256 pixel images to 512*512 pixel images with Adobe Photoshop and imported into Fiji-ImageJ (Schindelin et al., 2012) to generate time projections using the Stacks function. CSC tracks were recorded using the segmented lines tool and analyzed by the Kymograph function in ImageJ. Velocities were calculated based on the distances measured in the kymograph over time. Photobleaching experiments (shown in Supplemental Figure 3) were performed by excitation of an ROI (red box) using a 405 nm laser, followed by collection of images at 10 second intervals. The red boxed region was cropped post-collection, using Adobe Photoshop, and CSC complexes numbers were analyzed using the Spot Counter function in ImageJ (Box size, 3; Noise Tolerance, 30). For co-localization analysis, YFP/citrine and GFP fluorescence were excited at 488 nm and visualized from 524 nm to 650 nm, and 494 nm to 520 nm, respectively.

Yeast protein extraction, purification, and proteoliposome reconstitution

5 g of yeast cells (corresponding to 8 L of SC-Ura + Galactose medium) expressing His-tagged CESA6, CSLD3, CSLA9, or an empty vector were resuspended in 20 ml lysis buffer (50 mM Hepes pH=7.4, 300 mM NaCl, 1 mM MgCl2, 1 mM MnCl2, 5 mM cellobiose, 5% glycerol, 50 mM Pefabloc SC plus (Sigma, Cat#: 11873601001), 1 mM PMSF (Thermo Fisher, Cat#: 36978)). Cells were lysed by passage through a French Press (20,000 PSI) twice at 4°C. Post-nuclear supernatant (PNS) was isolated by spinning in a SORVALL SS-34 rotor at 10,000 x g for 20 minutes at 4°C. A total membrane pellet was isolated by spinning the PNS fraction at 100,000 x g in a Fiberlite F65L-6 X 13.5 rotor at 4°C for 1 hour. The supernatant was discarded and the total membrane pellet was gently resuspended in 5 ml resuspension buffer (50 mM Hepes pH=7.4, 300 mM NaCl, 1 mM MgCl2, 1 mM MnCl2, 5 mM cellobiose, 50 mM Pefabloc SC plus, 1 mM PMSF, 2% LFCE-14 (Anatrace, Cat#: L414)) and incubated at 4°C for 30 minutes with gentle end-over-end shaking. Resuspended membranes were then spun at 100,000 x g in a Fiberlite F65L-6 X 13.5 rotor at 4°C for 1 h, and the supernatant was carefully collected and incubated at room temperature with Ni-NTA slurry (Thermo Fisher, Cat#: 88221) for 1 h. The slurry was transferred to a disposable chromatography column (BioRad, Cat#: 7321010) and washed with 5 ml wash buffer (50 mM Hepes pH=7.4, 300 mM NaCl, 1 mM MgCl2, 1 mM MnCl2, 5 mM cellobiose, 0.05% LFCE-14, 30 mM imidazole). Protein fractions (2.5 ml) were eluted from the Ni-NTA column with a 10 ml linear gradient of 30–250 mM imidazole in wash buffer. Protein fractions containing the His-tagged cell wall synthase enzymes were concentrated into wash buffer lacking imidazole using an Amicon Ultra 15 ultracel 100k centrifugal filter units (Sigma, Cat#: UFC910024) at 4,000 x g for 10 minutes. For reconstitution of purified cell wall synthases into proteoliposomes, 10 mg of yeast lipids (Avanti, Cat#: 190000P) were

dissolved in 1 ml chloroform in a glass test tube, and then evaporated with nitrogen and dried in a vacuum chamber at room temperature for 1 h. The resulting yeast lipid film was resuspended in reconstruction buffer (50 mM Hepes pH=7.4, 300 mM NaCl, 1 mM MgCl2, 1 mM MnCl2, 5 mM cellobiose, 6% LFCE-14), and mixed with vigorous vortexing. Purified, detergent-solubilized proteins were mixed with 300 ml of the solubilized lipid fraction in a protein-to-lipid molar ratio of 1: 4000 and incubated for 1 h at 4°C with gentle end-over-end shaking. Meanwhile, 0.2 g SM2 Adsorbent beads (Bio-Rad, Cat#: 1528920) were washed with 1 ml bead buffer (50 mM Hepes pH=7.4, 300 mM NaCl, 1 mM MgCl2, 1 mM MnCl2, 5 mM cellobiose) for 1 h at 4°C with gentle end-over-end shaking. The 300 ml protein-lipid mixture was diluted with 600 ml bead buffer and incubated with 0.2 g of pre-washed SM2 Adsorbent beads for 1 h. An additional 900 ml of bead buffer was added to the protein-lipid mixture and the resulting 1800 ml protein-lipid mixture was transferred to a new tube containing 0.2 g of pre-washed SM2 Adsorbent beads and incubated for 1 h with gentle end-over-end rotation. This step was repeated twice more (for a total of four SM2 Adsorbent bead extractions) to completely extract the detergent. The resulting proteoliposomes were layered over a discontinuous sucrose gradient (200 ml of 10%, 500 ml of each 15%, 25%, 35% and 60% w/v sucrose in bead buffer) and spun for 2 h in a TH-660 swinging bucket rotor at 150,000 x g at 4°C. The proteoliposome layer (Figure S5D, fraction 6) was collected and transferred to an Avanti Mini Extruder equipped with a 200 nm pore filter (Cat#: 610020) and passed through 20–30 times to generate unilamellar proteoliposomes of similar size, and then spun for 1 h in a Thermo Fisher TH-660 swinging bucket rotor at 150,000 x g at 4°C, and resuspended with 100~200 ml bead buffer for UDP-Glo or GDP-Glo glycosyltransferase assays (Promega, Cat#: V6961, VA1090). Briefly, 500–1000 ng proteoliposomes were incubated with 1 mM UDP-Glc in a 20 ml reaction containing 50 mM

Hepes pH=7.4, 300 mM NaCl, 1 mM MgCl2, 1 mM MnCl2, and 5 mM cellobiose for 1 h. 20 ml of freshly prepared nucleotide detection reagent was added and incubated for 15 minutes. Total luminescence was measured using a Tecan plate reader (infinite 200Pro, S/N: 1501003733), and the amount of UDP produced was calculated based on a UDP standard curve. For *in vitro* radiolabeling experiments with UDP-[3H]-Glc, proteoliposomes equivalent to 1–2 μg of purified, plant cell wall synthases were incubated with 0.25 μCi UDP-[3H]-Glucose (ARC, Cat#: ART 0127), 5 mM UDP-Glucose in a 20 μl reaction containing 20 mM Tris (pH=7.5), 100 mM NaCl, 20 mM MgCl2, 20 mM MnCl2, 5 mM cellobiose, and 10% (vol/vol) glycerol at 37°C for 2 h. 0.1% Triton X-100 was added for reaction termination. Water-insoluble polymer was isolated by sedimentation in an Eppendorf 5415D centrifuge at 16,000 x g for 20 minutes at room temperature. The pellet was gently resuspended and incubated in 20 μl of 50 mM sodium acetate (pH=4.5), 100 mM NaCl and 0.1 mg/ml of either endo-1,4-β-D-glucanase (Megazyme, Cat#: E-CELTR), or endo-1,3-β-D-glucanase (Megazyme, Cat#: E-LAMSE) at 37°C for 1 h. The pellet was collected by centrifuging at 16,000 x g for 20 minutes at room temperature and quantified by scintillation counting.

Size exclusion chromatography and immunoblot analysis

3 mg of purified, detergent-solubilized His-CSLD3, His-CESA6, and His-CSLA9 proteins in 5 ml wash buffer (50 mM Hepes pH=7.4, 300 mM NaCl, 1 mM MgCl2, 1 mM MnCl2, 5 mM cellobiose, 0.05% LFCE-14), were injected onto a HiPrep Sephacryl S-300 HR column equilibrated with wash buffer and run at a continuous flow rate of 0.5 ml/minute. 2 ml fractions were collected starting at 30 ml, concentrated using Ultra 15 ultracel 100k centrifugal filter units,

and every second fraction was analyzed by SDS-PAGE followed by either Coomassie Blue staining or immunoblotting. For immunoblotting, proteins were transferred to nitrocellulose membrane (GE Healthcare, Cat#: 10600003) by wet transfer at 15 V overnight. Membranes were blocked with 5% skim milk in PBST containing 0.05% Tween-20. Membranes were then incubated with primary (Invitrogen, Cat#: MA1-21315, Lot#: NI176305) and secondary (Thermo Fisher, Cat#: 31430, Lot#: UB278606) antibodies at a 1:2000 dilution, respectively, washing 5X with PBST between steps. HRP chemi-luminescence signal was then detected by x-ray film (Thermo Fisher, Cat#: 34090) exposure.

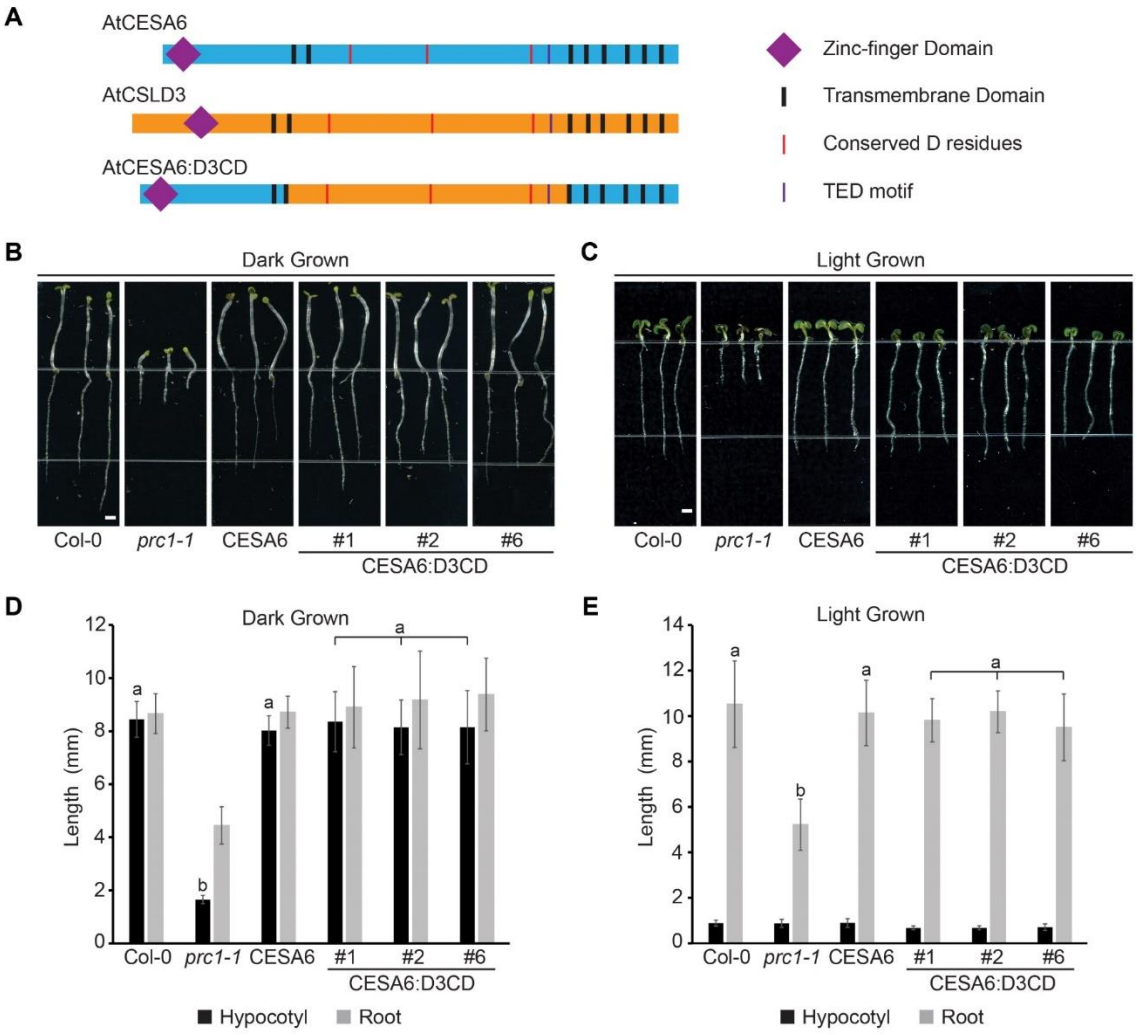
A
AtCESA6
AtCSLD3
AtCESA6:D3CD
Zinc-finger Domain
Transmembrane Domain
Conserved D residues
TED motif
B
Dark Grown
C
Light Grown
Col-0
prc1-1
CESA6
#1
#2
#6
CESA6:D3CD
D
Dark Grown
E
Light Grown
Length (mm)
Hypocotyl
Root

Figure 2.1: Expression of Citrine-CESA6:D3CD chimera proteins driven by CESA6 promoter fully rescue *cesa6* hypocotyl and root elongation defects.

(A) Schematic diagram of CESA6 (blue), CSLD3 (orange), and the chimeric CESA6:D3CD protein structures. Five-day old seedlings grown in darkness **(B, D)** and light **(C, E)** were analyzed and measured by Fiji-ImageJ (Schindelin et al., 2012). The *cesa6prc1-1* mutants displayed both hypocotyl and root elongation defects when compared with *Col-0* **(D, E)**. Independently transformed plants expressing either YFP-CESA6 **(**lane 3 in **B, C)** or Citrine-CESA6:D3CD proteins **(**lane 4, 5, 6 in **B, C)** in the *cesa6prc1-1* mutant background quantitatively restored hypocotyl and root elongation to wild-type levels **(D, E)**. Twelve individual plants were measured for each group. Scale bar in **B, C:** 1 mm. Error bars in **D, E** represent standard deviation. Labels a, b indicate significantly different groups: $p < 0.05$. (One-way ANOVA).

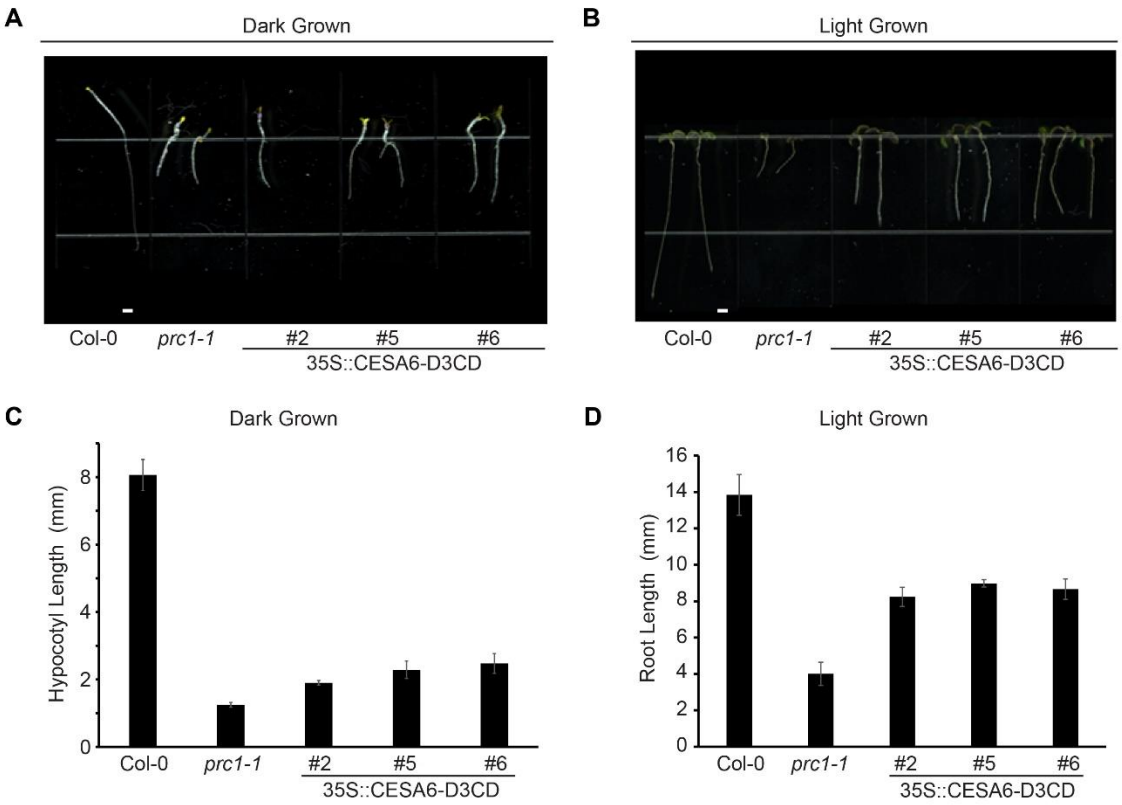

Figure 2.2 Expression of Citrine-CESA6:D3CD chimera proteins driven by *35S* promoter partially rescues *cesa6* root elongation defects.

Seven-day old seedlings grown in darkness **(A, C)** and light **(B, D)** were analyzed and measured by Fiji-ImageJ (Schindelin et al., 2012). The *cesa6* mutants displayed both hypocotyl and root elongation defects when compared with *Col-0* **(C, D)**. Independently transformed plants expressing Citrine-CESA6:D3CD proteins **(**lane 3, 4, 5 in **A, B)** in the *cesa6prc1-1* mutant background partially restored root elongation to wild-type levels. The hypocotyl length maintained indistinguishable compared to mutant background **(C, D)**. Twelve individual plants were measured for each group. Scale bar in **A, B:** 1 mm. Error bars in **C, D** represent standard deviation.

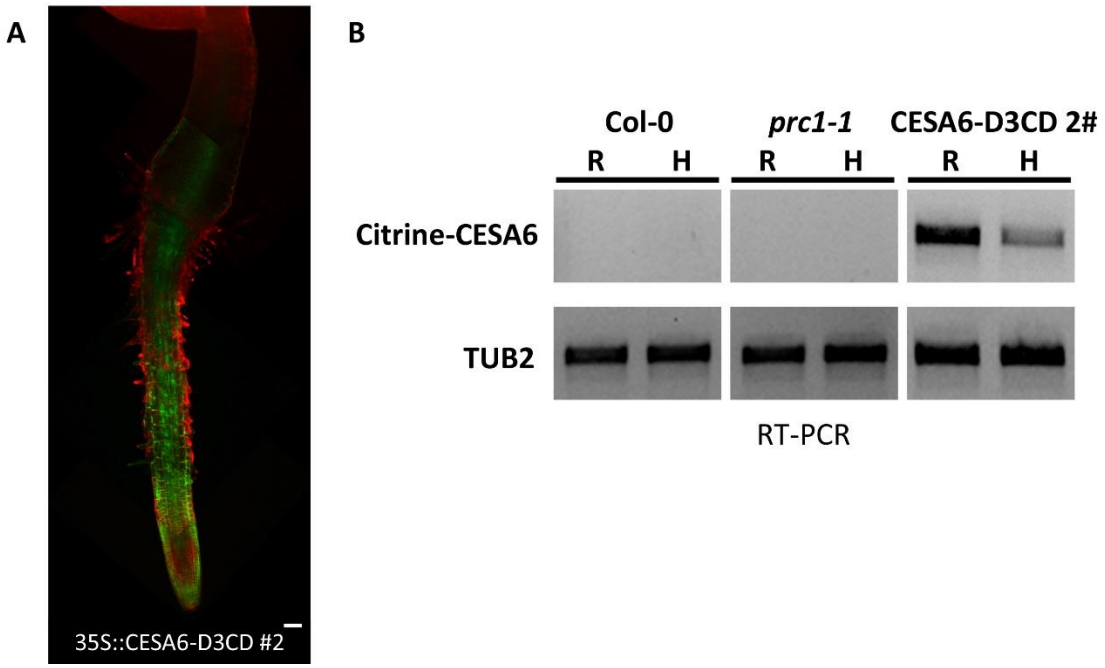

Figure 2.3: Expression pattern of Citrine-CESA6:D3CD chimera proteins driven by *35S* promoter.

Spinning-Disk Confocal microscopy was performed on three-day old, dark-grown seedlings **(A)**. Multiple frames were overlapped to display the expression pattern of Citrine-CESA6:D3CD proteins driven by *35S* promoter in whole seedlings. Green signals (Citrine-CESA6:D3CD) accumulated in root tissues, while displayed very weak strength in hypocotyl tissues **(B)**. RT-PCR analysis was performed using RNA collected from hypocotyl (H) and root (R) tissues. In stably transformed lines, the relative expression level of CESA6:D3CD was much higher in root tissues compared to hypocotyl tissues. TUB2 serves as the system control. Scale bar in **A:** 100 μm.

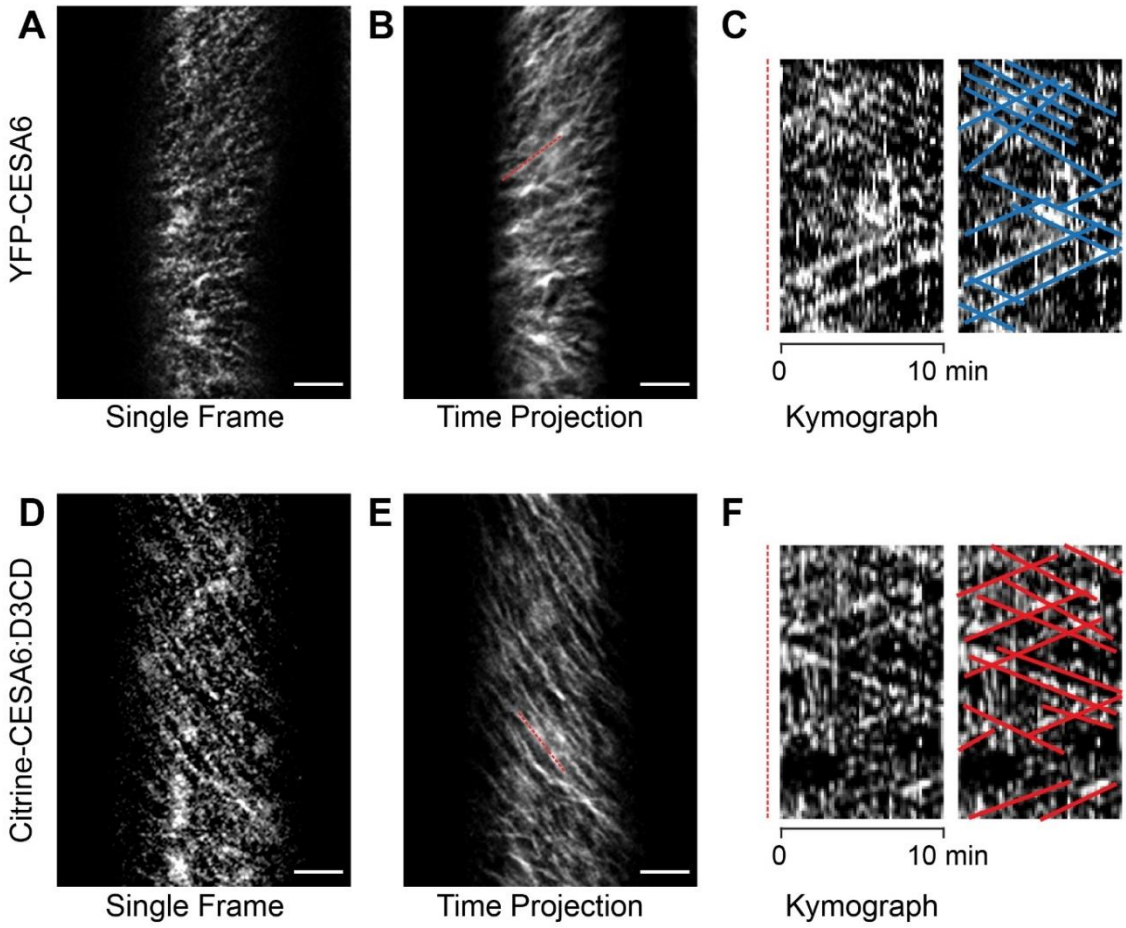
A
B
C
YFP-CESA6
Single Frame
Time Projection
0
10 min
Kymograph
D
E
F
Citrine-CESA6:D3CD
Single Frame
Time Projection
0
10 min
Kymograph

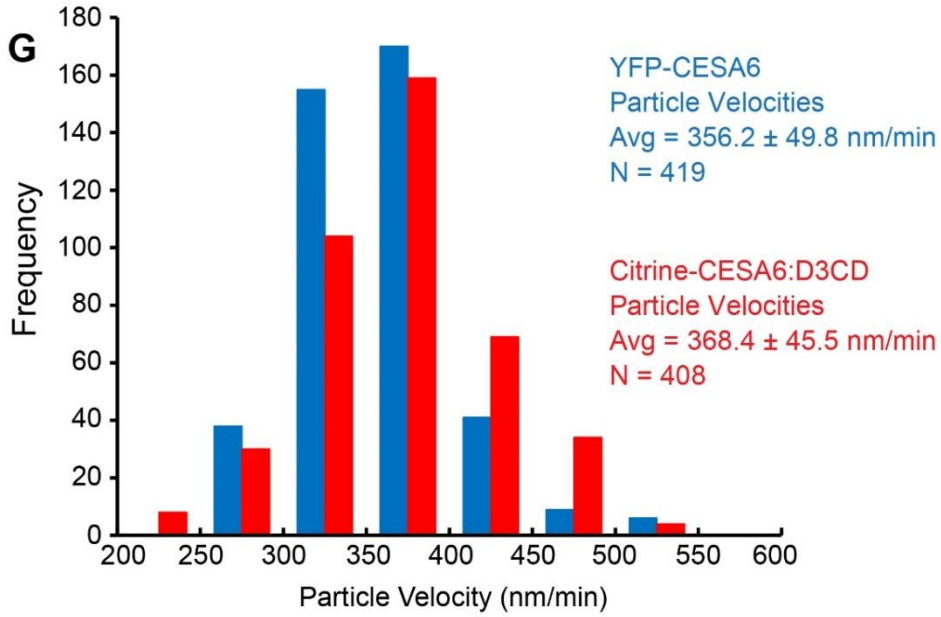
G
Frequency
Particle Velocity (nm/min)
YFP-CESA6
Particle Velocities
Avg = 356.2 ± 49.8 nm/min
N = 419
Citrine-CESA6:D3CD
Particle Velocities
Avg = 368.4 ± 45.5 nm/min
N = 408

Figure 2.4: Citrine-CESA6:D3CD chimeric proteins integrate into CSC complexes and display similar mobility as CSCs containing YFP-CESA6.

Confocal laser-scanning microscopy was performed on hypocotyl epidermal cells of three-day-old, dark-grown seedlings. Fluorescent CSC complexes containing YFP-CESA6 were observed and presented as **(A)** single frame, **(B)** time-lapse projection, and **(C)** a time-resolved kymograph of region labeled in red dashed line in **(B)**. **(D)** Single frame, **(E)** time-lapse projection, and **(F)** kymograph of red dashed line in **(E)** of Citrine-CESA6:D3CD, respectively. Scale bar: 5 μm. Blue lines **(C)** and red lines **(F)** represent the tracks of YFP-CESA6 and Citrine-CESA6:D3CD labeled CSCs, respectively. **(G)**, Histogram showed the distribution of CSCs velocities labeled by YFP-CESA6 (blue), calculated from 419 particles in 7 individual seedlings (9 cells total) and Citrine-CESA6:D3CD (red), calculated from 408 particles in 6 individual seedlings (9 cells total).

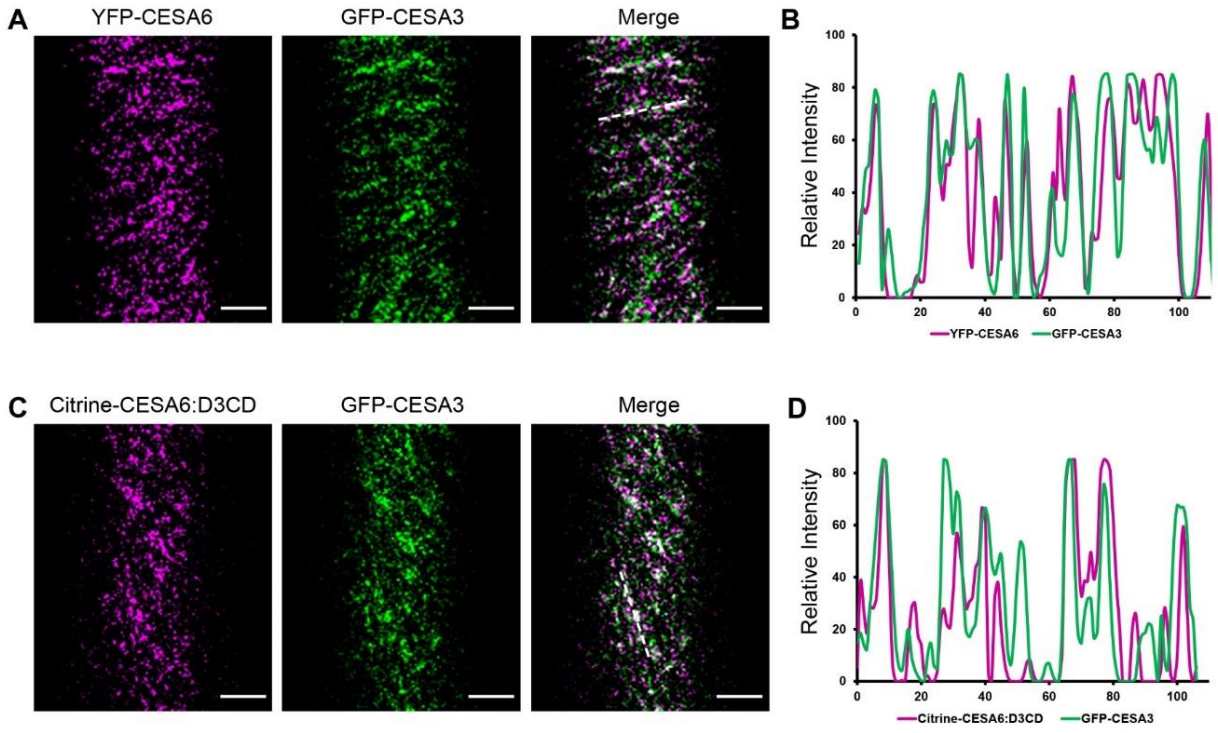

Figure 2.5: Citrine-CESA6:D3CD chimeric proteins co-localize with GFP-CESA3 proteins and integrate into the same CSC complexes.

Three-day-old, dark-grown F2 seedlings expressing both YFP-CESA6 and GFP-CESA3 were imaged by simultaneous two-channel confocal microscopy. **(A)** Single frame of YFP-CESA6 (magenta), GFP-CESA3 (green) and a merged image. **(B)** Plot of relative intensity through the white dashed line in **(A)** showing a strong association between the localization of YFP-CESA6 and GFP-CESA3. **(C, D)**, Single frame, and plot of relative intensity of F2 seedlings expressing both Citrine-CESA6:D3CD (magenta) and GFP-CESA3 (green), respectively. Scale bar in **A, C**: 5 μm.

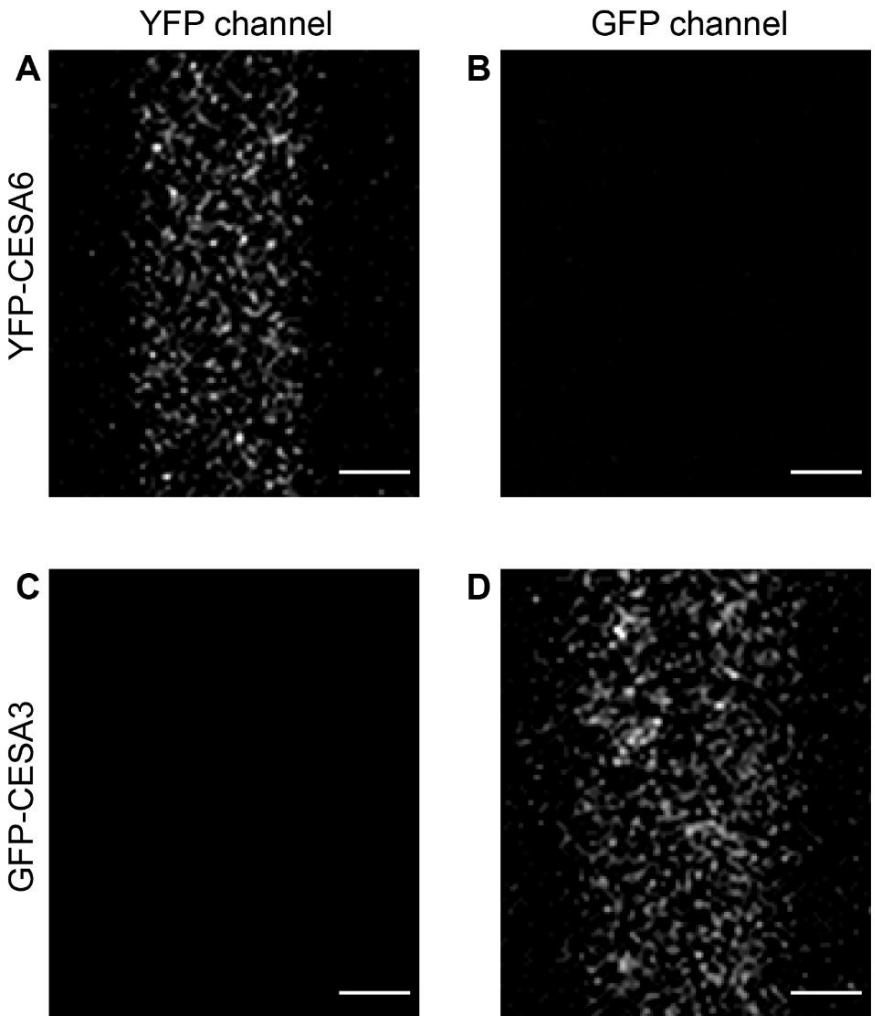

Figure 2.6: YFP and GFP signal can be distinguished using different emission spectrum ranges.

Confocal laser-scanning microscopy was performed on hypocotyl epidermal cells of three-day-old, dark-grown seedlings. Fluorescent CSC complexes containing YFP-CESA6 were observed only in the YFP channel **(A)**, not the GFP channel **(B)**. GFP-CESA3 labeled CSC complexes were not visible in the YFP channel **(C)**, and were visible only in the GFP channel **(D)**. Scale bars = 5 um.

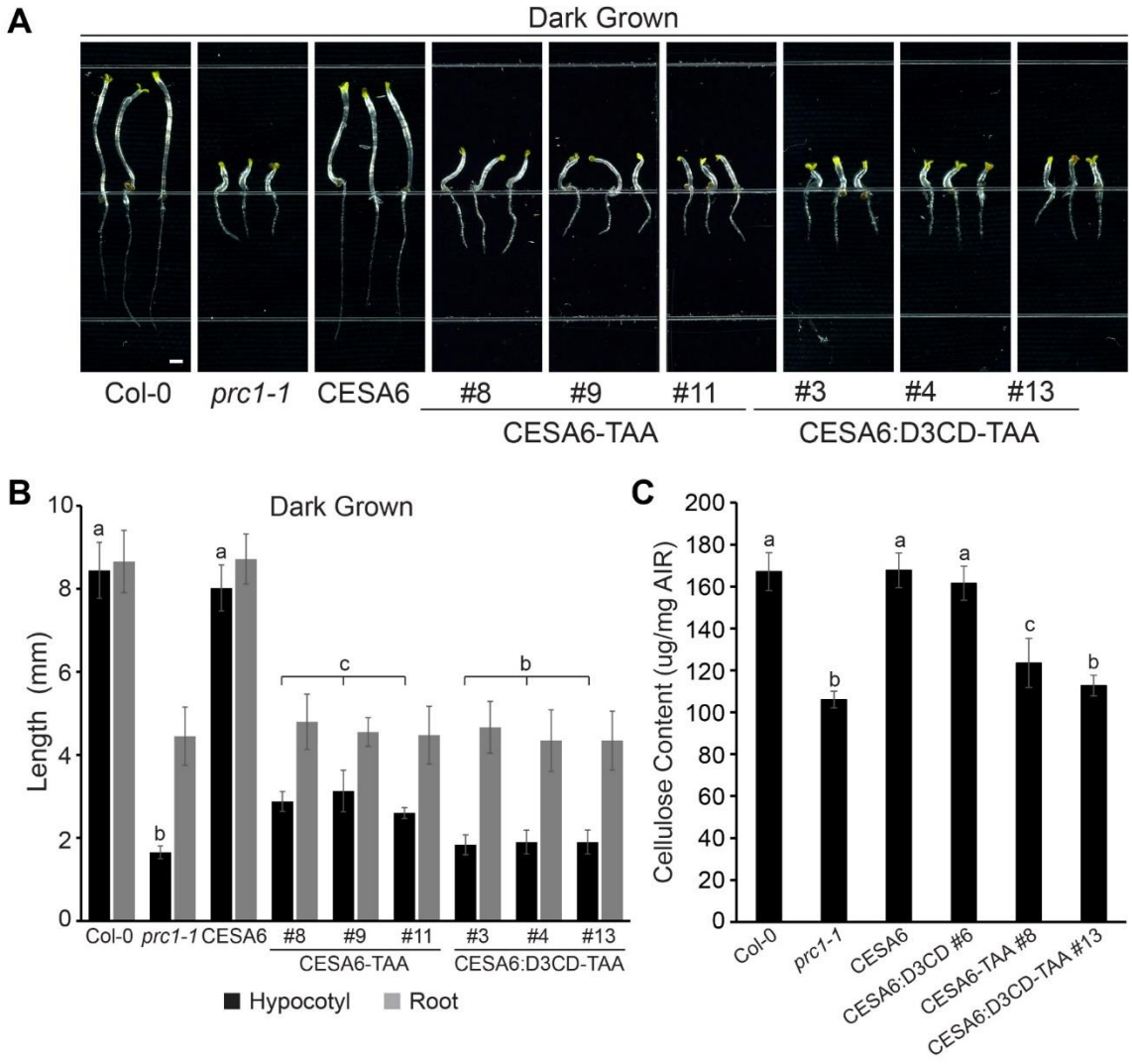
A
Dark Grown
Col-0
prc1-1
CESA6
#8
#9
#11
#3
#4
#13
CESA6-TAA
CESA6:D3CD-TAA
B
Dark Grown
Length (mm)
Hypocotyl
Root
C
Cellulose Content (ug/mg AIR)
CESA6:D3CD #6
CESA6-TAA #8
CESA6:D3CD-TAA #13

Figure 2.7: Citrine-CESA6 and Citrine-CESA6:D3CD proteins must be catalytically active to rescue *cesa6* hypocotyl elongation defects.

(A) Five-day-old dark-grown seedlings were analyzed and measured by ImageJ. Three independent transgenic lines expressing either Citrine-CESA6-TAA (#8, #9 and #11) or Citrine-CESA6:D3CD-TAA (#3, #4 and #13) failed to rescue *cesa6prc1-1* hypocotyl elongation defects. Quantification shown in **(B)**. **(C)** Crystalline cellulose content of tenday-old seedlings was measured using Updegraff methods on alcohol insoluble residue (AIR). The cellulose content of the *cesa6prc1-1* mutant was reduced compared to wild type (Col-0). This deficiency was rescued in both YFP-CESA6 and Citrine-CESA6:D3CD (CESA6:D3CD line #6, from Figure 1) seedlings, but not in Citrine-CESA6-TAA (CESA6-TAA line #8, in panel A) and Citrine-CESA6:D3CD-TAA (CESA6:D3CD-TAA line #13, in panel A) transgenic lines. Scale bar in **A**: 1 mm. Error bars in **B, C** represent standard deviation. Labels a, b, c indicate significantly different groups: $p < 0.05$. (One-way ANOVA).

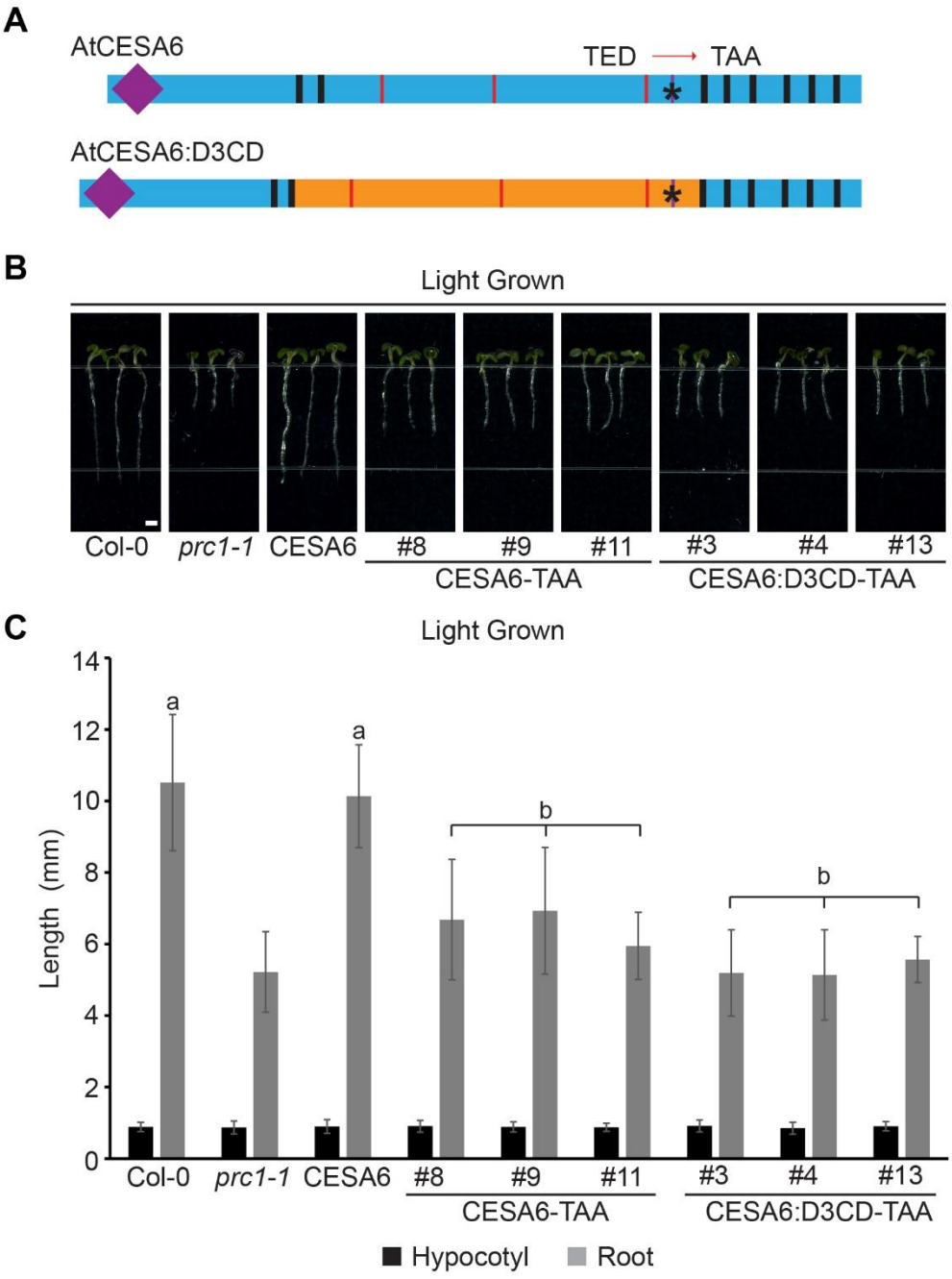
A
AtCESA6
TED
TAA
AtCESA6:D3CD
B
Light Grown
Col-0
prc1-1
CESA6
#8
#9
#11
#3
#4
#13
CESA6-TAA
CESA6:D3CD-TAA
C
Light Grown
Length (mm)
14
12
10
8
6
4
2
0
a
a
b
b
Col-0
prc1-1
CESA6
#8
#9
#11
#3
#4
#13
CESA6-TAA
CESA6:D3CD-TAA
Hypocotyl
Root

Figure 2.8: Inactive Citrine-CESA6-TAA and Citrine-CESA6:D3CD proteins are unable to rescue *cesa6* root elongation defects.

(A) Schematic diagram of CESA6 and the chimeric CESA6:D3CD protein structures. Marks were described in Figure 2. Asterisk: substitution points. Both aspartic acid and glutamic acid in the TED motif were mutated to alanine (TAA). **(B)** Five-day-old light-grown seedlings were analyzed and measured by Fiji-ImageJ (Schindelin et al., 2012). Transformed plants expressing Citrine-CESA6-TAA and Citrine-CESA6:D3CD-TAA failed to rescue *cesa6prc1-1* root elongation defects. Scale bar = 1 mm. Quantification shown in **(C)**. Labels a, b indicate significantly different groups: $p < 0.05$ (One-way ANOVA).

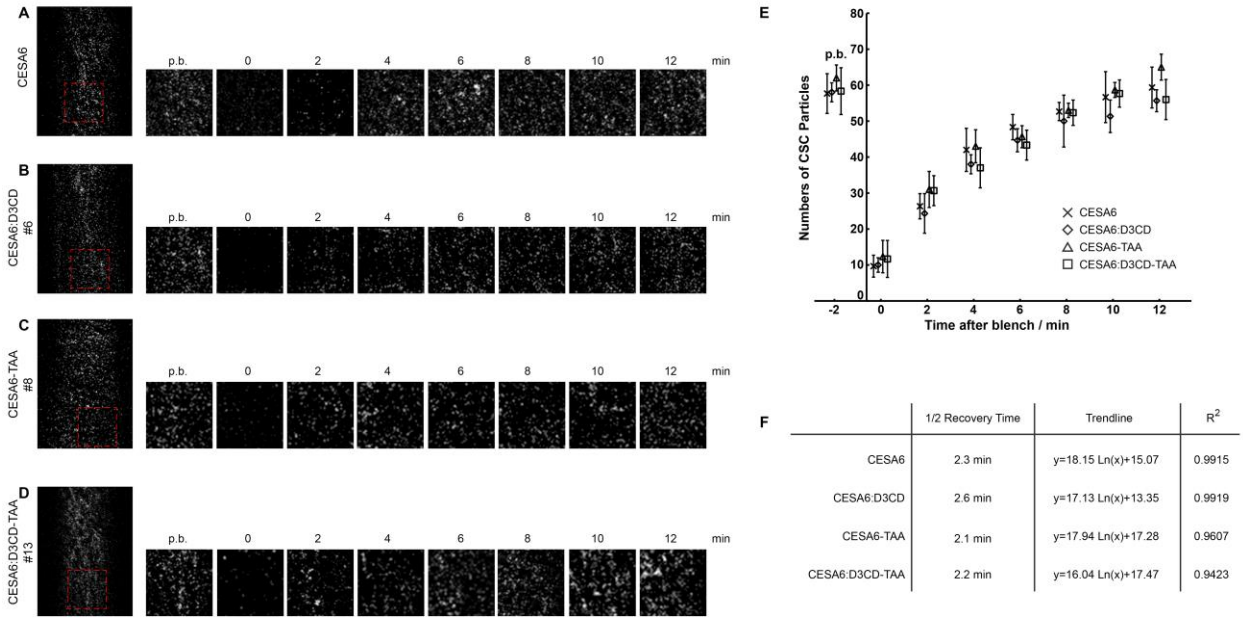

	1/2 Recovery Time	Trendline	R^2
CESA6	2.3 min	y=18.15 Ln(x)+15.07	0.9915
CESA6:D3CD	2.6 min	y=17.13 Ln(x)+13.35	0.9919
CESA6-TAA	2.1 min	y=17.94 Ln(x)+17.28	0.9607
CESA6:D3CD-TAA	2.2 min	y=16.04 Ln(x)+17.47	0.9423

Figure 2.9: The fluorescence recovery rates of CSCs labeled with either Citrine-CESA6-TAA or Citrine-CESA6:D3CD-TAA after photobleaching.

Single frames of CSC complexes recovery (2-min intervals) after photobleaching in hypocotyl epidermal cells of three-day-old dark-grown seedlings expressing YFP-CESA6 **(A)**, Citrine-CESA6:D3CD (line #6) **(B)**, Citrine-CESA6-TAA (line #9) **(C)**, and Citrine-CESA6:D3CD-TAA (line #13) **(D)**. Red dashed box represents the bleach area used for CSCs counting **(E)** and the logarithmic regression of recovery **(F)**. Scale bar = 5 um. All experiments were performed in triplicate. Error bars in E represent standard deviation. For each time point in **(E)**, One-way ANOVA was performed with $p > 0.05$, indicates insignificant difference. R2 in **(F)** represents the coefficient of determination of logarithmic correlation calculated using MS excel.

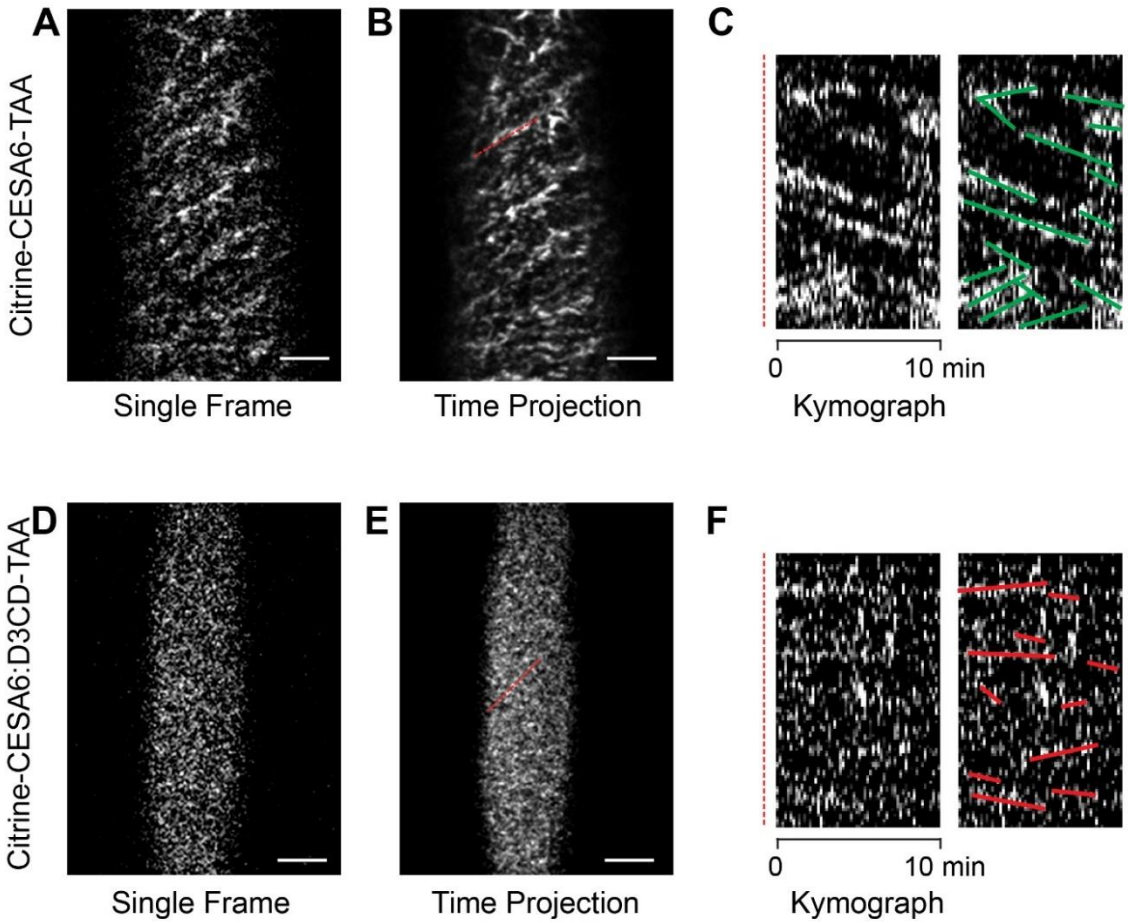
A
B
C
Citrine-CESA6-TAA
Single Frame
Time Projection
0
10 min
Kymograph
D
E
F
Citrine-CESA6:D3CD-TAA
Single Frame
Time Projection
0
10 min
Kymograph

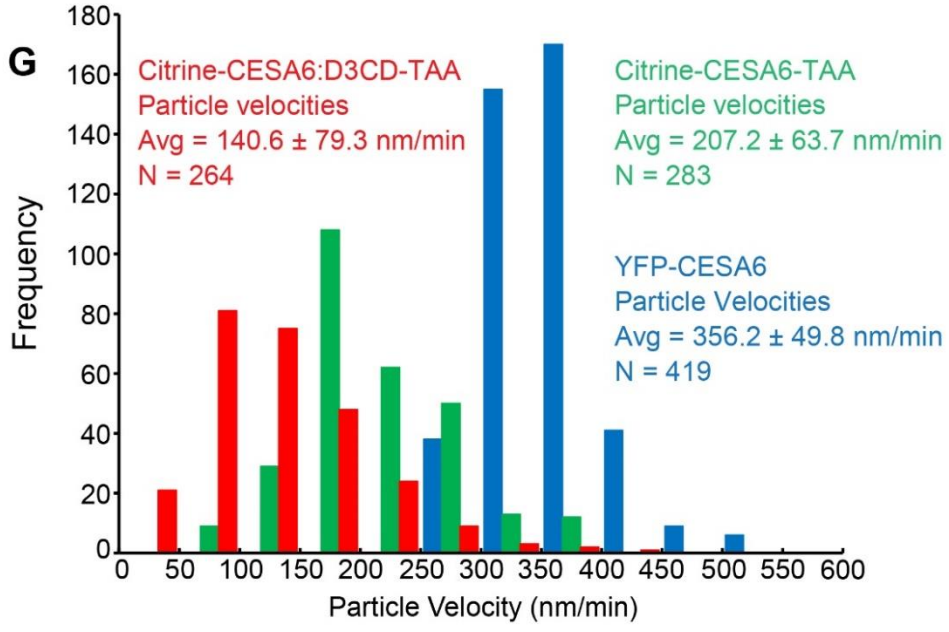
G
Citrine-CESA6:D3CD-TAA
Particle velocities
Avg = 140.6 ± 79.3 nm/min
N = 264
Citrine-CESA6-TAA
Particle velocities
Avg = 207.2 ± 63.7 nm/min
N = 283
YFP-CESA6
Particle Velocities
Avg = 356.2 ± 49.8 nm/min
N = 419
Frequency
Particle Velocity (nm/min)

Figure 2.10: TAA mutants of Citrine-CESA6 and Citrine-CESA6:D3CD integrate into CSCs, but display altered mobility compared to functional complexes.

(A) Single frame, **(B)** time-lapse projection, and **(C)** kymograph of red dashed line in **(B)** of Citrine-CESA6-TAA containing CSCs imaged by confocal scanning microscopy of three-day-old, dark-grown seedlings. **(D)** Single frame, **(E)** time-lapse projection, and **(F)** kymograph of red dashed line in **(E)** of Citrine-CESA6:D3CD-TAA containing CSCs. Scale bar: 5 μm. Green lines **(C)** and red lines **(F)** represent the tracks of Citrine-CESA6-TAA and Citrine-CESA6:D3CD-TAA labeled complexes, respectively. **(G)** Histogram showing the relative distribution of particle velocities labeled by both Citrine-CESA6-TAA (green), calculated from 283 particles in 6 individual seedlings (6 cells total), and Citrine-CESA6:D3CD-TAA (red), calculated from 264 particles in 8 individual seedlings (8 cells total). YFP-CESA6 (blue) particle velocities (reproduced from Fig 2G) are presented as reference.

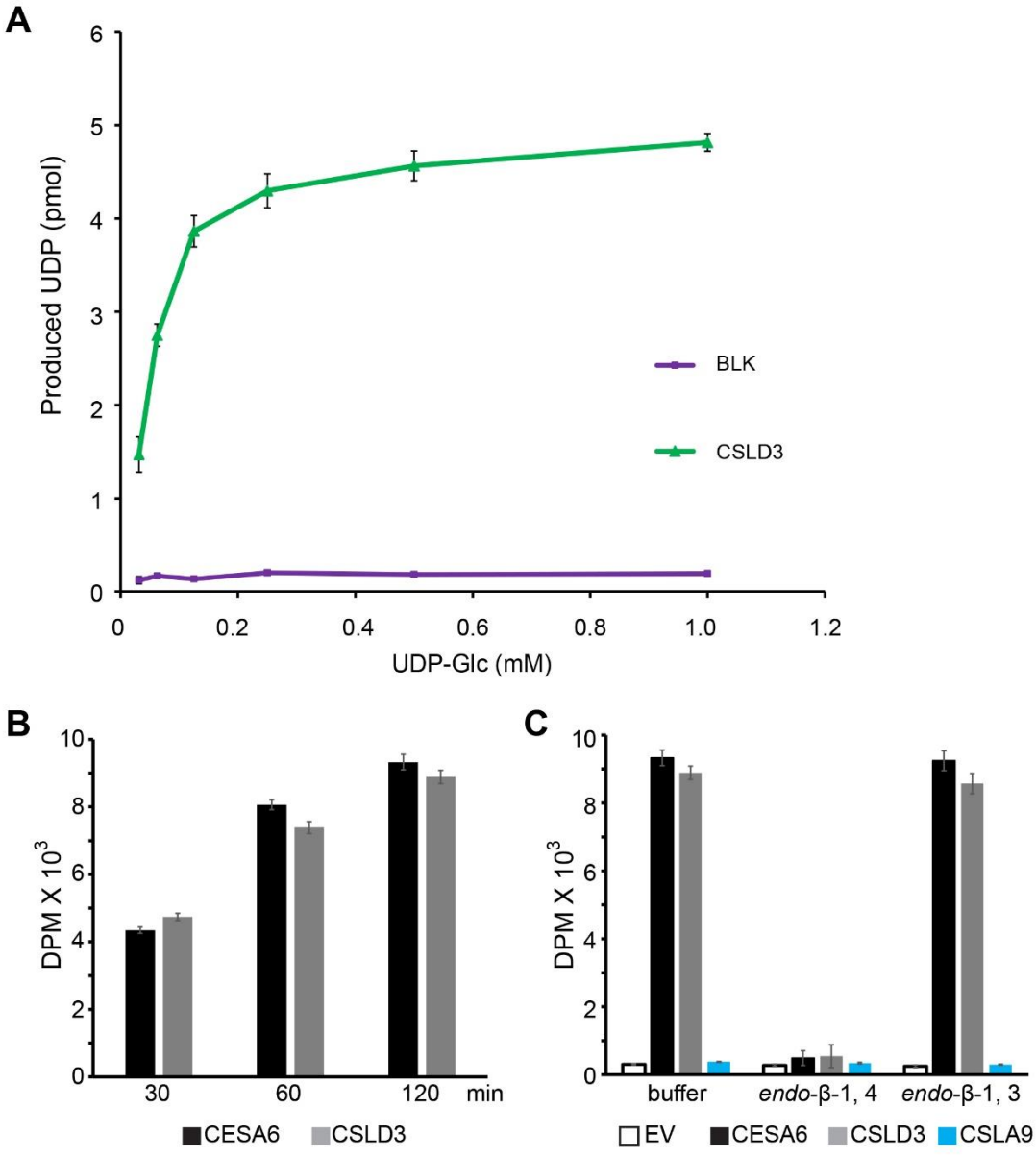
A
Produced UDP (pmol)
UDP-Glc (mM)
BLK
CSLD3
B
DPM X 10^3
30
60
120
min
CESA6
CSLD3
C
DPM X 10^3
buffer
endo-β-1, 4
endo-β-1, 3
EV
CESA6
CSLD3
CSLA9

Figure 2.11: Detection of β-1,4-glucan polysaccharides in proteoliposomes reconstituted with purified His-CSLD3 and His-CESA6.

(A) Proteoliposomes containing purified His-CSLD3 displayed saturable UDP-forming activities when supplied with UDP-Glc. The Km value is 62 uM. **(B)** Time-dependent β-1,4-glucan synthesis by both CESA6 and CSLD3 using UDP-[3H]-glucose as tracer. **(C)** Enzymatic digestion of CESA6 and CSLD3 synthesized glucan by β-1,4-endoglucanase. DPM, disintegrations per minute. EV, empty vector. All experiments were performed in triplicate. Error bars in **B, C** represent standard deviation.

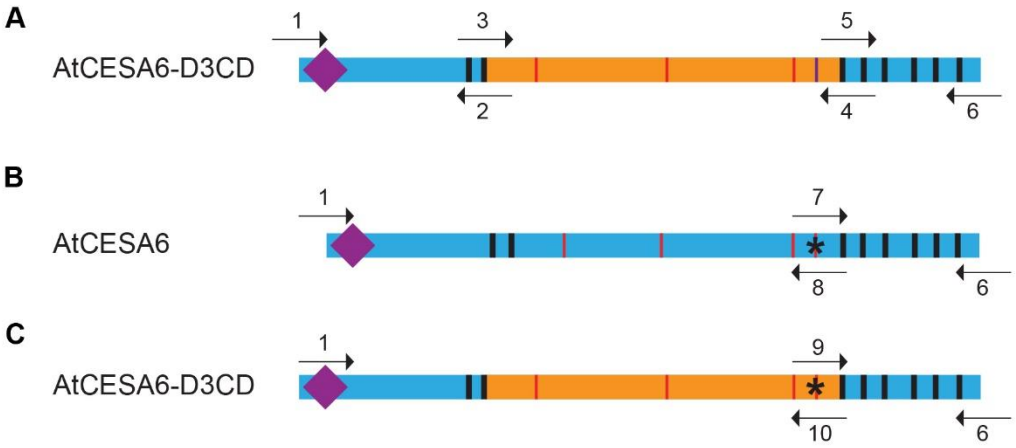

D

Primers Name	Primer Sequences (5'-3')
1: CESA6-N'-F-Gibson	TGCAGTCGACGGTACCATGAACACCGGTGGTCGG
2: CESA6-N'-lower	CAGCTTTGGAAGCTGATCAAGAACCCATGAAACAGC
3: CSLD3-CD-upper	GCTGTTTCATGGGTTCTTGATCAGCTTCCAAAGCTG
4: CSLD3-CD-lower	CCACGGGTAAACCACAGAGTTTAGGTAAGCGATTCT
5: CESA6-C'-upper	AGAATCGCTTACCTAAACTCTGTGGTTTACCCGTGG
6: CESA6-C'-R-Gibson	TTATCTAGATCCGGTGGATTCTCACAAGCAGTCTAAACC
7: CESA6-TAA-upper	GGTTCTGTTACCGCAGCTATTCTTACGGG
8: CESA6-TAA-lower	CCCGTAAGAATAGCTGCGGTAACAGAACC
9: CSLD3-TAA-upper	TATGGATCTGTCACGGCAGCTGTGGTCAC
10: CSLD3-TAA-lower	GTGACCACAGCTGCCGTGACAGATCCATA
11: pCESA6-F	CAGCTATGACCATGATTACGAATTCAACGTTTTTCTATTCTATAGTCTTG
12: pCESA6-R	CAGCTCCTCGCCCTTGCTCACCATGGTCAAGATTTGTCTGAAAACAGACACAG

Figure 2.12: Primers used for assembling CESA6:D3CD, CESA6-TAA and CESA6:D3CD-TAA constructs.

(A, B, C) Schematic diagram of CESA6 (blue), CSLD3 (orange) and the chimeric CESA6:D3CD protein structures. Purple diamond: Zinc-finger domain; Black bar: Transmembrane domains; Red bar: Conserved D residues; Purple bar: TED motif. Asterisk: substitution points. Both aspartic acid and glutamic acid in the TED motif were mutated to alanine (TAA). Arrows represent the primers **(D)** used to amplify fragments for construct assembly.

Chapter 3 Functional Relations of CSLD2, CSLD3, and CSLD5 Proteins during Cell Wall Synthesis

3.1 ABSTRACT

Plant cell expansion is a dynamic process that is physically constrained by the deposition of new cell wall components. In the process of tip growth, the new cell wall materials are delivered at a restricted plasma membrane domain and result in a highly polarized expansion within that specified domain. Previous studies demonstrated that this process requires the activities of members of the *Cellulose Synthase-Like D (CSLD)* subfamily. Furthermore, CSLD3 displayed β-1,4 glucan synthase activity *in vitro,* and a chimeric fusion protein in which the catalytic domain of CSLD3 was inserted into a CESA6 sequence was able to fully replace CESA6 activity during hypocotyl expansion in *cesa6* mutants. However, it is not clear whether other members of CSLD subfamily share the conserved biochemical activity, and whether CSLD proteins require formation of a higher-order complex to perform β-1,4 glucan synthase activities as CESA proteins do. Here, I used genetic methods to demonstrate that CSLD2 and CSLD3 proteins are interchangeable with each other during root hair elongation and cell plate formation. CSLD5 could partially rescue the root hair elongation defects. However, it displayed a unique function during cell plate formation. *In vitro* biochemical activity experiments showed that CSLD2, CSLD3, and CSLD5 proteins displayed conserved β-1,4 glucan synthases activities.

Taken together, these results indicated that while all three vegetatively expressed CSLD proteins possess conserved β-1,4 glucan synthases activities, CSLD5 has a more complicated and specialized role during cell plate formation.

3.2 INTRODUCTION

Plant cells are surrounded by rigid extracellular cell walls. To change the size and shape of plant cells, new cell wall material must be properly delivered and incorporated into existing cell walls during cell expansion. Two major mechanisms that control changes in plant cell shape are called diffuse growth and tip growth. During diffuse growth, the load-bearing components of cell wall, cellulose microfibrils, are synthesized directly at the plasma membranes by large integral membrane protein complexes called cellulose synthase complexes (CSCs), comprised of multiple catalytic subunits encoded by CESA (Cellulose Synthase) proteins. The new cellulose microfibrils are deposited and integrated in ordered arrays along the entire expanding faces of the cells, which are often transversely oriented to the major axis of cell expansion (Grierson et al., 2014). On the other hand, during tip growth, new cell wall material is selectively delivered and deposited by polarized secretion only at a restricted plasma membrane domains within the cell, resulting in a highly polarized expansion within that particular domain.

Root hairs are tip-growing tubular extensions of root epidermal cells, which play an important role in the uptake of water and nutrients (Peterson and Farquhar, 1996). Root hairs are formed by two separate processes: bulge initiation and subsequent tip growth (Vissenberg et al., 2001). In *Arabidopsis*, the initiation of bulge formation in root hair cells typically occurs at the apical end of the root hair precursor cell (nearest the root tip; Schiefelbein and Somerville, 1990). This initial bulge formation is thought to be regulated by the establishment of an apically

focused auxin gradient within the root hair cell precursor (Molendijk et al., 2001; Jones et al., 2002; Singh et al., 2008), and appears to be primarily regulated by cell wall expansion rather than incorporation of new cell wall materials (Jones et al., 2002; Sampedro and Cosgrove, 2005; Lin et al., 2011). Once the bulge is formed, new polarized cell wall deposition is initiated and confined to the expanding tip of the growing hair, leading to the elongated outgrowth (Schepf, 1986; Foreman and Dolan, 2001; Singh et al., 2008; Shibata and Sugimoto, 2019). During this process, the Golgi-derived secretory vesicles containing polysaccharides such as hemicellulose, pectin, and cell wall proteins are enriched in the subapical cytoplasm in the growing hairs, called the "vesicle rich zone" (Grierson et al., 2014). These cell wall cargoes are released to the extracellular matrix through exocytosis and are incorporated into the newly forming cell wall. Cellulose is deposited at the apical region of growing root hair cells and cellulose synthase inhibitor treatment causes the termination of elongation and popped root hairs (Park et al., 2011), indicating cellulose synthesis and deposition at the growing tip is essential for root hair elongation. Electron microscopy confirmed that the random arrangement of cellulose microfibrils was found in the initial cell wall layer at the tip region. (Newcomb and Bonnett, 1965; Galway et al., 1997; Emons and Mulder, 2000). An additional inner cell wall layer was found ~25 um from the growing tip (subapical region), which contains parallel arrays of cellulose microfibrils that organized in a helical orientation along the length of root hair (Emons and Wolters-Arts, 1983; Emons, 1994; Emons and Mulder, 2000). In the mutants of *cesa1*, *cesa3*, and *cesa6*, which are required for the cellulose synthesis of the primary cell wall, normal root hairs are generated and no significant defects in tip-restricted elongation were observed (Park et al., 2011; Gu and Nielsen, 2013). Additionally, both EYFP-CESA3 and EGFP-CESA6 proteins are excluded from the apical plasma membranes of growing hairs, and no accumulation

of these proteins is observed at the “vesicle rich zone” (Park et al., 2011). Taken together, these results suggest that CESA protein activities are required for cellulose synthesis at the tip of root hair cells.

Interestingly, root hair elongation is abolished, with root hair precursor cells undergoing cell rupture upon transition to tip-restricted elongation, resulting in a hairless phenotype in *csld3* mutants (Favery et al., 2001). Furthermore, the eYFP-CSLD3 proteins are enriched at the apical plasma membranes, and specifically accumulate in transport vesicles that accumulate in the "vesicle rich zone” of actively growing root hair cells (Park et al., 2011). Both *CESAs* and *CSLDs* belong to the *Cellulose Synthase-Like (CSL)* superfamily, whose members are predicted to encode glycosyltransferases that synthesize plant cell wall polysaccharide backbones (Fry et al., 2008). In *Arabidopsis*, there are seven CSL families including CSLA, CSLB, CSLC, CSLD, CSLE, CSLG, and CESA, among which the CSLD family shares the highest protein sequential similarity to CESA family (Richmond and Somerville, 2000). Functions of several CSL proteins have been determined in recent years. CSLA proteins are shown to catalyze the β-1,4-linkage between mannose subunits and are required for the synthesis of the backbone of mannan and glucomannan hemicelluloses (Liepman et al., 2005; Goubet et al., 2009). AtCSLC4 contributes to the synthesis of the β-1,4-glucan backbone of xyloglucan in the Golgi apparatus in *Arabidopsis* (Cocuron et al., 2007). The differential localization of distinct CSLC proteins has been observed in barley (*Hordeum vulgare*), raising the possibility that different CSLC family members may provide distinct biosynthetic activities during cell wall polysaccharide biosynthesis (Dwivany et al., 2009). Co-expression analysis showed that *HvCSLC3* was coordinately expressed with putative xylosyltransferase genes, consistent with *AtCSLCs* function in biosynthesis of xylogucan (Dwivany et al., 2009). However, HvCSLC2 displayed a plasma

membrane localization, and was not observed in internal membranes such as endoplasmic reticulum or Golgi apparatus (Dwivany et al., 2009). This raised the question whether all members of these subclades of CSL proteins synthesize the same types of polysaccharides.

To test if CSLD3 serves as β-1,4-glucan synthase during tip growth, previous research in our laboratory has demonstrated that a chimeric CSLD3 protein containing the CESA6 catalytic domain manages to rescue the hairless defects observed in *kjk-2* (*csld3* null) mutant (Park et al., 2011). Additionally, genetic complementation of a *cesa6* mutant with a chimeric CESA6 protein containing a CSLD3 catalytic domain demonstrated that the CSLD3 catalytic domain successfully generates β-1,4-glucan polymers for cellulose synthesis (Yang et al., 2020). Time-lapse fluorescence microscopy demonstrated that these CESA6-CSLD3 chimeric proteins assembled into CSC complexes with other CESA proteins and displayed similar mobility characteristics as CESA6-labeled complexes in hypocotyl cells (Yang et al., 2020). Proteoliposomes containing purified, detergent-solubilized CSLD3 proteins could specifically utilize UDP-glucose as enzymatic substrates and synthesize products that are only sensitive to endo-β-1,4-glucanase (Yang et al., 2020). Taken together, these results supported that the biochemical activity of the CSLD3 represents a UDP-glucose-dependent β-1,4-glucan synthase.

In *Arabidopsis,* there are six members in the CSLD protein family. *CSLD6* is currently thought to be a pseudogene and has not been found to be expressed in any plant tissues (Bernal et al., 2008). *CSLD1* and *CSLD4* exhibited high expression levels in pollen, and *csld1* and *csld4* mutants are male sterile due to defects in tip-restricted pollen tube elongation (Wang et al., 2001). The remaining *CSLD2, CSLD3,* and *CSLD5* are broadly expressed in vegetative tissues (Brady et al., 2007). Similar to CSLD3, CSLD2 also accumulates in root hair cells during root hair development. Shorter and irregular root hairs were observed in *csld2* mutants, indicating CSLD2

is also important for proper tip-restricted root hair growth (Bernal et al., 2008). The functional roles of CSLD enzymes are not restricted solely to cells undergoing tip-restricted expansion. While *csld5* mutants display no root hair defects, they have measurably shorter roots, smaller rosettes, and slightly reduced overall stature when compared to wild type (Col-0) (Bernal et al., 2007). Previous research in our laboratory demonstrated that CSLD5, along with CSLD2 and CSLD3, all participated in the construction of newly-forming cell plates during plant cytokinesis (Gu et al., 2016). Cellulose deposition has been observed in newly-forming cell plates (Miart et al., 2014). However, the predominant cell wall polysaccharide that accumulates at cell plates is likely the β-1,3-glucan callose (Meikle et al., 1991; Samuels et al., 1995; Ferguson et al., 1998; Chen and Kim, 2009; Drakakaki, 2015). Given that members of some CSL clades, notably CSLCs which accumulate in distinct compartments (Richmond and Somerville, 2000; Cocuron et al., 2007), may have distinct biochemical activities, we decided to test to what degree different CSLD proteins were functionally interchangeable. Additionally, at least three distinct CESA proteins are needed in order to assemble functional CSCs during synthesis of cellulose microfibrils (Arioli et al., 1998; Taylor et al., 1999; Fagard et al., 2000; Taylor et al., 2000; Scheible et al., 2001; Taylor et al., 2003; Desprez et al., 2007; Persson et al., 2007; Taylor, 2007). We therefore also wanted to determine whether, like CESA proteins, multiple CSLD proteins were required to assemble functional complexes in vivo, and directly test the biochemical activities of multiple CSLD family proteins.

Here, I used genetic methods to demonstrate that CSLD2 and CSLD3 proteins are functionally interchangeable with each other during root hair elongation and cell plate formation. While ectopic expression of *CSLD5* in root hair cells could partially rescue *csld3* root hair elongation defects, this rescue was directly linked to the relative accumulation of this protein

which is rapidly degraded in non-dividing cells. While CSLD2 and CSLD3 were largely interchangeable, CSLD5 displayed a unique function during cell plate formation that neither CSLD2 nor CSLD3 could functionally replace. *In vitro* biochemical activity experiments showed that CSLD2, CSLD3, and CSLD5 proteins displayed conserved β-1,4 glucan synthases activities.

3.3 RESULTS

3.3.1 Single *csld* mutants showed different degrees of growth defects

To better understand the functions of three vegetatively expressed CSLD proteins, I carefully analyzed the growth phenotypes of three single mutants (Figure 3.2A). To quantify the overall size of plants, the length of rosette leaves was used as the reference. While the *csld2* mutants showed indistinguishable overall sizes to wild type (Col-0), the *csld3* and *csld5* mutants displayed a ~15% reduction in the length of rosette leaves of three-week old plants (Figure 3.2D). 5-day old seedlings of three *csld* single mutants growing on ¼ MS plate showed a 10%~20% reduction on root length (Figure 3.2B, E), which is consistent with the overall size reduction in mutants. Among them, the *csld3* mutants displayed the most severe root length reduction. To distinguish whether the reduction is due to a slower growth rate or the growth defects in the absence of CSLD proteins. I recorded the root lengths of these mutant lines over seven days after germination (Figure 3.2E). In 7-day old seedlings, the mutants can reach to the length as 5-day old wild type (Col-0) seedlings (Figure 3.2C), indicating that the growth reduction shown in *csld* mutants is due to an overall slower growth rate, which might relate to insufficient cellulose synthesis at early stages of root elongation, and could be restored with extended growth time. The growth defects were enhanced in *csld2/3*, csld2/5, or csld3/5 double mutants (Figure 3.5A) resulting in a ~60% reduction in root length of 5-day old seedlings, indicating that three vegetative

CSLD proteins played important and at least partially redundant roles in root elongation during early stages of seedling development. Interestingly, this growth reduction cannot be restored with extended growth time, indicating that *CSLD* function in development of these tissues is not solely restricted to their roles in root hair tip-growth.

When examining the root hair phenotypes, the root hair morphology in *csld5* mutants was indistinguishable to that of wild type (Col-0) (Figure 3.3A, B), which was both consistent with the relatively low expression level of *CSLD5* in root hair cells (Brady et al., 2011), as well as reflective of the expected low levels of CSLD5 protein accumulation we would expect to observed in these non-dividing cells. *csld2* and *csld3* mutants phenotypes were most prominent during tip-restricted root hair elongation as previously described (Favery et al., 2001; Wang et al., 2001; Bernal et al., 2008; Galway et al., 2011; Park et al., 2011; Hu et al., 2019). In *csld2* mutants, bulges were formed at the base of growing root hairs (Figure 3.3A), and early termination of root hair elongation resulted in significantly shorter hair length compared to wild type (Col-0) (Figure 3.3B). In *csld3* mutants, essentially no root hairs could be observed (Figure 3.3A). These phenotypes were consistent with the expression patterns of *CSLD2* and *CSLD3* generated using the *Arabidopsis* eFP Browser (http://bar.utoronto.ca/efp/cgi-bin/efpWeb.cgi). (Figure 3.9). Both *CSLD2* and *CSLD3* displayed increased expression levels in root hair cells. *CSLD3* was expressed in hair cells initiating root hair growth (region 8), while *CSLD2* expression level increased later when root hair undergoing elongation (Brady et al., 2011).

3.3.2 CSLD2 and CSLD3 are functionally interchangeable in root hair cells undergoing tip growth

To examine whether the root hair tip-growth defects observed in the *csld2* and *csld3* mutants were due to distinct genetic or biochemical functions between *CSLD2* and *CSLD3*, or simply the results of gene dosage effects due to differential expression patterns, I first tested whether *CSLD2* could functionally replace *CSLD3* during root hair elongation. To address this, a previous laboratory member, Fangwei Gu, generated the stably transformed *kjk-2* (*csld3* null) plant lines expressing a fluorescently tagged Cerulean-CSLD2 under control of the endogenous CSLD3 promoter. This transgenic plant quantitatively rescued the hairless defects of *kjk-2* (*csld3* null) plant lines (Figure 3.4A), and generated normal root hairs that quantitatively indistinguishable to wild type (Col-0) (Figure 3.4B), indicating the CSLD2 protein could functionally replace CSLD3 protein function during root hair elongation. Interestingly, in the stably transformed plant lines expressing Cerulean-CSLD5 driven by the endogenous CSLD3 promoter, we also observed root hair formation (Figure 3.4A). However, the length of root hairs varied dramatically with an average of about 40% compared to wild type (Col-0), as well as the *pCSLD3*:Citrine-CSLD3 fully restored plants (Figure 3.4B).

To determine if the fluorescently-tagged CSLD proteins in these transgenic lines were accurately delivered to the tip region of the elongating root hair cells, I examined the localization of ectopic expressed CSLD2 and CSLD5 proteins by laser-confocal microscopy (Figure 3.4C). Similar to EYFP-CSLD3, Cerulian-CSLD2 localized to the apical plasma membranes in these transgenic lines, as well as the compartments that accumulated in the vesicle-rich zone in the tips of growing root hairs. This tip-localized accumulation could be observed in lines expressing these fluorescent CSLD fusions driven either by the constitutive *35S* promoter or the endogenous

CSLD3 promoter (Figure 3.4C, middle panel). When driven by the endogenous CSLD3 promoter, the signals of Cerulean-CSLD5 were barely detectable in root hair cells (Figure 3.4C, lower left panel), consistent with early observations that CSLD5 proteins are actively degraded in non-dividing cells in plants (Gu et al., 2016). When localization of fluorescent CSLD5 fusions was examined in lines where this fluorescent fusion was driven by the constitutive *35S* promoter, some accumulation of Cerulean-CSLD5 proteins was detected and displayed accumulation within the apical region of growing tip (Figure 3.4C lower right panel), a localization similar to those observed for fluorescent fusions of CSLD2 and CSLD3 proteins. When considering the instability of CSLD5 proteins in non-dividing cells from previous research (Gu et al., 2016), these results suggest that the functions of CSLD2, CSLD3, and CSLD5 during root hair elongation may be interchangeable, but that the instability of CSLD5 in non-dividing root hair cells may reduce the ability of this protein to rescue CSLD function.

3.3.3 CSLD5 is essential and irreplaceable for cell wall deposition in cell plate formation during cytokinesis

Previous research in the laboratory demonstrated that *csld5* displayed cell wall stub defects in root cortical cells and developing stomatal cells. These defects in *csld2/5* and *csld3/5* double mutants were dramatically enhanced (Figure 3.5C, D), indicating the CSLD2 and CSLD3 are also involved in the formation of cell plates during plant cell division (Gu et al., 2016). Interestingly, although *csld2/3* double mutants suffered enhanced growth reduction defects and displayed shorter roots similar to *csld2/5* and *csld3/5* double mutants (Figure 3.5A, B), the cell wall stubs were not observed in *csld2/3* double mutants (Figure 3.5C). This result might indicate either that CSLD5 performs an essential function during cell plate formation, or as with earlier

results with *CSLD2* and *CSLD3*, *CSLD5* may simply need to be expressed at the appropriate time with a *CSLD5* promoter sequence.

To investigate these possibilities, I generated stably transformed transgenic lines expressing Citrine-CSLD2 or Citrine-CSLD3 driven by the *CSLD5* promoter sequence, and examined if the ectopically expressed CSLD2 or CSLD3 could functionally replace CSLD5 and restore the cell wall stubs observed in *csld5* mutants during cell plate formation. The fluorescently-tagged Citrine-CSLD2 and Citrine-CSLD3 driven by the endogenous *CSLD5* promoter were first transformed to *csld5* mutants (Figure 3.6A, upper panel). In the stably-transgenic plants expressing *pCSLD5*:Citrine-CSLD2, cell wall stubs were still observed, indicating that simply expressing Citrine-CSLD2 with *CSLD5* promoter sequences could not replace endogenous CSLD5 activity. Similarly, *pCSLD5*:Citrine-CSLD3 was unable to rescue the cell wall stub defects in *csld5* mutants. Importantly, in both cases, the percentage of cells displaying wall stub defects were indistinguishable from the *csld5* mutant alone (Figure 3.6B).

Due to the fact that *csld5* mutants displayed a relatively low percentage of cells in which we detect cell wall stubs (Figure 3.5D), we also examined the propensity of *CSLD5* promoter-driven CSLD2 and CSLD3 fluorescent fusions to rescue the cell division defects observed in *csld2/5* and *csld3/5* double mutant backgrounds (Figure 3.6A lower panel). When expressing Citrine-CSLD2 driven by the endogenous *CSLD5* promoter in *csld3/5* double mutants, Citrine-CSLD2 would be the sole CSLD isoform present during cell plate formation. Quantification of the percentage of cell wall stubs present in this line indicated that while expression of *pCSLD5*:Citrine-CSLD2 could reduce the incidence of cell wall stubs versus the *csld3/csld5* double mutant background, this reduction was only back to the levels observed in the *csld5* mutant alone (Figure 3.6B). When expressing *pCSLD5*:Citrine-CSLD3 in *csld2/5* double

mutants, where Citrine-CSLD3 would be the sole CSLD isoform present during cell plate formation, again the incidence of cell wall stubs was only rescued back to levels observed in the *csld5* single mutant background (Figure 3.6B). Taken together, these results suggest that simply expressing CSLD2 or CSLD3 behind the *CSLD5* promoter is insufficient to rescue the cell division defects observed in *csld5* mutants.

3.3.4 Mutations in the TED motif do not cause complete functional loss of CSLD3 proteins

While these results supported that three vegetative CSLD proteins, CSLD2, CSLD3, and CSLD5 may act cooperatively but provide non-redundant functions, they did not directly address whether the CSLD proteins need to be catalytically active *in vivo* to rescue the corresponding defects. To address this question, I took advantage of a recently published crystal structure of bacterial cellulose synthase (BcsA) to design catalytically-dead versions of CESA and CSLD proteins. Based on the BcsA structure, a trio of highly conserved amino acid residues, Threonine - Glutamic acid - Aspartic acid (TED) were identified, and within this TED motif, the aspartic acid has been proposed to function as a catalytic base during the formation of the β-1,4-glycosidic linkages of forming glucan polysaccharides (Morgan et al., 2013; Omadjela et al., 2013; Morgan et al., 2016). When examining the catalytic domains of the plant cellulose synthases, CESA and CSLDs, we found this TED motif is absolutely conserved in higher plant CESA and CSLD protein sequences (Figure 3.1C). While in BcsA mutation of the aspartic acid alone inactivates this cellulose synthase, we wanted to examine mutants in which only the aspartic acid was changed, but also examine functions of mutants in which both aspartic acid and the neighboring glutamic acid residues were changed.

To examine whether the Glutamic acid and Aspartic acid residues of CSLDs might display some functional redundancy due to the similar chemical nature of their sidechains, I substituted the Aspartic acid residue and the neighboring Glutamic residue with Alanine residue to remove the carboxylic groups. I called these mutants "TEA" and "TAA" mutations, respectively. The plants expressing Citrine-CSLD3-TAA were unable to rescue the hairless defects in *kjk-2 (csld3 null mutant)* (Figure 3.7B). Interestingly, the stably transformed plants expressing Citrine-CSLD3-TEA driven by endogenous *CSLD3* promoter were able to generate root hairs and partially rescue the *csld3* hairless defects (Figure 3.7B). Quantification of root showed an about 60% reduction of hair length in these plants compared to wild type (Col-0), as well as the *pCSLD3*:Citrine-CSLD3 fully restored plants (Figure 3.7C). To assess whether either the early termination of growth hair growth, or an overall slower growth rate caused the shorter root hair phenotypes, I recorded the root hair growth in wild type (Col-0), *pCSLD3*:Citrine-CSLD3-TEA, and *pCSLD3*:Citrine-CSLD3-TAA expressing lines and measured the length of growing root hair cells at different time points (Figure 3.7D). Transgenic *csld3* plants expressing *pCSLD3*:Citrine-CSLD3-TEA showed a slower elongation rate compared to wild type (Col-0), while transgenic *csld3* mutants expressing *pCSLD3*:Citrine-CSLD3-TAA displayed no root hair growth, consistent with this protein being catalytically inactive. From these results we concluded that a catalytically active form of CSLD3 was required to rescue loss of this protein in *csld3* mutants, and second that unlike the bacterial cellulose synthase, BcsA, the glutamic acid in the TED motif appears capable of providing some residual level of activity in this enzyme.

To further distinguish the partial rescue shown in plants expressing Citrine-CSLD3-TEA was due to whether the catalytic activities were reduced, or disruption of CSLD complex assembly directly, I performed the kinetics analysis on His-tagged CSLD3-TEA and CSLD3-

TAA proteins *in vitro* system. Using the yeast-based protein expression and purification system, proteoliposomes containing His-CSLD3-TEA proteins displayed a nearly four-fold increase in the K_m value for the UDP-glucose substrate (~255uM), compared to His-CSLD3 which had a K_m value of ~62uM for UDP-glucose (Figure 3.8A). The K_m value of CSLD3 for UDP-glucose was consistent compared to previous CSLD3 and CESA6 K_m values (Yang et al., 2020). Consistent with the genetic rescue results, the His-CSLD3-TAA proteins failed to utilize the UDP-Glc as substrates and displayed only background levels of UDP formation when compared with a blank control. Taken together, these results are consistent with the conclusion that the quantitative rescue of *csld3* hairless defects observed in seedlings expressing *pCSLD3*:Citrine-CSLD3 requires the catalytic activity of a β-1,4-glucan synthase, and that the partial rescue of root hair growth defects observed in lines expressing *pCSLD3*:Citrine-CSLD3-TEA is linked to reduced catalytic activity in these mutants.

3.3.5 *In vitro* activity experiments confirmed that CSLD2 and CSLD5 displayed β-1,4 glucan synthase activities

To further explore whether all CSLD proteins maintain the conserved β-1,4 glucan synthase activities, His-tagged CSLD2, CSLD3, and CSLD5 proteins were heterologously expressed in *S. cerevisiae*. To more specifically assess the enzymatic activities of these plant cell wall synthases, previous laboratory member, Gwangbae Bak, developed this yeast-based protein expression and purification system, where the microsomal light membrane fractions were isolated from yeast expressing CSLD2, CSLD3, and CSLD5, and subsequently resuspended with detergent LFCE14. The solubilized His-tagged proteins were purified with Ni-NTA slurry incubation. The purified proteins were further enriched and mixed with *S. cerevisiae* total lipid

extracts to reconstitute the artificial proteoliposomes containing purified cell wall polysaccharide synthases. These proteoliposomes were further treated with UDP-Glc, the substrate to generate β-1,4 glucan polysaccharides. Both CSLD2 and CSLD5 could utilize UDP-Glc as substrates and generate free UDP with a similar reaction rate to CSLD3 (Figure 3.8B), indicating all three vegetatively expressed CSLD proteins have conserved biochemical function as a β-1,4 glucan synthase.

3.4 DISCUSSION

Plant cells are surrounded by a rigid cell wall matrix. In order to grow and elongate, plant cells must synthesize new cell wall components and properly deliver these components and enzymes that modify or synthesize cell wall polysaccharides to specific sites where cell expansion is occurring (Richmond and Somerville, 2000; Cosgrove, 2005). In the past decades, the roles of CESA proteins in the synthesis of cellulose microfibrils, and the cellular mechanisms responsible for targeting these enzyme complexes to cortical microtubule arrays during diffuse growth has been well studied (Crowell et al., 2009; Gutierrez et al., 2009; Gu et al., 2010; Li et al., 2012; Liu et al., 2016; Zhu et al., 2018). On the other hand, the role that cellulose synthesis plays during construction of new cell walls and the mechanisms responsible for delivering enzymes involved in synthesis of this cell wall polysaccharide during tip-restricted cell expansion is still limited. Previous studies in our laboratory have shown that a member of the *CSLD* family, *CSLD3*, participates in the synthesis of cellulose during tip growth where it provides a β-1,4-glucan cellulose synthase-like activity (Park et al., 2011; Yang et al., 2020). However, whether the other two vegetatively expressed CSLD proteins (CSLD2, CSLD5, Figure 3.9) share a conserved biosynthetic activity, and how these three vegetatively expressed isoforms

of the CSLD protein family cooperate in an *in vivo* environment was not yet clear. To examine these questions, I first performed a detailed phenotypic analysis of growth and developmental defects of mutants of the three vegetatively expressed *CSLD* genes, *CSLD2*, *CSLD3*, and *CSLD5*, and found that *csld3* and *csld5* mutants caused varying degrees of growth reduction in root expansion (Figure 3.2), which was enhanced in *csld2/3* and *csld2/5* double mutants (Figure 3.5). This observation indicates that CSLD proteins have positive roles in plant growth and development outside of their prominent roles in tip growth in root hairs. During the root hair elongation process, the stably transformed *kjk-2* (*csld3* null) plant lines expressing *pCSLD3*:Cerulean-CSLD2 could fully rescue the *csld3* hairless defects, indicating the CSLD2 functionally replaced CSLD3 in these developmental processes. Interestingly, partial rescue and shorter root hairs were observed in the stably transformed *kjk-2* (*csld3* null) lines expressing *pCSLD3*:Cerulean-CSLD5 (Figure 3.4). Considering the instability of CSLD5 proteins in non-dividing cells (Gu et al., 2016), lack of accumulation of ectopically-expressed *CSLD5* might be responsible for this partial rescue. We further compared the expression levels of fluorescently-tagged CSLD5 driven by different promoters (Figure 3.4C). Accumulation of Cerulean-CSLD5 was enhanced in root hair cells when driven by the constitutive *35S* promoter compared to the signals of CSLD5 driven by the endogenous *CSLD3* promoter. This genetic evidence demonstrated a gene dosage effect when rescuing the *csld3* mutants: as long as a sufficient amount of CSLD proteins are accumulated in the apical region of the growing tip, root hair extension can be promoted. This dosage effect of CSLD2 and CSLD3 was further supported by genetic rescue analysis of *csld2/csld5*, *csld3/csld5* double mutant plants expressing *pCSLD5*:Citrine-CSLD3 and *pCSLD5*:Citrine-CSLD2, respectively. The fact that both plant lines displayed a reduction of cell wall stubs versus the parental double mutant backgrounds

indicated that when a sufficient amount of CSLD proteins are provided, CSLD2 and CSLD3 are functionally interchangeable during cell plate formation.

The dosage effect of CSLD proteins during root hair elongation and cell plate formation indicated that CSLD proteins, unlike CESA proteins does not require the simultaneous presence of different isoforms to perform catalytic cell wall synthase activities. It further suggest that unlike CESA proteins, CSLD proteins do not need multiple isoforms to form a heterologous complex to perform cellulose synthases activities. The partial rescue in the plants expressing *pCSLD3*:Cerulean-CSLD5 also supports the idea that a minimum amount of cellulose synthases is required to compensate defects caused by lacking cellulose.

Unlike *CSLD2* and *CSLD3,* the expression level of *CSLD5* is highly regulated by the cell cycle (Gu et al., 2016). With a relatively low expression level in non-dividing cells, CSLD5 accumulation rapidly increases upon the initiation of M phase and is highly apparent during anaphase and telophase when cell plate formation occurs. Cerluean-CSLD5 proteins accumulated to the growing cell plate along with Citrine-CSLD2 and Citrine-CSLD3 during anaphase and telophase (Gu et al., 2016).

After completion of cell plate formation, CSLD5 proteins are rapidly degraded in an ubiquitin-dependent process, as MG132 (26S proteasome inhibitor) could stabilize CSLD5 proteins (Gu et al., 2016). The interaction between CSLD5 and APC activator, CCS52A2, confirmed that the CSLD5 protein level is highly regulated by $APC^{CCS52A2}$ cell cycle regulatory complexes (Gu et al., 2016). The instability of CSLD5 might explain why ectopic expression of *CSLD5* could only partially restore root hair elongation. Based on these results, we proposed that despite the β-1,4-glucan synthase activity, CSLD5 might also serve as a “check point” protein

during cytokinesis. The degradation and depletion of CSLD5 protein may represent an M/S1 checkpoint for progression from cytokinesis to new cycles of cell division.

In the process of cell plate formation, neither CSLD2 nor CSLD3 were able to functionally restore the absence of CSLD5. In *csld3/csld5* double mutant plants expressing Citrine-CSLD2, CSLD2 is the solely CSLD protein in dividing cells. The ectopic expression of *CSLD2* causes a reduction in the cell wall stub rate with relation to *csld5* single mutant levels. Similar results were obtained for *csld3/csld5* double mutant plants expressing Citrine-CSLD3. Furthermore, no cell wall stubs were observed in *csld2/csld3* double mutants further supported that CSLD5 is essential and irreplaceable during cell plate formation.

To further investigate whether the CSLD proteins would form a higher-order complexes, I generated transgenic plants expressing inactive versions of CSLD3 proteins. The TAA mutation fully abolished the activity of CESA6 protein without affecting its ability to integrate into a higher-order complexes (Figure 2.9, 2.10). CSCs containing the non-functional CESA6-TAA protein still displayed linear movement with a reduced speed (Figure 2.10). If the CSLD proteins assemble into polymers with other cellulose synthases, then we expect the non-functional CSLD3 subunits might still promote the assembly of complex, and perform some degree of activity. However, this is not the case. The TAA mutation fully abolished the *in vitro* activities of CSLD3 proteins, and no hairs were generated in plants expressing CSLD3-TAA proteins. Combined with the fact that the stably transformed *kjk-2* (*csld3* null) plant lines expressing *pCSLD3*:Cerulean-CSLD2 could fully rescue the *csld3* hairless defects, this result further supported the idea that CSLD proteins do not need multiple isoforms to form a complex to perform cellulose synthases activities. It is intriguing that plants expressing CSLD3-TEA proteins showed a recovery of approximately 50% of the root hair length. Further kinetics

analysis demonstrated that CSLD3-TEA protein displayed higher K_m value, indicating reduced affinity to its substrate. This result is consistent with the slower growth rate of root hairs observed in these plants (Figure 3.7). When the cellulose synthase needs more time to utilize the substrate and synthesize the β-1,4 glucan chain, the deposition rate of newly synthesized cellulose would be reduced, leading to the slower elongation rate in root hairs.

In the end, I confirmed that both CSLD2 and CSLD5 share the conserved β-1,4 glucan synthase activities as CSLD3 protein. This result further supports our view of the CSLD proteins as a distinct family of cellulose synthases.

Why are there two different families of cellulose synthase in plants? One hint comes from the cell wall structures of root hairs, which contain two layers of cell walls. The rapidly growing tip only contains one outer layer of the cell wall. Fibrillar cell wall structures, which are thought to represent cellulose microfibrils in this layer were typically shorter and displayed random arrangement, whereas the inner layer microfibrils were ordered and longer, similar to what is observed in cells primarily undergoing diffuse expansion (Emons and Wolters-Arts, 1983; Emons, 1994; Emons and Mulder, 2000; Newcomb and Bonnett, 1965; Galway et al., 1997; Emons and Mulder, 2000). During diffuse growth, the orientation of cellulose microfibrils synthesized by CESA proteins is consistent with the cortical microtubules arrays underneath the cell membranes (Paredez et al., 2006). These well-organized cellulose microfibrils will further form a rigid extracellular matrix with other cell wall materials. Interestingly, there is no distribution of MTs in the rapidly growing root tip, and treatment with MT depolymerization drugs didn't induce root hair extension defects (Van Bruaene et al., 2004). Due to the fact that CSLD3 accumulated at the tip region of growing hairs, it is reasonable to assume that CSLD proteins are responsible for synthesizing these disordered cellulose structures. However, this soft

and flexible extracellular matrix is very conducive to the development of root hair tip growth in the presence of rapid cell elongation. Similar to root hair elongation, during pollen tube extension and cell plate formation, the speed of elongation is the first priority compared to the stability of the overall structure.

The second layer of the inner cell wall is found at the subapical region of the root hairs and serves to strengthen the overall structural stability. Consistent with the presence of the second layer of the inner cell wall, cortical microtubules also appears in the subapical region (Van Bruaene et al., 2004). Furthermore, CESA proteins are found to localize on the cell membrane in this region. Taken together, these findings strongly support the idea that compared to CESA proteins involved in synthesizing classic cellulose microfibrils in most cell wall structures, CSLD proteins might play a "pioneer" role during certain specific developmental processes, where the cells are trying to use the shortest time to form a soft and flexible extracellular matrix to meet the needs of rapid cell elongation. The balance between "fast rate" vs "rigid structure" forces the plants to maintain two types of cellulose synthases that could meet different needs in various developmental processes.

Another piece of evidence supporting this idea comes from how CSLD proteins perform β-1,4 glucan synthase activity. Unlike CESA proteins, multiple pieces of evidence in this chapter indicated that CSLDs do not require multiple isoforms to form higher-order heteropolymers. The smaller polymer or monomer format of CSLD proteins might be more adapted to the rapid synthesis of cellulose. Taken together, these results indicate that while all three vegetative expressed CSLD proteins maintain conserved β-1,4 glucan synthases activities, CSLD5 plays essential roles during cell plate formation. CSLD proteins do not require different isoforms to synthesize heterologous complexes *in vivo*.

3.5 MATERIALS AND METHODS

Plant material and growth conditions

Arabidopsis thaliana lines used in this study were derived from *Col-0* ecotype. Seeds were sterilized with 10% Clorox bleach solution, rinsed five times with distilled water, then stored at 4°C for 2 days before being plated on growth medium comprised of 0.25X Murashige and Skoog Basal Medium,1% sucrose, and 0.6% phytagel. Plates were placed vertically in a growth chamber at 21°C and grown under long-day conditions (16 hours light (200 uE/m^2s)/8 hours dark photoperiod). Three-day-old dark-grown seedlings were used for microscopy analysis. Five-day-old seedlings were used for morphology analysis. For propagation of mature plants, 14-day old seedlings were transferred to soil and grown in environmental chambers at 21°C under long-day conditions (16 hours light/8 hours dark photoperiod).

Yeast expression plasmid construction and growth conditions

S. cerevisiae (Strain INVSc1, Thermo Fisher, Cat#: C81000) was used for protein expression. Untransformed yeast was cultured in YPD medium. Positive colonies containing pYES2/NT C plasmids (Thermo Fisher, Cat#: V825220), expressing N-terminal His-tagged CSLD2, CSLD3, CSLD5, CSLD3-TEA, were selected and cultured overnight at 30°C and 180 rpm in SC-Ura + Glucose medium composed of 1.9 g/L SC-Ura (uracil drop-out) powder, 1.7 g/L yeast nitrogen base without amino acids and ammonium sulfate, 5 g/L ammonium sulfate, and 20 g/L glucose. Yeast cells were harvested, rinsed in sterile water, and used to inoculate 200 ml of SC-Ura + Raffinose medium with the same nitrogenous base composition containing 20 g/L raffinose to an OD_{600} equal to 0.03. Cultures were grown for 14 to 16 h at 30°C and 180 rpm until

the OD_{600} reached 2.0. Protein expression was induced by addition of 800 ml of SC-Ura + Galactose medium containing 20 g/L galactose, and cells were incubated for an additional 6 h at 30°C and 180 rpm. Yeast cells were harvested, weighed, flash frozen in liquid nitrogen, and stored at -80°C.

Morphology analysis

The whole plant were pictured at three weeks old stage using Canon Kiss 5 digital camera. The raw images were collected at 5184*3456 pixel and cropped using Adobe Photoshop using the same scale bar level.

Root length measurement

Images of 5-day-old seedlings were recorded using an Epson Perfection 4990 Photo scanner. The lengths of root regions were measured using Fiji-ImageJ (Schindelin et al., 2012). All transformed lines were grown side by side on the same plate, and at least 15 individuals were measured per line. Three independent biological replicates were performed for each line.

Fluorescent imaging analysis

Images were acquired using a Leica confocal laser scanning microscope SP8 using a 60X oil lens (Type F Immersion oil, NA=1.518) and processed with the Leica Application Suite X (LAS X) Life Science Microscope software. YFP and citrine fluorescence were excited at 514 nm and visualized from 519 nm to 650 nm. Cell wall was stained using FM4-64, which was excited at 488 nm and visualized from XXX nm to XXX nm. Raw images were collected using 512*512 pixel images. Brightness and contrast were adjusted accordingly using Adobe Photoshop.

Yeast protein extraction, purification, and proteoliposome reconstitution

5 g of yeast cells (corresponding to 8 L of SC-Ura + Galactose medium) expressing His-tagged CESA6, CSLD3, CSLA9, or an empty vector were resuspended in 20 ml lysis buffer (50 mM Hepes pH=7.4, 300 mM NaCl, 1 mM $MgCl_2$, 1 mM $MnCl_2$, 5 mM cellobiose, 5% glycerol, 50 mM Pefabloc SC plus (Sigma, Cat#: 11873601001), 1 mM PMSF (Thermo Fisher, Cat#: 36978)). Cells were lysed by passage through a French Press (20,000 PSI) twice at 4°C. Post-nuclear supernatant (PNS) was isolated by spinning in a SORVALL SS-34 rotor at 10,000 x g for 20 minutes at 4°C. A total membrane pellet was isolated by spinning the PNS fraction at 100,000 x g in a Fiberlite F65L-6 X 13.5 rotor at 4°C for 1 hour. The supernatant was discarded and the total membrane pellet was gently resuspended in 5 ml resuspension buffer (50 mM Hepes pH=7.4, 300 mM NaCl, 1 mM $MgCl_2$, 1 mM $MnCl_2$, 5 mM cellobiose, 50 mM Pefabloc SC plus, 1 mM PMSF, 2% LFCE-14 (Anatrace, Cat#: L414)) and incubated at 4°C for 30 minutes with gentle end-over-end shaking. Resuspended membranes were then spun at 100,000 x g in a Fiberlite F65L-6 X 13.5 rotor at 4°C for 1 h, and the supernatant was carefully collected and incubated at room temperature with Ni-NTA slurry (Thermo Fisher, Cat#: 88221) for 1 h. The slurry was transferred to a disposable chromatography column (BioRad, Cat#: 7321010) and washed with 5 ml wash buffer (50 mM Hepes pH=7.4, 300 mM NaCl, 1 mM $MgCl_2$, 1 mM $MnCl_2$, 5 mM cellobiose, 0.05% LFCE-14, 30 mM imidazole). Protein fractions (2.5 ml) were eluted from the Ni-NTA column with a 10 ml linear gradient of 30–250 mM imidazole in wash buffer. Protein fractions containing the His-tagged cell wall synthase enzymes were concentrated into wash buffer lacking imidazole using an Amicon Ultra 15 ultracel 100k centrifugal filter units (Sigma, Cat#: UFC910024) at 4,000 x g for 10 minutes. For reconstitution of purified cell wall synthases into

proteoliposomes, 10 mg of yeast lipids (Avanti, Cat#: 190000P) were dissolved in 1 ml chloroform in a glass test tube, and then evaporated with nitrogen and dried in a vacuum chamber at room temperature for 1 h. The resulting yeast lipid film was resuspended in reconstruction buffer (50 mM Hepes pH=7.4, 300 mM NaCl, 1 mM $MgCl_2$, 1 mM $MnCl_2$, 5 mM cellobiose, 6% LFCE-14), and mixed with vigorous vortexing. Purified, detergent-solubilized proteins were mixed with 300 μl of the solubilized lipid fraction in a protein-to-lipid molar ratio of 1: 4000 and incubated for 1 h at 4°C with gentle end-over-end shaking. Meanwhile, 0.2 g SM2 Adsorbent beads (Bio-Rad, Cat#: 1528920) were washed with 1 ml bead buffer (50 mM Hepes pH=7.4, 300 mM NaCl, 1 mM $MgCl_2$, 1 mM $MnCl_2$, 5 mM cellobiose) for 1 h at 4°C with gentle end-over-end shaking. The 300 μl protein-lipid mixture was diluted with 600 μl bead buffer and incubated with 0.2 g of pre-washed SM2 Adsorbent beads for 1 h. An additional 900 μl of bead buffer was added to the protein-lipid mixture and the resulting 1800 μl protein-lipid mixture was transferred to a new tube containing 0.2 g of pre-washed SM2 Adsorbent beads and incubated for 1 h with gentle end-over-end rotation. This step was repeated twice more (for a total of four SM2 Adsorbent bead extractions) to completely extract the detergent. The resulting proteoliposomes were layered over a discontinuous sucrose gradient (200 μl of 10%, 500 μl of each 15%, 25%, 35% and 60% w/v sucrose in bead buffer) and spun for 2 h in a TH-660 swinging bucket rotor at 150,000 x g at 4°C. The proteoliposome layer (Figure S5D, fraction 6) was collected and transferred to an Avanti Mini Extruder equipped with a 200 nm pore filter (Cat#: 610020) and passed through 20–30 times to generate unilamellar proteoliposomes of similar size, and then spun for 1 h in a Thermo Fisher TH-660 swinging bucket rotor at 150,000 x g at 4°C, and resuspended with 100~200 μl bead buffer for UDP-Glo or GDP-Glo glycosyltransferase assays (Promega, Cat#: V6961, VA1090). Briefly, 500–1000 ng proteoliposomes were incubated with 1 mM UDP-Glc in a 20 μl reaction containing

50 mM Hepes pH=7.4, 300 mM NaCl, 1 mM $MgCl_2$, 1 mM $MnCl_2$, and 5 mM cellobiose for 1 h. 20 μl of freshly prepared nucleotide detection reagent was added and incubated for 15 minutes. Total luminescence was measured using a Tecan plate reader (infinite 200Pro, S/N: 1501003733), and the amount of UDP produced was calculated based on a UDP standard curve.

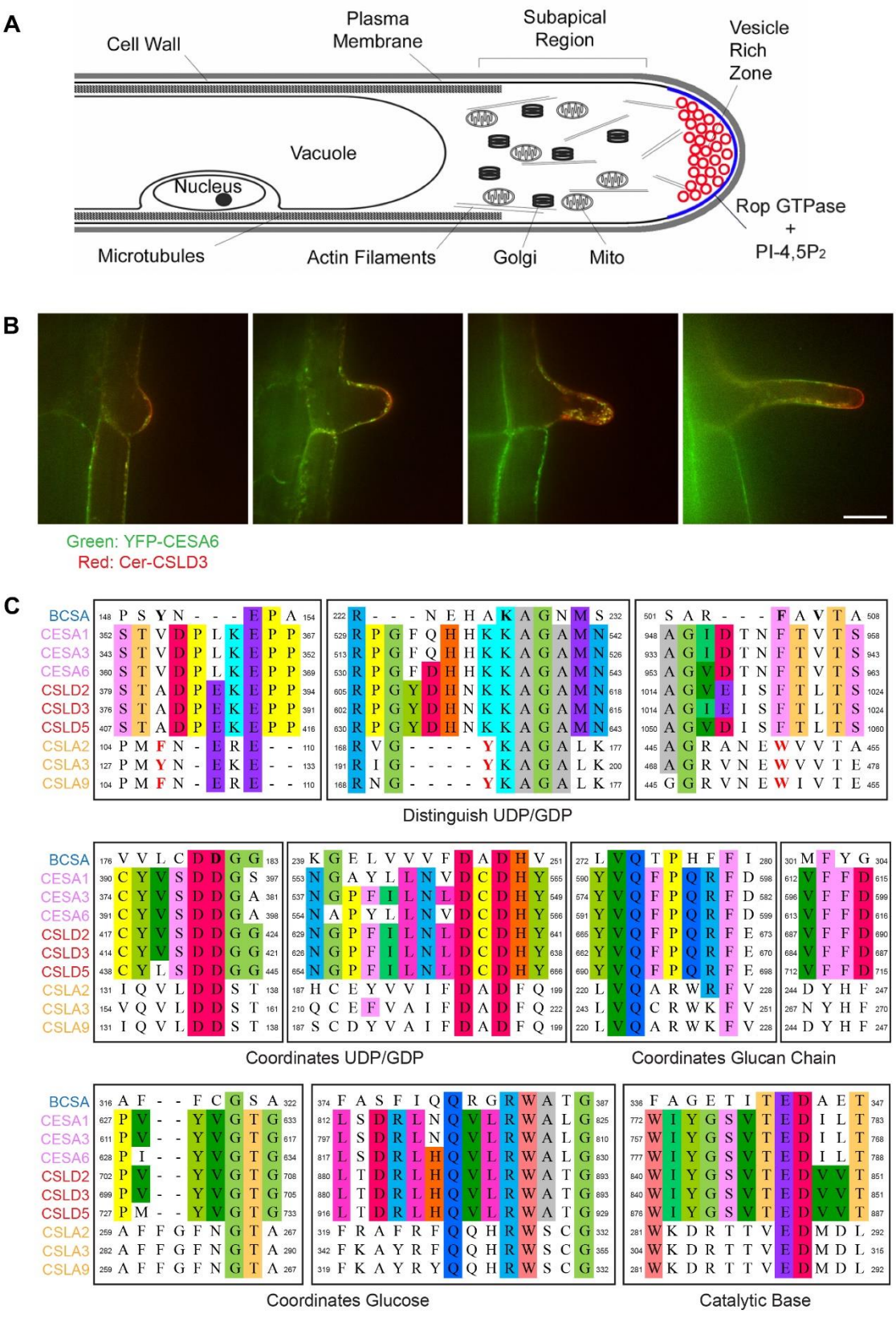
A
Cell Wall
Plasma Membrane
Subapical Region
Vesicle Rich Zone
Vacuole
Nucleus
Rop GTPase + PI-4,5P2
Microtubules
Actin Filaments
Golgi
Mito
B
Green: YFP-CESA6
Red: Cer-CSLD3
C
BCSA
CESA1
CESA3
CESA6
CSLD2
CSLD3
CSLD5
CSLA2
CSLA3
CSLA9
Distinguish UDP/GDP
Coordinates UDP/GDP
Coordinates Glucan Chain
Coordinates Glucose
Catalytic Base

Figure 3.1. Sub-cellular localization of CESA6 and CSLD3 proteins in root hairs.

(A) A schematic model of root hairs display the vesicle rich zone close to the apical region of plasma membrane of growing root tip. The Golgi is accumulated in subapical region, where no cortical microtubules are observed. **(B)** The fluorescence of CESA6 and CSLD3 proteins was recorded in growing root hairs of five-day old seedlings. Green signals represent YFP-CESA6, Red signals represent Cer-CSLD3. The distinct localization from two colors represents the specific accumulation of CSLD3 at the apical of plasma membrane. **(C)** Alignment of amino acid residues of AtCESAs (pink), AtCSLDs (red) and AtCSLAs (yellow) was constructed by MEGA7 (Kumar et al., 2016). The amino acids in bold represent the identical sequences in three families including nucleotide coordinating regions (DD, DxD motifs), sugar coordinating regions (Q/RxxRW motif), and catalytic bases (TED motif). AtCSLD sequences showed higher identity to cellulose-synthesizing CESAs in these regions.

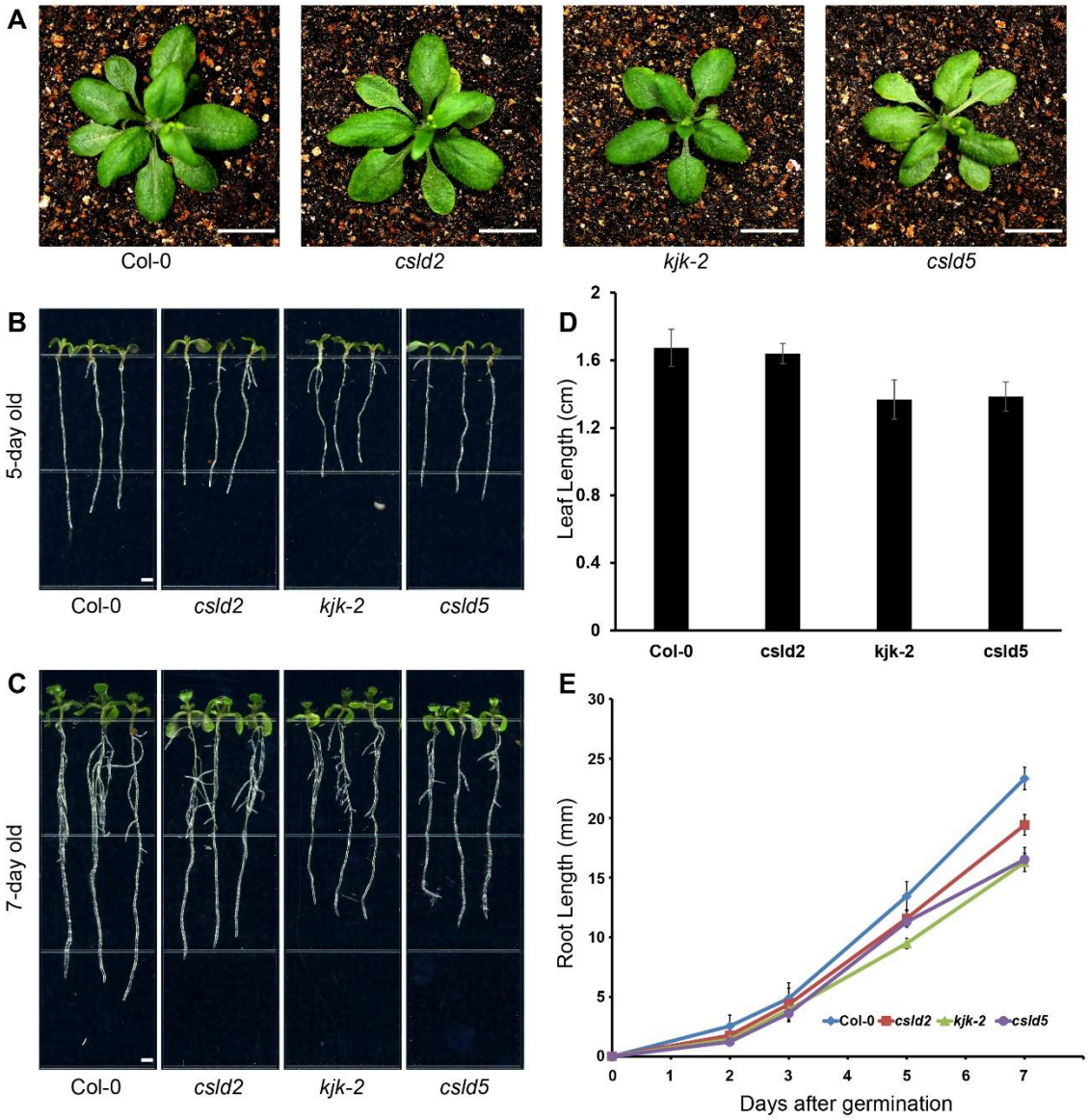
A
Col-0
csld2
kjk-2
csld5
B
5-day old
Col-0
csld2
kjk-2
csld5
C
7-day old
Col-0
csld2
kjk-2
csld5
D
Leaf Length (cm)
2
1.6
1.2
0.8
0.4
0
Col-0
csld2
kjk-2
csld5
E
Root Length (mm)
30
25
20
15
10
5
0
Col-0
csld2
kjk-2
csld5
0
1
2
3
4
5
6
7
Days after germination

Figure 3.2. The single mutant of CSLDs displayed growth defects.

(A) Rosette size of three-week old plants. *csld3*$^{kjk-2}$ and *csld5* mutants displayed smaller overall size of rosette leaves, while no significant changes was observed in *csld2* mutants. The length of rosette leaves was measured and quantified in **(D)**. Five-day-old **(B)** and seven-day-old **(C)** seedlings were recorded using an Epson Perfection 4990 Photo scanner. The lengths of root regions were measured using Fiji-ImageJ (Schindelin et al., 2012). *csld2*, *csld3*$^{kjk-2}$ and *csld5* single mutants displayed varying degrees of growth reduction in root expansion. The length of roots is recorded and quantified in **(E)**. The *csld* mutants displayed a slower growth rate compared to wild type (Col-0).

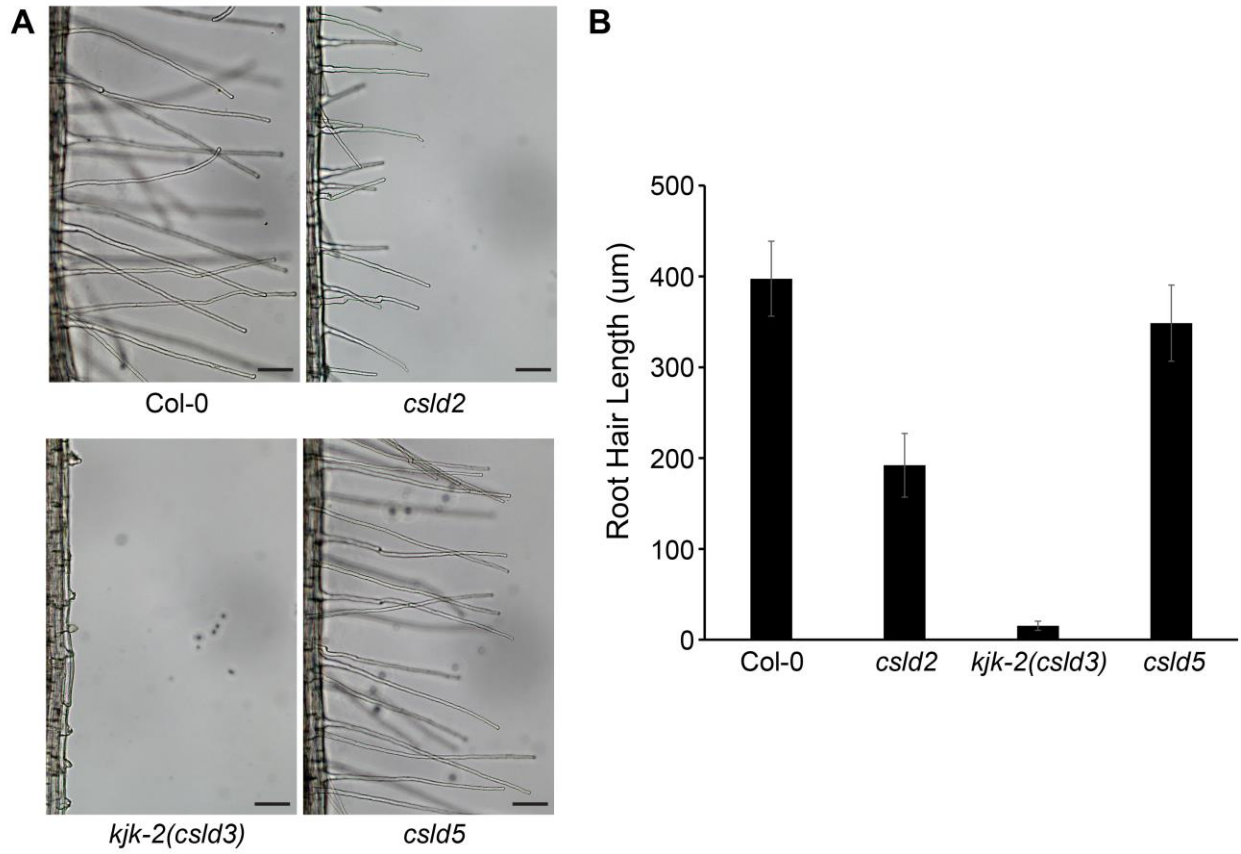

Figure 3.3. CSLD2 and CSLD3 displayed root hair defects.

(A) Root hair morphology analysis in three *csld* single mutants. Five-day-old seedlings were used to observe and record the phenotypes. In *csld2* mutants, the root hair length displayed a nearly ~50% reduction compared to wild type (Col-0). Bulges were formed at the base of growing root hairs. In *csld3*$^{kjk-2}$mutants, bulges were able to initiation, while nearly no root hair cells were able to continue the tip-restricted expansion, and results in a hairless defect. In *csld5* mutants, the morphological shape of root hair is not affected compared to wild type (Col-0). The length of root hairs is quantified in **(B)**.

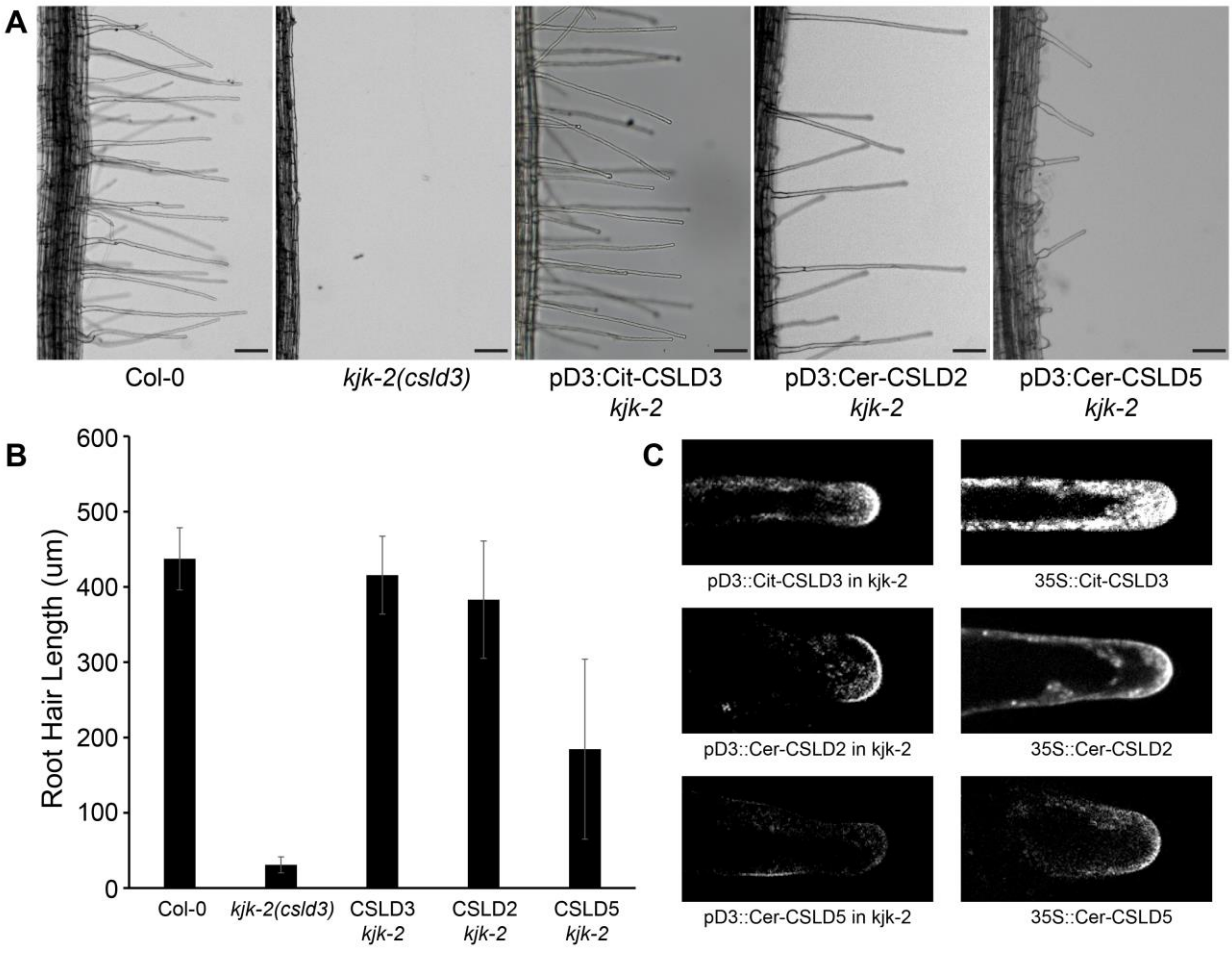
A
Col-0
kjk-2(csld3)
pD3:Cit-CSLD3
kjk-2
pD3:Cer-CSLD2
kjk-2
pD3:Cer-CSLD5
kjk-2
B
Root Hair Length (um)
600
500
400
300
200
100
0
Col-0
kjk-2(csld3)
CSLD3
kjk-2
CSLD2
kjk-2
CSLD5
kjk-2
C
pD3::Cit-CSLD3 in kjk-2
35S::Cit-CSLD3
pD3::Cer-CSLD2 in kjk-2
35S::Cer-CSLD2
pD3::Cer-CSLD5 in kjk-2
35S::Cer-CSLD5

Figure 3.4. Ectopic expressed CSLD2 and CSLD5 driven by the *CSLD3* promoter promoted the root hair elongation.

(A) Root hair morphology analysis of stably transformed *csld3*$^{kjk-2}$ mutant plants expressing fluorescence tagged CSLD2, CSLD3, and CSLD5 under the endogenous CSLD3 promoter. When expressing Citrine-CSLD3, the hairless defects is fully restored, and root hair length is indistinguishable to wild type (Col-0). When expressing Cerulean-CSLD2, normal root hairs are generated as well. Shorter root hairs are observed in plant expressing Cerulean-CSLD5. The lengths of root hairs in these plants are quantified in **(B)**. **(C)** Localization of fluorescence tagged CSLD2, CSLD3, and CSLD5 driven by the endogenous CSLD3 promoter (left three panels) and *35S* promoter (right three panels) in growing root hair cells.

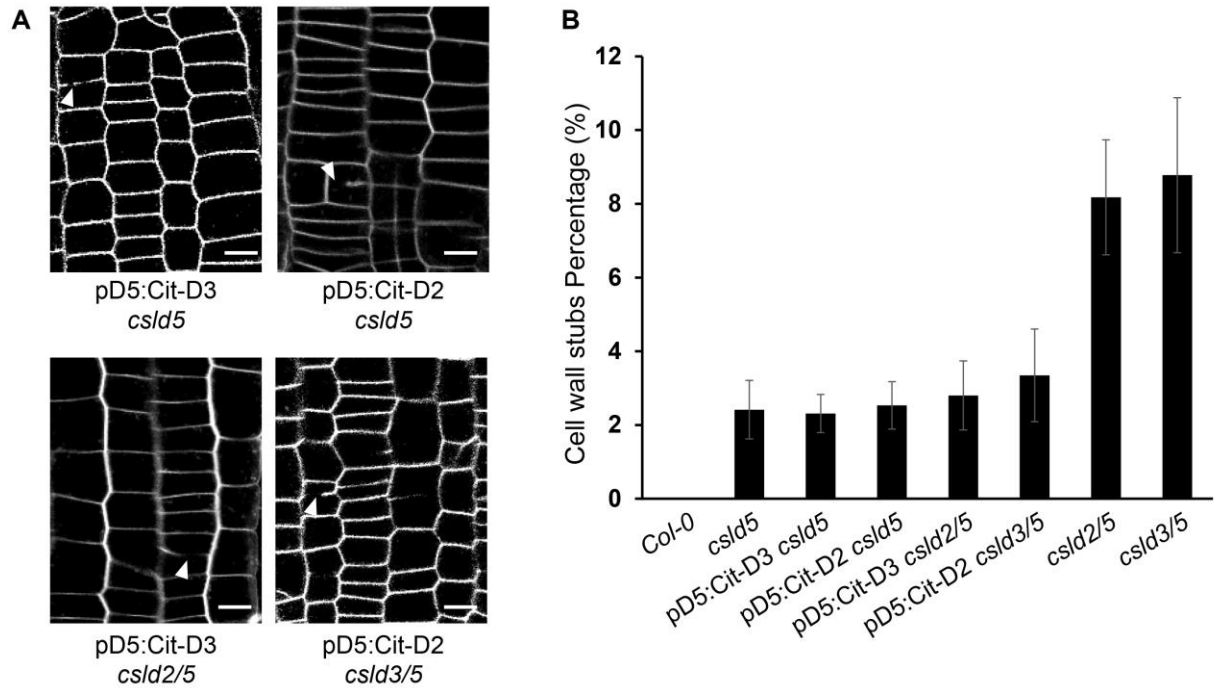

Figure 3.5. CSLD5 is essential and irreplaceable for cell wall deposition in cell plate formation during cytokinesis.

(A) Root length analysis of five-day-old seedlings. The growth reduction of root tissue expansion is significant enhanced in *csld2/csld3, csld2/csld5,* and *csld3/csld5* double mutants. The length of roots was recorded and quantified in **(B). (C)** Confocal images of root epidermal cells from five-day-old seedlings. The seedlings were first stained with FM4-64 to visualize the edges of the root cortical cells. The cell division defects (cell wall stub) exhibited in *csld5* mutant are highly enhanced in *csld2/csld5, csld3/csld5* double mutants (white arrowheads). No cell wall stub is observed in *csld2/csld3* double mutants. The percentage of cell wall stubs is quantified in **(D).**

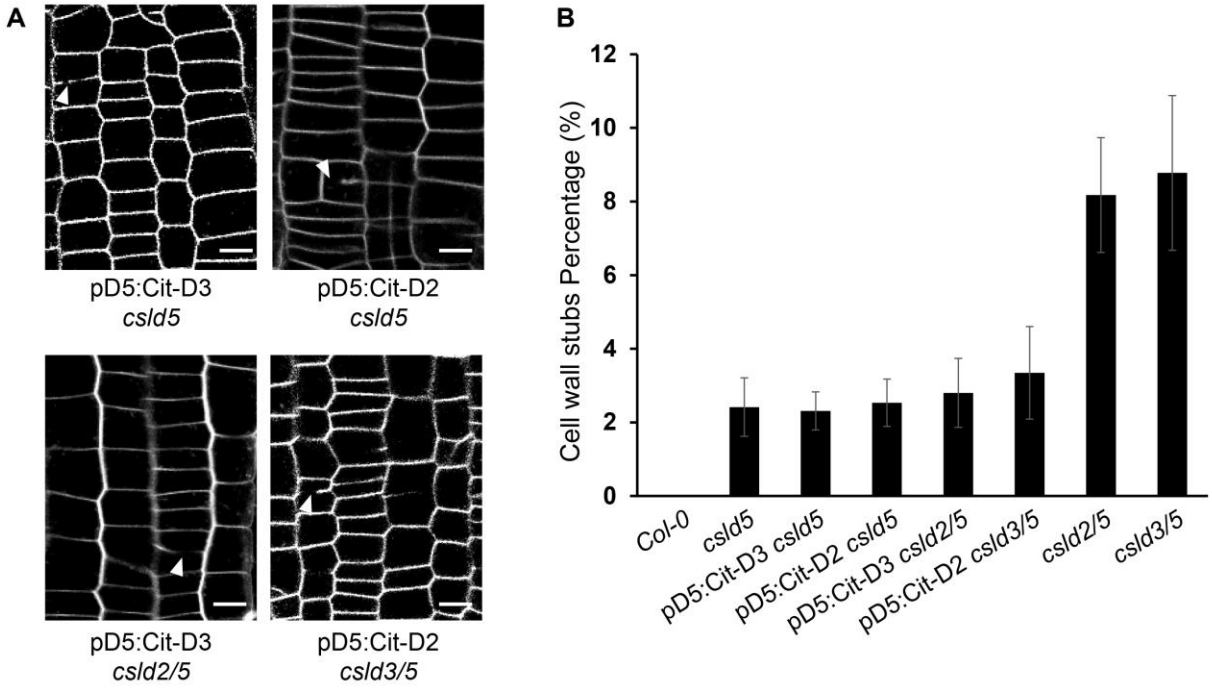

Figure 3.6. Neither Citrine-CSLD2 nor Citrine-CSLD3 can replace CSLD5 activity in *csld5* mutant backgrounds.

(A) Confocal images of root epidermal cells from five-day-old seedlings. The cell division defects (cell wall stub) exhibited in *csld5* mutant cannot be restored in stably transformed plants expressing CSLD2 or CSLD3 driven by the endogenous CSLD5 promoter (upper two panels). When expressing CSLD2 or CSLD3 in *csld2/csld5, csld3/csld5* double mutant background, the presence of CSLD2 and CSLD3 could reduce the percentage of cell wall stubs compared to the parental *csld2/csld5, csld3/csld5* double mutants, and reaches to similar level to single *csld5* mutants. The percentage of cell wall stubs is quantified in **(B).**

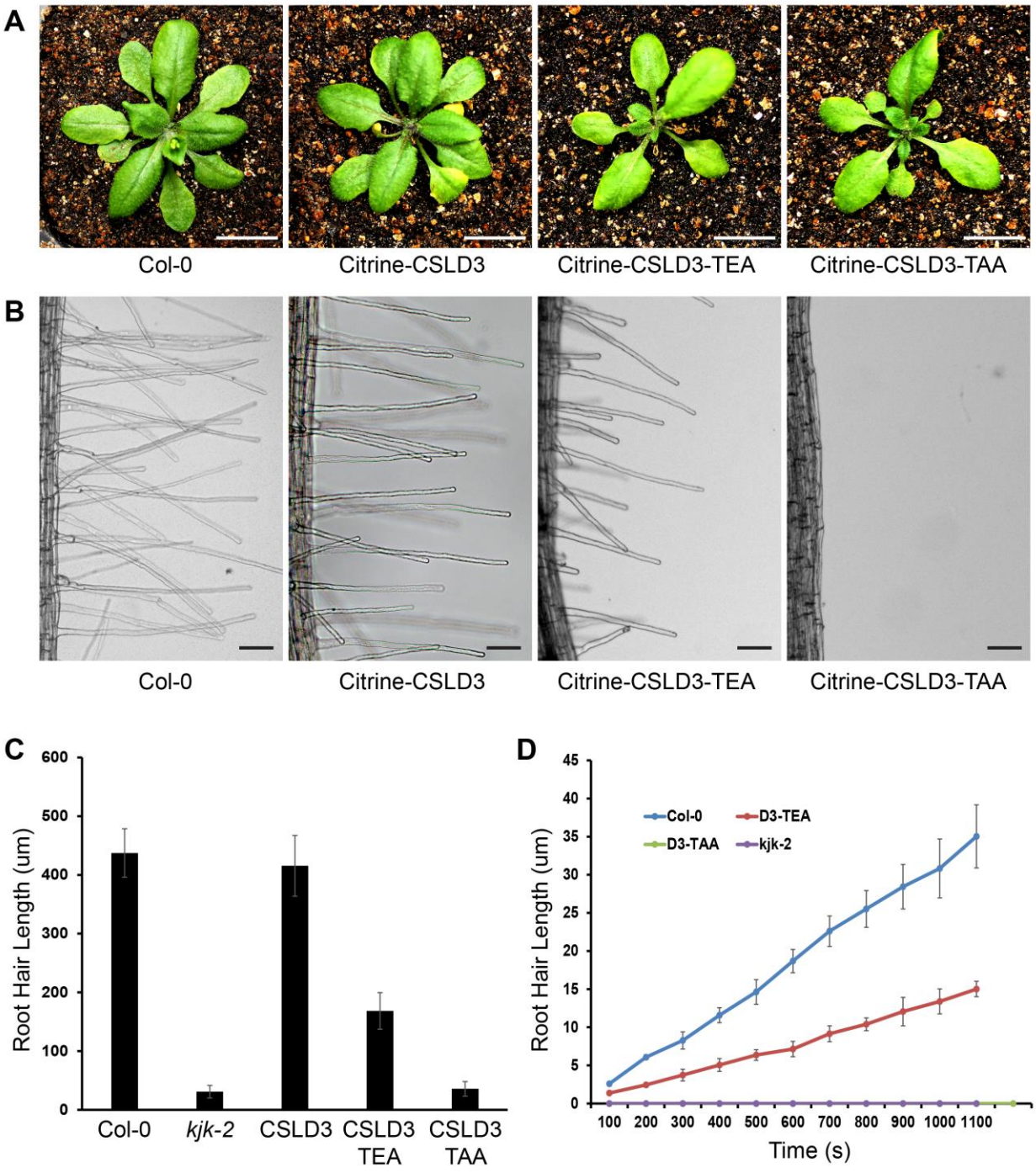
A
Col-0
Citrine-CSLD3
Citrine-CSLD3-TEA
Citrine-CSLD3-TAA
B
Col-0
Citrine-CSLD3
Citrine-CSLD3-TEA
Citrine-CSLD3-TAA
C
Root Hair Length (um)
600
500
400
300
200
100
0
Col-0
kjk-2
CSLD3
CSLD3 TEA
CSLD3 TAA
D
Root Hair Length (um)
45
40
35
30
25
20
15
10
5
0
Col-0
D3-TEA
D3-TAA
kjk-2
100 200 300 400 500 600 700 800 900 1000 1100
Time (s)

Figure 3.7. The quantitative rescue of *csld3^{kjk-2}* hairless defects requires the catalytic activity of a β-1,4-glucan synthase.

(A) Rosette size of three-week old plants. The stably transformed *csld3^{kjk-2}* plants expressing Citrine-CSLD3 exhibits indistinguishable rosette size compared to wild type (Col-0). A smaller rosette size is observed in plants expressing Citrine-CSLD3-TEA and Citrine-CSLD3-TAA. The newly formed second layer of rosette leaves are still very small compared to wild type (Col-0), where the second layer of rosette leaves are in mature stage. **(B)** Root hair morphology analysis of five-day-old seedlings. The stably transformed *csld3^{kjk-2}* plants expressing Citrine-CSLD3-TEA partially rescue the hairless defects and managed to generate root hairs are half long compared to wild type (Col-0). The length of root hairs is quantified in **(C)**. **(D)** The root hair length over time was recorded every 100 seconds for these plants. The slope represents the growth rate of root hairs. The stably transformed *csld3^{kjk-2}* plants expressing Citrine-CSLD3-TEA display slower growth rate compared to wild type (Col-0), while plants expressing Citrine-CSLD3-TAA has no growth rate due to failures of promoting the tip-restricted expansion in root hair cells.

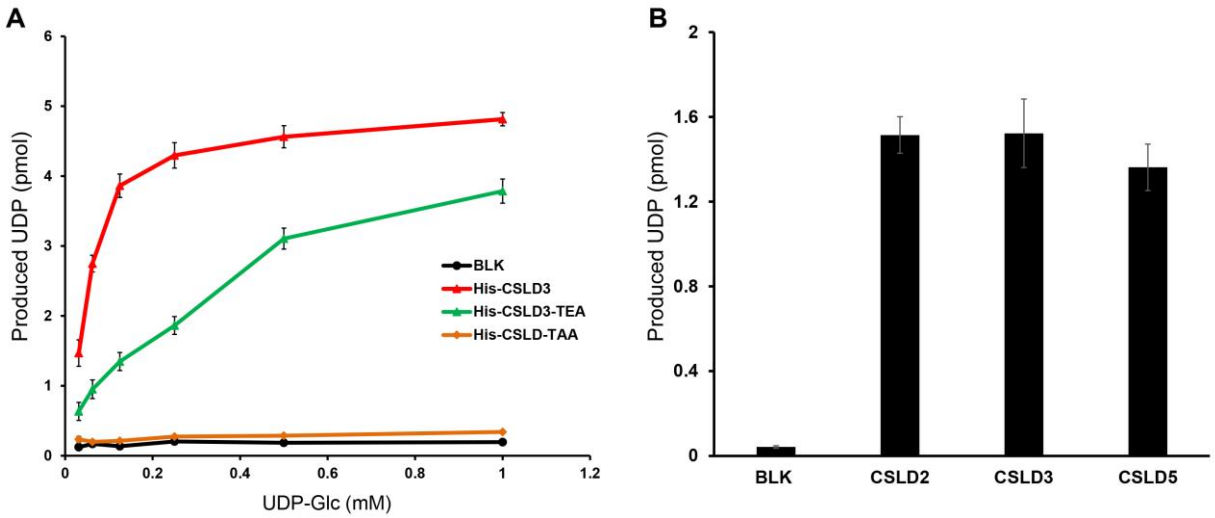

Figure 3.8. Purified CSLD2 and CSLD5 displayed β-1,4 glucan synthase activities *in vitro*.

(A) Proteoliposomes containing His-CSLD3 (red line) and His-CSLD3-TEA (green line) displayed saturable UDP-forming activities when supplied with UDP-Glc. The Km values are 62 uM and 255 uM, respectively. Proteoliposomes containing His-CSLD3-TAA (yellow line) displayed no UDP-forming activities, similar to the negative control (BLK, black line). **(B)** Proteoliposomes containing His-CSLD2, His-CSLD3, and His-CSLD5 displayed similar UDP-forming activities when supplied with UDP-Glc.

A

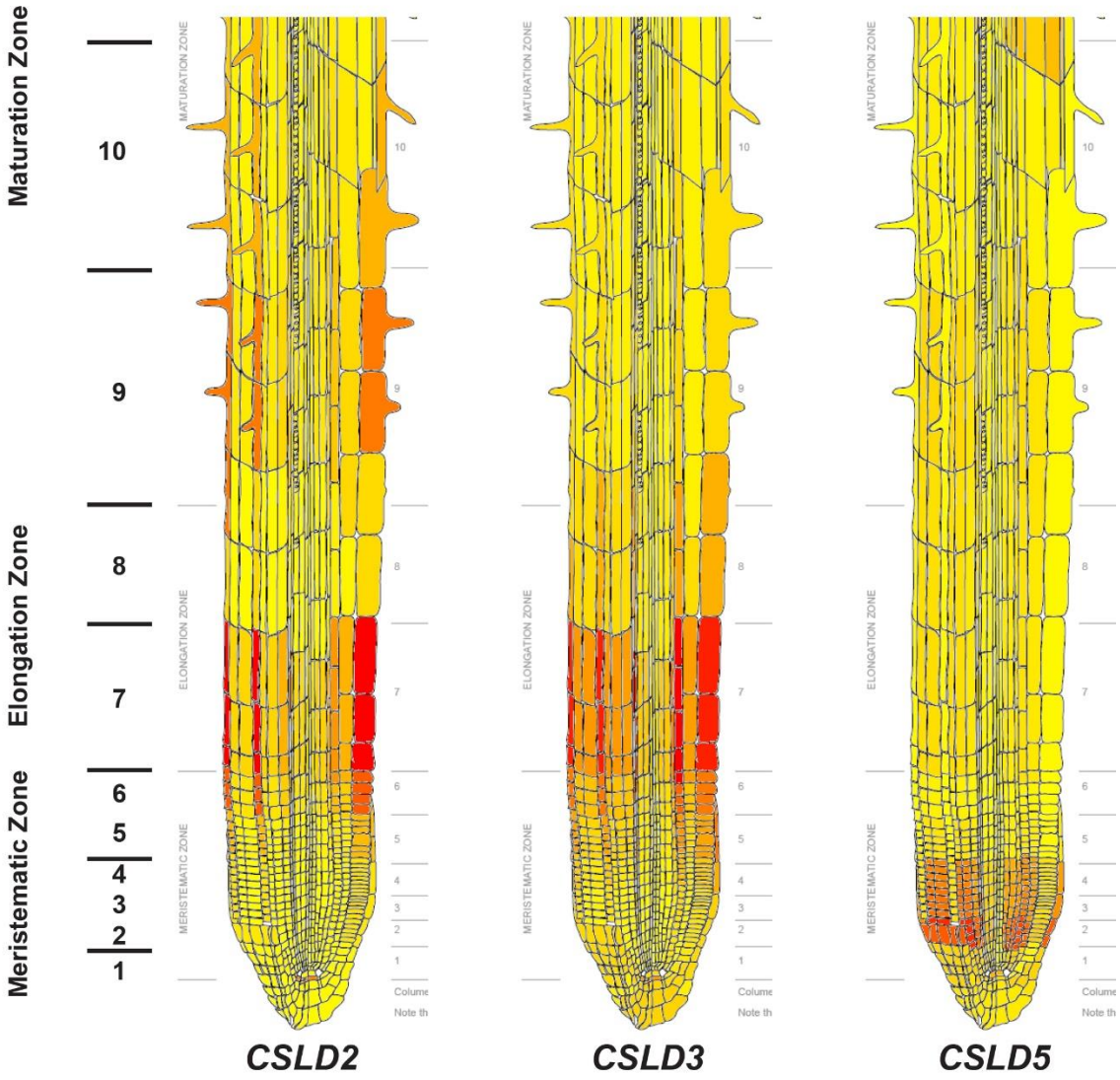

B

Region	*CSLD2*	*CSLD3*	*CSLD5*
2 (Cortex cells)	143.41	144.55	**333.98**
8 (Root hair initiation)	744.69	**1091.58**	14.79
9 (Root hair tip growth)	**2699.68**	484.02	18.35
10 (Root hair tip growth)	1527.0	442.38	8.92

Figure 3.9. *CSLD2*, *CSLD3*, and *CSLD5* are differently expressed in root hair cells.

(A) Root expression patterns of *CSLD2* (left), *CSLD3* (middle), and *CSLD5* (right) genes generated using the *Arabidopsis* eFP Browser (http://bar.utoronto.ca/efp/cgi-bin/efpWeb.cgi). Both *CSLD2* and *CSLD3* displayed increased expression levels in root hair cells, while CSLD5 was accumulated in root cortical cells meristematic zone (region 2) and displayed lowly expressed in root hair cells. *CSLD3* was expressed in hair cells initiating root hair growth (region 8), while *CSLD2* had high expression level after the root hairs were initiated (region 9). **(B)** Absolute expression level of *CSLD2*, *CSLD3*, and *CSLD5* in various regions. The highest values were highlighted in red.

Chapter 4 Conclusions and Future Directions

4.1 CONCLUSIONS

My research work during my Ph.D. training focused on the functions of CSLD proteins during plant cell wall deposition in *Arabidopsis*. CSLD proteins were first identified at the pollen tubes of *Nicotiana alata* (Doblin et al., 2001). Given the high similarity to CESA proteins, CSLDs were initially proposed as β-1,4-glucan synthases involved in pollen-tube wall synthesis (Doblin et al., 2001). Later research showed that *csld5* mutants displayed reduced growth and altered xylan occurrence, which indicated a reduction of xylan, and homogalacturonan synthase activity in the absence of CSLD5 protein (Bernal et al., 2007). More recently, detailed biochemical activities were described for CSLD proteins expressed in isolated microsomal membranes from tobacco. These results indicated that CSLD proteins are utilizing GDP-Man as the substrate to form β-1,4-mannan (Verhertbruggen et al., 2011, Yin er al, 2011). Previous studies in our laboratory supported an alternate interpretation that CSLD3 is a cellulose synthase (Park et al., 2011, Yang et al., 2020). A functional YFP-CSLD3 protein accumulated to the apical region of plasma membranes in hair cells undergoing tip growth. Genetic complementation of hairless defects in *csld3* mutants with the functional chimeric proteins where the CSLD3 catalytic region (residues 340–921) was replaced with the corresponding CESA6 catalytic domain supported a UDP-glucose-dependent cellulose synthase-like activity for CSLD3 (Park et al., 2011). In addition, we showed that a functional CESA6 chimeric fusion protein

containing the corresponding CSLD3 catalytic domain integrates into plasma membrane-localized CSCs and can fully rescue both the hypocotyl elongation and cellulose accumulation defects in the *cesa6* mutants (Yang et al., 2020). Furthermore, we showed that proteoliposomes containing purified CESA6 and CSLD3 utilize UDP-glucose and accumulate β-1,4-glucan products (Yang et al., 2020). One significant conclusion based on my work described in chapter two has been to conclusively address questions regarding whether CSLD3, and by extension other CSLDs, are β-1,4-mannan synthases that utilize GDP-mannose substrates or β-1,4-glucan synthases that utilize UDP-glucose. Using genetic, biochemical, and cell biology approaches, I provided multiple pieces of evidence to support that a member of the CSLD protein family, CSLD3, is a β-1,4-glucan synthase. The fact that β-1,4- polysaccharides synthesized by the catalytic domain of CSLD are able to assemble into cellulose microfibrils indicates the nature of these polysaccharides is chemically equivalent.

My work described in chapter three mainly focused on how CSLD proteins perform the β-1,4-glucan synthase activity *in vivo*. Proteoliposomes containing purified CSLD2 and CSLD5 displayed similar β-1,4 glucan synthase activities as observed initially for CSLD3. These results further confirmed that in *Arabidopsis*, in addition to the CESA protein family, the CSLD protein family is the second cellulose synthase family. The fact that ectopic expressed CSLD2 or CSLD5 driven by the endogenous CSLD3 promoter could fully (CSLD2) or partially (CSLD5) rescue the *csld3* hairless defects (Figure 3.4) supports that CSLD proteins are functionally interchangeable during tip-restricted expansion, therefore demonstrated gene dosage effects when rescuing the *csld* mutant defects. The rescue analysis of a catalytically dead version of CSLD3 proteins showed high consistencies between the degrees of activities of CSLD3 proteins and the degrees of the rescue of root hair lengths. When the activity of CSLD3 was reduced with

a four-fold Km value increase (CSLD3-TEA), root hair length displayed a partial reduction (Figure 3.7, 3.8). When the activity of CSLD3 was fully abolished (CSLD3-TAA), no root hair formation was observed (Figure 3.7, 3.8). Together, these results indicated that CSLD proteins do not require the concurrence of multiple isoforms and the formation of the heterologous higher-order complex. Even though all three vegetatively expressed CSLD proteins are important for cell plate formation, CSLD5 plays essential and irreplaceable roles during this process, which is probably closely related to cell cycle regulation of the expression level of CSLD5.

According to the differences between CESA and CSLD proteins, I proposed a hypothesis explaining the functional diversity of these two distinct cellulose synthases. CESA proteins are involved in synthesizing β-1,4 glucan chains that assemble into well-organized cellulose microfibrils, which serve as the major load-bearing components in the classic cell wall matrix providing necessary mechanical support for plant cells. On the other hand, CSLD proteins play a "pioneer" role of cell wall synthases and are essential for the *de novo* synthesis of cellulose during certain specific developmental processes such as tip growth and cell plate formation. These developmental processes share two important similarities: the requirement of rapid and *de novo* synthesis of cell walls. Differences of cellulose in two layers of root hair cell walls, to some extent, supported this hypothesis. Due to the fact that the nature of β-1,4 glucan chains synthesized by CESA protein and CSLD proteins are chemically equivalent, studies on whether CSLD proteins form higher order complexes *in vivo* are a key piece needed to support this hypothesis.

4.2 FUTURE DIRECTIONS

Genetic evidence suggests that CSLD proteins do not require the formation of heterologous higher-order complexes. Structure analysis demonstrated that detergent-solubilized CSLD3 proteins are able to assemble into a complex similar in size and shape to the trimeric structures of individual lobes of cellulose synthase rosette complexes *in vitro* (Yang et al., 2020). It is unclear whether CSLD proteins form higher order, homopolymeric complexes *in vivo* to perform synthase activities. Co-immunoprecipitation (Co-IP) analysis could help to directly answer this question. The mating-based split ubiquitin yeast two-hybrid system (mbSU-Y2H) system and bimolecular fluorescence complementation (BiFC) could be alternative approaches to test to what extent different CSLD proteins could assemble into higher order complexes, and to what degree different CSLDs might integrate into these complexes. Following this direction, it will be interesting to investigate the potential differences of cellulose microfibril diameters synthesized by CESA proteins and CSLD proteins. However, the direct observation of cellulose deposition in root hair cells would be a challenge due to the cylindrical shape of root hairs, and the apical region of root hair cells is too small for microscopy. Inspired by the fibrillar structures observed in recent reconstitution experiments with plant CESAs (Purushotham et al., 2016; Cho et al., 2017), the protoplast expression system could be a potential approach to overcome this problem. Feeding UDP-Glc as substrates, protoplast fractions generated from stably transformed plants expressing CESA or CSLD proteins could serve as the enzymatic platform, and we could determine whether any fibril structure is detected using electron microscopy.

To further supplement the work described in chapter three and make it publishable, some additional experiments will likely be needed. While the *in vitro* activity assay with proteoliposomes containing purified CSLD2 and CSLD5 confirmed their β-1,4-glucan synthases

activities, the Km values of these two proteins were not determined. Furthermore, it would be interesting to know whether the TEA mutation of CSLD3 protein impacts the ability of these enzymes to actually form β-1,4-linkaged glucan. While it is likely this synthesis step would be reduced based on the observed lower affinity for UDP-glucose, we may observe much more significant inhibition of the ability to form new glycosidic bonds than we observe for hydrolysis of the UDP-glucose substrate. *In vitro* radiolabeling experiments with UDP-[^{3}H]-Glc could answer this question.

To further understand the essential roles of CSLD5 during cell plate formation, we could test whether the catalytically dead version of CSLD5 could restore the cell wall stub defect displayed in *csld5* mutants. The rationale is based on these facts: first, CSLD proteins demonstrated gene dosage effects, and CSLD2, CSLD3, and CSLD5 are functionally interchangeable. Both *CSLD2* and *CSLD3* displayed a stable expression level in dividing cells during the formation of the cell plate. Second, the essential function of CSLD5 does not solely appear to be related to its biochemical activities. According to sequence similarities (Figure 3.1), CSLD5 also contains the conserved TED motif that is responsible for catalytic activity. Therefore, it would be very interesting to analyze whether *csld5* plants expressing tagged CSLD5-TEA or CSLD5-TAA proteins could restore the cell wall stubs defects. Following this direction, domain swap analysis could be performed between CSLD5 and other CSLD proteins to narrow down the regions that are responsible for the "extra" function of CSLD5.

Given the fact that the expression level of CSLD5 is highly regulated by the cell cycle, it would also be very interesting to investigate the regulation of CSLD protein activity. Studies have shown that the stability of CESA proteins is affected by light and temperature (Jacob-Wilk et al., 2006, Hill et al., 2018). Phosphorylation also plays an important role in regulating CESA

protein activity. The phosphorylation of S180 and S185 leads to the degradation of AtCESA7 (Taylor, 2007). Based on the sequence similarities between CESA proteins and CSLD proteins, the corresponding residues can be identified. Point mutation targeting theses residues would uncover potential regulation of CSLD protein activity, and deepen our understanding of cellulose synthases in *Arabidopsis*.

Additionally, the fact that no cortical microtubules are present in the apical regions of growing root hairs leads to the question: how do CSLD proteins get delivered to the plasma membranes undergoing tip-restricted expansion? Studies have shown that CESA/CSCs are delivered to plasma membrane through the MASCs/SmaCCs (Crowell et al., 2009; Gutierrez et al., 2009). Disruption on the cortical microtubule arrays affected the movement of these compartments and resulted in reduced CSCs fusion to the plasma membrane (Crowell et al., 2009; Gutierrez et al., 2009). More proteins have been identified mediating the association between CESA/CSCs and cortical microtubules. CSI1 binds to the microtubules and serves as a target marker to MASCs/SmaCCs, in which PTL1 mediates the tethering of MASCs/SmaCCs to CSI1 (Gu et al., 2010; Li et al., 2012; Zhu et al., 2018). PTL1 functions as a subunit of exocyst complexes to mediate the fusion of MASCs/SmaCCs to the plasma membrane (Zhu et al., 2018). The CMUs are microtubule-associated proteins that are localize as static puncta along cortical microtubules to maintain lateral microtubule arrays positions at the cortex of plant cells (Liu et al., 2016). Taken together, these proteins are involved in mediating the CESA/CSCs targeting to cortical microtubules. The fact that no cortical microtubules are present in the apical regions of growing root hairs suggest that a different machinery is likely to be necessary for successful recruitment and fusion of CSLD containing secretory vesicles. To start the investigation on the trafficking of CSLD proteins, protein-protein interaction-based screening could be a good

approach to explore the potential binding partners of CSLD proteins. Both mating-based split ubiquitin yeast two-hybrid system (mbSU-Y2H) and Immunoprecipitation-Mass Spectrometry (IP-MS) are commonly used approaches to identify potential binding partners of proteins of interest. On the other hand, forward genetic screening could be applied to parental plants expressing fluorescently-tagged CSLD proteins to screen for mutants that display altered distribution of CSLD proteins.

Appendix Characterizing the Potential Function of CNIHs during the Delivery of CSLD3 in *Arabidopsis*

5.1 INTRODUCTION

The CSC complexes containing CESA proteins are proposed to be assembled in the Golgi apparatus and then transported to the plasma membranes (Lei et al., 2012; Bashline et al., 2014). The movement of CSC complexes was guided by cortical microtubules (Paredez et al., 2006), and recent studies showed that cellulose synthase-interactive protein 1 (CSI1) is involved in mediating the delivery of CSCs containing compartments to cortical microtubules (Li et al., 2012). However, due to the absence of cortical microtubules at the growing tip of root hairs, one of my rotation projects was to identify proteins that are involved in regulating the delivery of CSLD3 protein. Based on the analysis of the M.I.N.D database, I found one interesting CSLD3-interacting candidate, Cornichon1 (AtCNIH1), which is proposed to function as cargo-binding protein and is involved in vesicle trafficking in animal system (Bokel et al., 2006; Kato et al., 2010). Using the mating-based split ubiquitin yeast two-hybrid system (mbSU-Y2H) system, I confirmed the specific interaction between AtCSLD3 and AtCNIH1 proteins.

Cornichon (CNIH) proteins exist in both plant and animal cells. In mammalian neuronal cells, CNIH-2 was reported to act as an integral component of AMPA receptor complexes (TARPs) by modulating AMPA receptor activity through regulating its biosynthesis, trafficking,

and stability. The sub-cellular localization of CNIH-2 was detected associating with the Golgi apparatus in cultured hippocampal neurons (Kato et al., 2010). This result is consistent with the observation in *Arabidopsis* mesophyll protoplasts, where CNIH1 is also localized in the Golgi or endosomal compartments (Jones et al., 2014). Taken together, these facts strongly suggest that the plant Cornichon proteins might also work as protein sorting modulators and affect CSLD3 protein distribution. Five members of the Cornichon protein family are confirmed in *Arabidopsis*, and none of them were well studied yet. To test this hypothesis, I started my research by generating the homozygous knockout lines of all Cornichon genes and characterizing their phenotypes.

5.2 RESULTS

AtCNIH1 displayed a specific interaction to AtCSLD3 protein.

To confirm whether the interaction between AtCNIH1 and AtCSLD3 from the M.I.N.D database exists, I tested the direct interactions between AtCNIH1 and AtCSLD3 proteins using split ubiquitin-based yeast two-hybrid analysis. CSLA9, as the Golgi-localized CSL protein, was used as a negative control to exclude the universal interactions between AtCNIH1 and other Golgi proteins. A full-length AtCNIH1 was attached to the amino terminus of a construct consisting of the carboxy-terminal ubiquitin fragment transcription factor fusion protein (CNIH1-Cub-PLV). CSLD3 and CSLA9 were tested for interaction with CNIH1 by attaching their coding sequences to amino-terminal fragments of either wild-type ubiquitin (CSLD3/CSLA9-NubWT), or a mutated version (CSLD3/CSLA9-NubG), that only interacts with Cub-fusions upon the association of CNIH1 with the tested fusion protein. The presence of methionine inhibited yeast growth for clearer distinction. I found that with 50 uM of methionine, no growth was observed in yeast

expressing CSLA9-NubG and NubG constructs (Figure 5.1). In contrast, yeast expressing CSLD3-NubG displayed active growth (Figure 5.1), indicating the association of CNIH1 with CSLD3 protein. More importantly, the interaction is not universal to other Golgi-localized CSL proteins, suggesting the interaction might have a biological function, and a high possibility of CNIH1 involvement in the delivery of CSLD3 protein.

cnih mutants displayed root hair defects

In *Arabidopsis*, the Cornichon family contains five members: CNIH1, CNIH2, CNIH3, CNIH4, and CNIH5. When generating the homozygous T-DNA insertion knockout lines of all five genes, *cnih5 (AT4G12090)* seems to be a recessive lethal mutant (Figure 5.2C). Therefore, I focused on the morphological analysis of the other four mutants. Interestingly, all four single mutants of the CNIH gene displayed defects on root hair elongation (Figure 5.2A, B). When crossing *cnih1* with *cnih2* and *cnih4*, no enhanced defects were observed in *cnih1/cnih2* and *cnih1/cnih4* double mutants (Figure 5.2A, B). These results indicate that CNIH proteins are involved in root hair elongation, and functional redundancy might exist among different CNIHs.

5.3 DISCUSSION AND FUTURE DIRECTION

In the four *cnih* mutants I analyzed, *cnih2* and *cnih4* showed the most severe root hair defect and displayed a ~50% reduction on root hair length compared to the wild type (Col-0). It makes sense to assume that *cnih2/4* double mutants should provide more severe root hair defects. However, these two genes (*AT1G12340* and *AT1G12390*) are located at chromosome one with a distance of around 22 kb. CRISPR was applied to generate the double mutant lines. Based on the gene sequences, I designed primers that could target both genes. The CRISPR constructs were

transformed to both *cnih2* and *cnih4* single T-DNA insertion lines. Further screening and analysis are required for investigating the phenotypes of *cnih* mutants.

To test whether the delivery of CSLD3 is affected in the absence of CNIHs, I would like to check the sub-cellular localization of CSLD3 in *cnih* mutants. The *cnih2* and *cnih4* plants expressing *pCSLD3:Citrine-CSLD3* were generated. Further screening and confocal microscopy analysis on these lines are required as well.

5.4 METHODS AND MATERIALS

Plant material and growth conditions

Arabidopsis thaliana lines used in this study were derived from *Col-0* ecotype. Seeds were sterilized with 10% Clorox bleach solution, rinsed five times with distilled water, then stored at 4°C for 2 days before being plated on growth medium comprised of 0.25X Murashige and Skoog Basal Medium,1% sucrose, and 0.6% phytagel. Plates were placed vertically in a growth chamber at 21°C and grown under long-day conditions (16 hours light (200 uE/m^2s)/8 hours dark photoperiod). Three-day-old dark-grown seedlings were used for microscopy analysis. Five-day-old seedlings were used for morphology analysis. For propagation of mature plants, 14-day old seedlings were transferred to soil and grown in environmental chambers at 21°C under long-day conditions (16 hours light/8 hours dark photoperiod).

Morphology analysis

The whole plant were pictured at three weeks old stage using Canon Kiss 5 digital camera. The raw images were collected at 5184*3456 pixel and cropped using Adobe Photoshop using the same scale bar level.

Root length measurement

Images of 5-day-old seedlings were recorded using an Epson Perfection 4990 Photo scanner. The lengths of root regions were measured using Fiji-ImageJ (Schindelin et al., 2012). All transformed lines were grown side by side on the same plate, and at least 15 individuals were measured per line. Three independent biological replicates were performed for each line.

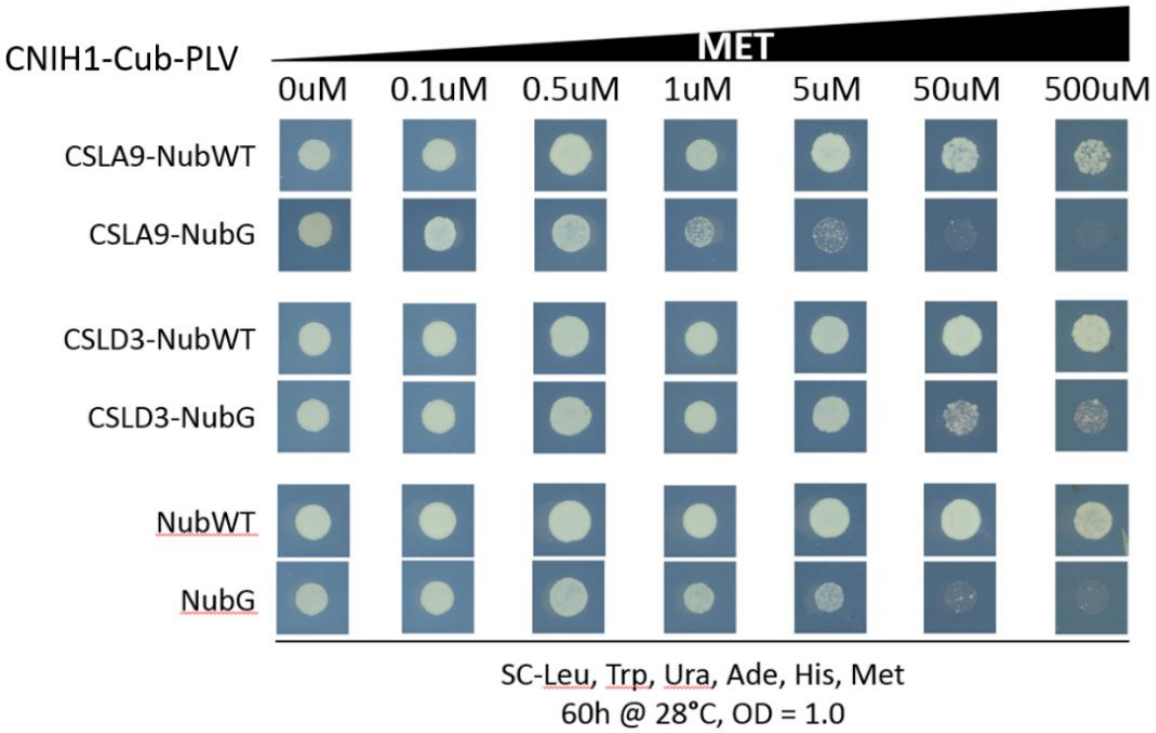

Figure 5.1. The yeast two-hybrid confirmed the interaction between AtCNIH1 and AtCSLD3.

Yeast cell expressing CNIH1-Cub-PLV and CSLD3-NubG survive in the selection medium in the presence of 50 uM methionine. No growth was observed in yeast expressing CSLA9-NubG. NubWT serve as positive controls. MET: methionine, growth inhibitor.

A

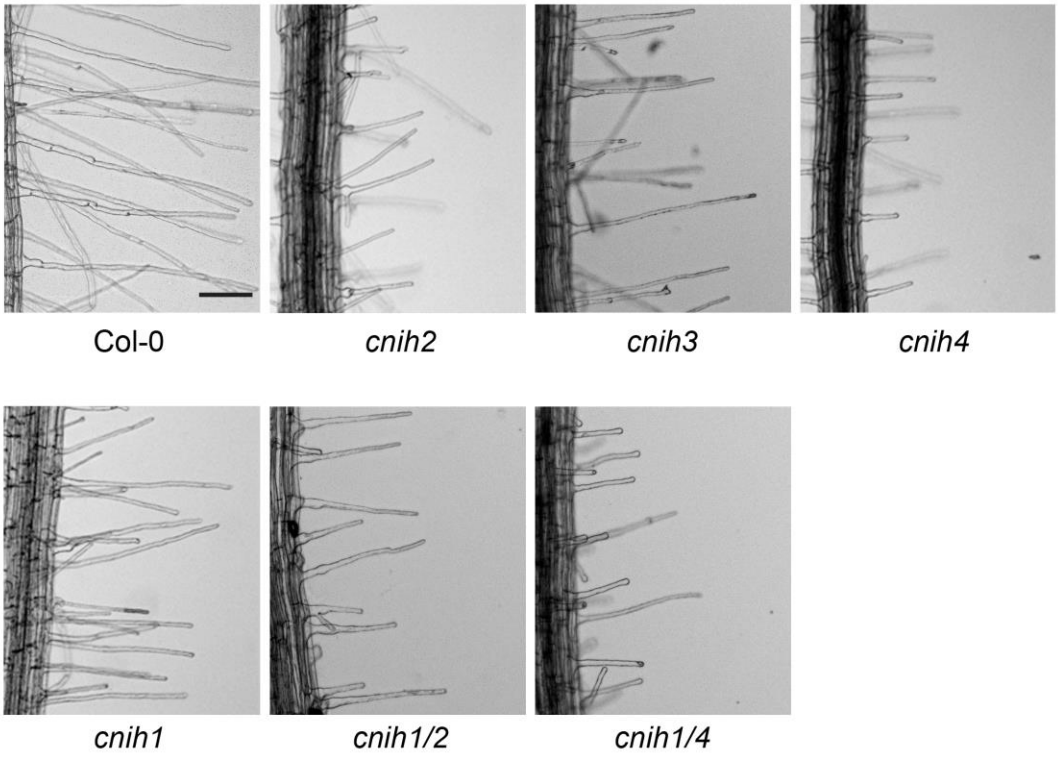

B

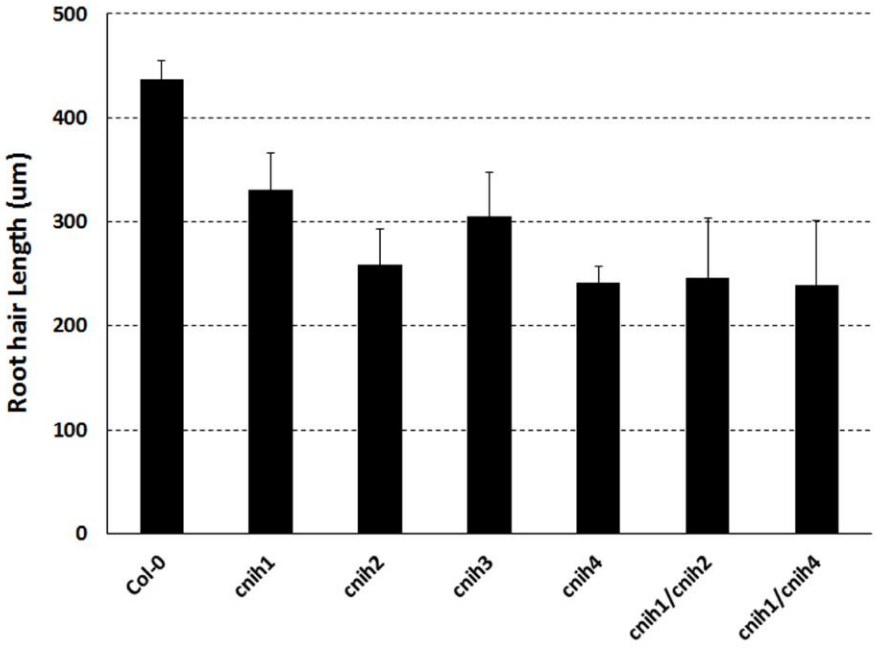

C

cnih5 (39 in total)	WT	hetero	homo
expected	13	26	N/A
observed	14	25	0

Figure 5.2. *cnih* mutants displayed root hair defects.

(A) Root hair of 5-day old seedlings. In *cnih1* and *cnih3* single mutants, ~20% reduction of root hair length was observed. In *cnih2* and *cnih4* single mutants, ~50% reduction of root hair length was observed. No significant enhanced defects displayed in *cnih1*/*cnih2* and *cnih1/cnih4* double mutants. Length of root hairs are quantified in **(B)**. **(C)** Homozygous T-DNA insertion knockout line of *cnih5 (AT4G12090)* is a recessive lethal mutant.

Bibliography

Akkerman, M., Franssen-Verheijen, M.A., Immerzeel, P., Hollander, L.D., Schel, J.H., and Emons, A.M. (2012). Texture of cellulose microfibrils of root hair cell walls of Arabidopsis thaliana, Medicago truncatula, and Vicia sativa. J Microsc **247,** 60-67.

Antoni Femenia, E.S.S., Susana Simal, Carmen Rosselló. (1999). Compositional features of polysaccharides from Aloe vera (Aloe barbadensis Miller) plant tissues. Carbohydrate Polymers **39,** 109-117.

Arioli, T., Peng, L.C., Betzner, A.S., Burn, J., Wittke, W., Herth, W., Camilleri, C., Hofte, H., Plazinski, J., Birch, R., Cork, A., Glover, J., Redmond, J., and Williamson, R.E. (1998). Molecular analysis of cellulose biosynthesis in Arabidopsis. Science **279,** 717-720.

Atmodjo, M.A., Sakuragi, Y., Zhu, X., Burrell, A.J., Mohanty, S.S., Atwood, J.A., 3rd, Orlando, R., Scheller, H.V., and Mohnen, D. (2011). Galacturonosyltransferase (GAUT)1 and GAUT7 are the core of a plant cell wall pectin biosynthetic homogalacturonan:galacturonosyltransferase complex. Proc Natl Acad Sci U S A **108,** 20225-20230.

Bacete, L., Melida, H., Miedes, E., and Molina, A. (2018). Plant cell wall-mediated immunity: cell wall changes trigger disease resistance responses. Plant J **93,** 614-636.

Basavaraju, P., Shailasree, S., Shetty, N.P., Kini, R.K., J⊘rgensen, H.J.L., de Neergaard, E., and Shetty, H.S. (2009). Infection induced oxidative cross-linking of hydroxyproline-rich glycoproteins (HRGPs) is associated with restriction of Colletotrichum sublineolum in sorghum. Journal of Plant Interactions **4,** 179-186.

Bashline, L., Li, S., and Gu, Y. (2014). The trafficking of the cellulose synthase complex in higher plants. Ann Bot **114,** 1059-1067.

Baskin, T.I. (2005). Anisotropic expansion of the plant cell wall. Annu Rev Cell Dev Bi **21,** 203-222.

Basu, D., Liang, Y., Liu, X., Himmeldirk, K., Faik, A., Kieliszewski, M., Held, M., and Showalter, A.M. (2013). Functional identification of a hydroxyproline-o-galactosyltransferase specific for arabinogalactan protein biosynthesis in Arabidopsis. J Biol Chem **288,** 10132-10143.

Benova-Kakosova, A., Digonnet, C., Goubet, F., Ranocha, P., Jauneau, A., Pesquet, E., Barbier, O., Zhang, Z., Capek, P., Dupree, P., Liskova, D., and Goffner, D. (2006). Galactoglucomannans increase cell population density and alter the protoxylem/metaxylem tracheary element ratio in xylogenic cultures of Zinnia. Plant Physiol **142,** 696-709.

Bernal, A.J., Yoo, C.M., Mutwil, M., Jensen, J.K., Hou, G., Blaukopf, C., Sorensen, I., Blancaflor, E.B., Scheller, H.V., and Willats, W.G.T. (2008). Functional Analysis of the Cellulose Synthase-Like Genes CSLD1, CSLD2, and CSLD4 in Tip-Growing Arabidopsis Cells. Plant Physiol **148,** 1238-1253.

Bernal, A.J., Jensen, J.K., Harholt, J., Sorensen, S., Moller, I., Blaukopf, C., Johansen, B., de Lotto, R., Pauly, M., Scheller, H.V., and Willats, W.G.T. (2007). Disruption of

ATCSLD5 results in reduced growth, reduced xylan and homogalacturonan synthase activity and altered xylan occurrence in Arabidopsis. Plant J **52,** 791-802.

Biswal, A.K., Hao, Z., Pattathil, S., Yang, X., Winkeler, K., Collins, C., Mohanty, S.S., Richardson, E.A., Gelineo-Albersheim, I., Hunt, K., Ryno, D., Sykes, R.W., Turner, G.B., Ziebell, A., Gjersing, E., Lukowitz, W., Davis, M.F., Decker, S.R., Hahn, M.G., and Mohnen, D. (2015). Downregulation of GAUT12 in Populus deltoides by RNA silencing results in reduced recalcitrance, increased growth and reduced xylan and pectin in a woody biofuel feedstock. Biotechnol Biofuels **8,** 41.

Bokel, C., Dass, S., Wilsch-Brauninger, M., and Roth, S. (2006). Drosophila Cornichon acts as cargo receptor for ER export of the TGFalpha-like growth factor Gurken. Development **133,** 459-470.

Bringmann, M., Li, E.Y., Sampathkumar, A., Kocabek, T., Hauser, M.T., and Persson, S. (2012). POM-POM2/CELLULOSE SYNTHASE INTERACTING1 Is Essential for the Functional Association of Cellulose Synthase and Microtubules in Arabidopsis. Plant Cell **24,** 163-177.

Brown, D.M., Zhang, Z., Stephens, E., Dupree, P., and Turner, S.R. (2009). Characterization of IRX10 and IRX10-like reveals an essential role in glucuronoxylan biosynthesis in Arabidopsis. Plant J **57,** 732-746.

Brown, D.M., Goubet, F., Wong, V.W., Goodacre, R., Stephens, E., Dupree, P., and Turner, S.R. (2007). Comparison of five xylan synthesis mutants reveals new insight into the mechanisms of xylan synthesis. Plant J **52,** 1154-1168.

Brown, R.M. (1996). The Biosynthesis of Cellulose. Journal of Macromolecular Science, Part A **33,** 1345-1373.

Bruce, D.M. (2003). Mathematical modelling of the cellular mechanics of plants. Philos Trans R Soc Lond B Biol Sci **358,** 1437-1444.

Bucher, G.L., Tarina, C., Heinlein, M., Di Serio, F., Meins, F., Jr., and Iglesias, V.A. (2001). Local expression of enzymatically active class I beta-1, 3-glucanase enhances symptoms of TMV infection in tobacco. Plant J **28,** 361-369.

Burton, R.A., Gidley, M.J., and Fincher, G.B. (2010). Heterogeneity in the chemistry, structure and function of plant cell walls. Nat Chem Biol **6,** 724-732.

Burton, R.A., Wilson, S.M., Hrmova, M., Harvey, A.J., Shirley, N.J., Stone, B.A., Newbigin, E.J., Bacic, A., and Fincher, G.B. (2006). Cellulose synthase-like CslF genes mediate the synthesis of cell wall (1,3;1,4)-beta-D-glucans. Science **311,** 1940-1942.

Cannon, M.C., Terneus, K., Hall, Q., Tan, L., Wang, Y., Wegenhart, B.L., Chen, L., Lamport, D.T., Chen, Y., and Kieliszewski, M.J. (2008). Self-assembly of the plant cell wall requires an extensin scaffold. Proc Natl Acad Sci U S A **105,** 2226-2231.

Chebli, Y., Kaneda, M., Zerzour, R., and Geitmann, A. (2012). The Cell Wall of the Arabidopsis Pollen Tube-Spatial Distribution, Recycling, and Network Formation of Polysaccharides. Plant Physiol **160,** 1940-1955.

Chen, S., Ehrhardt, D.W., and Somerville, C.R. (2010). Mutations of cellulose synthase (CESA1) phosphorylation sites modulate anisotropic cell expansion and bidirectional mobility of cellulose synthase. Proc Natl Acad Sci U S A **107,** 17188-17193.

Chen, X.Y., and Kim, J.Y. (2009). Callose synthesis in higher plants. Plant Signal Behav **4,** 489-492.

Cho, S.H., Purushotham, P., Fang, C., Maranas, C., Diaz-Moreno, S.M., Bulone, V., Zimmer, J., Kumar, M., and Nixon, B.T. (2017). Synthesis and Self-Assembly of

Cellulose Microfibrils from Reconstituted Cellulose Synthase. Plant Physiol **175,** 146-156.

Chonlong Chio, M.S., Wensheng Qin. (2019). Lignin utilization: A review of lignin depolymerization from various aspects. Renewable and Sustainable Energy Reviews **107,** 232-249.

Cocuron, J.C., Lerouxel, O., Drakakaki, G., Alonso, A.P., Liepman, A.H., Keegstra, K., Raikhel, N., and Wilkerson, C.G. (2007). A gene from the cellulose synthase-like C family encodes a beta-1,4 glucan synthase. Proc. Natl. Acad. Sci. U. S. A. **104,** 8550-8555.

Cosgrove, D.J. (2005). Growth of the plant cell wall. Nat Rev Mol Cell Bio **6,** 850-861.

Cosgrove, D.J. (2014). Re-constructing our models of cellulose and primary cell wall assembly. Curr Opin Plant Biol **22,** 122-131.

Crowell, E.F., Bischoff, V., Desprez, T., Rolland, A., Stierhof, Y.D., Schumacher, K., Gonneau, M., Hofte, H., and Vernhettes, S. (2009). Pausing of Golgi bodies on microtubules regulates secretion of cellulose synthase complexes in Arabidopsis. Plant Cell **21,** 1141-1154.

de O. Buanafina, M.M. (2009). Feruloylation in grasses: current and future perspectives. Mol Plant **2,** 861-872.

De Storme, N., and Geelen, D. (2014). Callose homeostasis at plasmodesmata: molecular regulators and developmental relevance. Frontiers in plant science **5,** 138.

DeBolt, S., Gutierrez, R., Ehrhardt, D.W., Melo, C.V., Ross, L., Cutler, S.R., Somerville, C., and Bonetta, D. (2007). Morlin, an inhibitor of cortical microtubule dynamics and cellulose synthase movement. Proc Natl Acad Sci U S A **104,** 5854-5859.

Del Bem, L.E., and Vincentz, M.G. (2010). Evolution of xyloglucan-related genes in green plants. BMC Evol Biol **10,** 341.

Desprez, T., Juraniec, M., Crowell, E.F., Jouy, H., Pochylova, Z., Parcy, F., Hofte, H., Gonneau, M., and Vernhettes, S. (2007). Organization of cellulose synthase complexes involved in primary cell wall synthesis in Arabidopsis thaliana. Proc. Natl. Acad. Sci. U. S. A. **104,** 15572-15577.

Dhugga, K.S., Barreiro, R., Whitten, B., Stecca, K., Hazebroek, J., Randhawa, G.S., Dolan, M., Kinney, A.J., Tomes, D., Nichols, S., and Anderson, P. (2004). Guar seed beta-mannan synthase is a member of the cellulose synthase super gene family. Science **303,** 363-366.

Didi, V., Jackson, P., and Hejatko, J. (2015). Hormonal regulation of secondary cell wall formation. J Exp Bot **66,** 5015-5027.

Ding, S.Y., Liu, Y.S., Zeng, Y., Himmel, M.E., Baker, J.O., and Bayer, E.A. (2012). How does plant cell wall nanoscale architecture correlate with enzymatic digestibility? Science **338,** 1055-1060.

Doblin, M.S., De Melis, L., Newbigin, E., Bacic, A., and Read, S.M. (2001). Pollen tubes of Nicotiana alata express two genes from different beta-glucan synthase families. Plant Physiol **125,** 2040-2052.

Doblin, M.S., Pettolino, F.A., Wilson, S.M., Campbell, R., Burton, R.A., Fincher, G.B., Newbigin, E., and Bacic, A. (2009). A barley cellulose synthase-like CSLH gene mediates (1,3;1,4)-beta-D-glucan synthesis in transgenic Arabidopsis. Proc. Natl. Acad. Sci. U. S. A. **106,** 5996-6001.

Dong, X., Hong, Z., Sivaramakrishnan, M., Mahfouz, M., and Verma, D.P. (2005). Callose synthase (CalS5) is required for exine formation during microgametogenesis and for pollen viability in Arabidopsis. Plant J **42,** 315-328.

Drakakaki, G. (2015). Polysaccharide deposition during cytokinesis: Challenges and future perspectives. Plant Sci **236,** 177-184.

Dwivany, F.M., Yulia, D., Burton, R.A., Shirley, N.J., Wilson, S.M., Fincher, G.B., Bacic, A., Newbigin, E., and Doblin, M.S. (2009). The CELLULOSE-SYNTHASE LIKE C (CSLC) Family of Barley Includes Members that Are Integral Membrane Proteins Targeted to the Plasma Membrane. Mol Plant **2,** 1025-1039.

Egelund, J., Petersen, B.L., Motawia, M.S., Damager, I., Faik, A., Olsen, C.E., Ishii, T., Clausen, H., Ulvskov, P., and Geshi, N. (2006). Arabidopsis thaliana RGXT1 and RGXT2 encode Golgi-localized (1,3)-alpha-D-xylosyltransferases involved in the synthesis of pectic rhamnogalacturonan-II. Plant Cell **18,** 2593-2607.

Emons, A.M.C., and Ketelaar, T. (2012). Root hairs. (Berlin; London: Springer).

Enns, L.C., Kanaoka, M.M., Torii, K.U., Comai, L., Okada, K., and Cleland, R.E. (2005). Two callose synthases, GSL1 and GSL5, play an essential and redundant role in plant and pollen development and in fertility. Plant Mol Biol **58,** 333-349.

Fagard, M., Desnos, T., Desprez, T., Goubet, F., Refregier, G., Mouille, G., McCann, M., Rayon, C., Vernhettes, S., and Hofte, H. (2000). PROCUSTE1 encodes a cellulose synthase required for normal cell elongation specifically in roots and dark-grown hypocotyls of arabidopsis. Plant Cell **12,** 2409-2423.

Favery, B., Ryan, E., Foreman, J., Linstead, P., Boudonck, K., Steer, M., Shaw, P., and Dolan, L. (2001). KOJAK encodes a cellulose synthase-like protein required for root hair cell morphogenesis in Arabidopsis. Gene Dev **15,** 79-89.

Ferguson, C., Teeri, T.T., Siika-aho, M., Read, S.M., and Bacic, A. (1998). Location of cellulose and callose in pollen tubes and grains of Nicotiana tabacum. Planta **206,** 452-460.

Fernandes, A.N., Thomas, L.H., Altaner, C.M., Callow, P., Forsyth, V.T., Apperley, D.C., Kennedy, C.J., and Jarvis, M.C. (2011). Nanostructure of cellulose microfibrils in spruce wood. Proc Natl Acad Sci U S A **108,** E1195-1203.

Fowler, T.J., Bernhardt, C., and Tierney, M.L. (1999). Characterization and expression of four proline-rich cell wall protein genes in Arabidopsis encoding two distinct subsets of multiple domain proteins. Plant Physiol **121,** 1081-1092.

Fry, S.C., Nesselrode, B.H., Miller, J.G., and Mewburn, B.R. (2008). Mixed-linkage (1-->3,1-->4)-beta-D-glucan is a major hemicellulose of Equisetum (horsetail) cell walls. New Phytol **179,** 104-115.

Fry, S.C., York, W.S., Albersheim, P., Darvill, A., Hayashi, T., Joseleau, J.-P., Kato, Y., Lorences, E.P., Maclachlan, G.A., McNeil, M., Mort, A.J., Grant Reid, J.S., Seitz, H.U., Selvendran, R.R., Voragen, A.G.J., and White, A.R. (1993). An unambiguous nomenclature for xyloglucan-derived oligosaccharides. Physiologia Plantarum **89,** 1-3.

Funakawa, H., and Miwa, K. (2015). Synthesis of borate cross-linked rhamnogalacturonan II. Frontiers in plant science **6,** 223.

Galway, M.E., Eng, R.C., Schiefelbein, J.W., and Wasteneys, G.O. (2011). Root hair-specific disruption of cellulose and xyloglucan in AtCSLD3 mutants, and factors affecting the post-rupture resumption of mutant root hair growth. Planta **233,** 985-999.

Gibson, L.J. (2012). The hierarchical structure and mechanics of plant materials. J R Soc Interface **9,** 2749-2766.

Gilbert, H.J., Knox, J.P., and Boraston, A.B. (2013). Advances in understanding the molecular basis of plant cell wall polysaccharide recognition by carbohydrate-binding modules. Curr Opin Struct Biol **23,** 669-677.

Gille, S., de Souza, A., Xiong, G., Benz, M., Cheng, K., Schultink, A., Reca, I.B., and Pauly, M. (2011). O-acetylation of Arabidopsis hemicellulose xyloglucan requires AXY4 or AXY4L, proteins with a TBL and DUF231 domain. Plant Cell **23,** 4041-4053.

Gonneau, M., Desprez, T., Guillot, A., Vernhettes, S., and Hofte, H. (2014). Catalytic subunit stoichiometry within the cellulose synthase complex. Plant Physiol **166,** 1709-1712.

Goubet, F., Misrahi, A., Park, S.K., Zhang, Z., Twell, D., and Dupree, P. (2003). AtCSLA7, a cellulose synthase-like putative glycosyltransferase, is important for pollen tube growth and embryogenesis in Arabidopsis. Plant Physiol **131,** 547-557.

Goubet, F., Barton, C.J., Mortimer, J.C., Yu, X., Zhang, Z., Miles, G.P., Richens, J., Liepman, A.H., Seffen, K., and Dupree, P. (2009). Cell wall glucomannan in Arabidopsis is synthesised by CSLA glycosyltransferases, and influences the progression of embryogenesis. Plant J **60,** 527-538.

Green, P.B. (1962). Mechanism for Plant Cellular Morphogenesis. Science **138,** 1404-1405.

Gu, F., and Nielsen, E. (2013). Targeting and regulation of cell wall synthesis during tip growth in plants. J Integr Plant Biol **55,** 835-846.

Gu, F., Bringmann, M., Combs, J.R., Yang, J., Bergmann, D.C., and Nielsen, E. (2016). Arabidopsis CSLD5 Functions in Cell Plate Formation in a Cell Cycle-Dependent Manner. Plant Cell **28,** 1722-1737.

Gu, Y., Kaplinsky, N., Bringmann, M., Cobb, A., Carroll, A., Sampathkumar, A., Baskin, T.I., Persson, S., and Somerville, C.R. (2010). Identification of a cellulose synthase-associated protein required for cellulose biosynthesis. Proc Natl Acad Sci U S A **107,** 12866-12871.

Guo, H., Li, L., Ye, H., Yu, X., Algreen, A., and Yin, Y. (2009). Three related receptor-like kinases are required for optimal cell elongation in Arabidopsis thaliana. Proc Natl Acad Sci U S A **106,** 7648-7653.

Guseman, J.M., Lee, J.S., Bogenschutz, N.L., Peterson, K.M., Virata, R.E., Xie, B., Kanaoka, M.M., Hong, Z., and Torii, K.U. (2010). Dysregulation of cell-to-cell connectivity and stomatal patterning by loss-of-function mutation in Arabidopsis chorus (glucan synthase-like 8). Development **137,** 1731-1741.

Gutierrez, R., Lindeboom, J.J., Paredez, A.R., Emons, A.M.C., and Ehrhardt, D.W. (2009). Arabidopsis cortical microtubules position cellulose synthase delivery to the plasma membrane and interact with cellulose synthase trafficking compartments. Nat Cell Biol **11,** 797-U743.

Harholt, J., Sorensen, I., Fangel, J., Roberts, A., Willats, W.G., Scheller, H.V., Petersen, B.L., Banks, J.A., and Ulvskov, P. (2012a). The glycosyltransferase repertoire of the spikemoss Selaginella moellendorffii and a comparative study of its cell wall. PLoS One **7,** e35846.

Harholt, J., Jensen, J.K., Verhertbruggen, Y., Sogaard, C., Bernard, S., Nafisi, M., Poulsen, C.P., Geshi, N., Sakuragi, Y., Driouich, A., Knox, J.P., and Scheller, H.V. (2012b). ARAD proteins associated with pectic Arabinan biosynthesis form complexes when transiently overexpressed in planta. Planta **236,** 115-128.

Hashimoto-Sugimoto, M., Higaki, T., Yaeno, T., Nagami, A., Irie, M., Fujimi, M., Miyamoto, M., Akita, K., Negi, J., Shirasu, K., Hasezawa, S., and Iba, K. (2013). A Munc13-like protein in Arabidopsis mediates H+-ATPase translocation that is essential for stomatal responses. Nat Commun **4,** 2215.

Hayashi, T. (1989). Xyloglucans in the primary cell wall. Annu. Rev. Plant Physiol. Plant Mol. biol. **40,** 139-168.

Hazen, S.P., Scott-Craig, J.S., and Walton, J.D. (2002). Cellulose synthase-like genes of rice. Plant Physiol **128,** 336-340.

Hematy, K., Sado, P.E., Van Tuinen, A., Rochange, S., Desnos, T., Balzergue, S., Pelletier, S., Renou, J.P., and Hofte, H. (2007). A receptor-like kinase mediates the response of Arabidopsis cells to the inhibition of cellulose synthesis. Curr Biol **17,** 922-931.

Hill, J.L., Jr., Hammudi, M.B., and Tien, M. (2014). The Arabidopsis cellulose synthase complex: a proposed hexamer of CESA trimers in an equimolar stoichiometry. Plant Cell **26,** 4834-4842.

Hill, J.L., Jr., Josephs, C., Barnes, W.J., Anderson, C.T., and Tien, M. (2018). Longevity in vivo of primary cell wall cellulose synthases. Plant Mol Biol **96,** 279-289.

Hong, Z., Delauney, A.J., and Verma, D.P. (2001). A cell plate-specific callose synthase and its interaction with phragmoplastin. Plant Cell **13,** 755-768.

Hooke, R. (1665). Micrographia; or, Some physiological descriptions of minute bodies made by magnifying glasses. With observations and inquiries thereupon. (London: Printed by J. Martyn and J. Allestry).

Hu, H., Zhang, R., Tang, Y., Peng, C., Wu, L., Feng, S., Chen, P., Wang, Y., Du, X., and Peng, L. (2019). Cotton CSLD3 restores cell elongation and cell wall integrity mainly by enhancing primary cellulose production in the Arabidopsis cesa6 mutant. Plant Mol Biol **101,** 389-401.

Iglesias, V.A., and Meins, F., Jr. (2000). Movement of plant viruses is delayed in a beta-1,3-glucanase-deficient mutant showing a reduced plasmodesmatal size exclusion limit and enhanced callose deposition. Plant J **21,** 157-166.

Jacob-Wilk, D., Kurek, I., Hogan, P., and Delmer, D.P. (2006). The cotton fiber zinc-binding domain of cellulose synthase A1 from Gossypium hirsutum displays rapid turnover in vitro and in vivo. Proc Natl Acad Sci U S A **103,** 12191-12196.

James M. Lau, M.M., Alan G. Darvill, Peter Albersheim. (1985). Structure of the backbone of rhamnogalacturonan I, a pectic polysaccharide in the primary cell walls of plants. Carbohydrate Research **137,** 111-125.

Jamet, E., Canut, H., Boudart, G., and Pont-Lezica, R.F. (2006). Cell wall proteins: a new insight through proteomics. Trends Plant Sci **11,** 33-39.

Jensen, J.K., Sorensen, S.O., Harholt, J., Geshi, N., Sakuragi, Y., Moller, I., Zandleven, J., Bernal, A.J., Jensen, N.B., Sorensen, C., Pauly, M., Beldman, G., Willats, W.G., and Scheller, H.V. (2008). Identification of a xylogalacturonan xylosyltransferase involved in pectin biosynthesis in Arabidopsis. Plant Cell **20,** 1289-1302.

Jones, A.M., Xuan, Y., Xu, M., Wang, R.S., Ho, C.H., Lalonde, S., You, C.H., Sardi, M.I., Parsa, S.A., Smith-Valle, E., Su, T., Frazer, K.A., Pilot, G., Pratelli, R., Grossmann, G., Acharya, B.R., Hu, H.C., Engineer, C., Villiers, F., Ju, C., Takeda, K., Su, Z., Dong, Q., Assmann, S.M., Chen, J., Kwak, J.M., Schroeder, J.I., Albert, R., Rhee, S.Y., and Frommer, W.B. (2014). Border control--a membrane-linked interactome of Arabidopsis. Science **344,** 711-716.

Jones, M.A., Shen, J.J., Fu, Y., Li, H., Yang, Z., and Grierson, C.S. (2002). The Arabidopsis Rop2 GTPase is a positive regulator of both root hair initiation and tip growth. Plant Cell **14,** 763-776.

Kato, A.S., Gill, M.B., Ho, M.T., Yu, H., Tu, Y., Siuda, E.R., Wang, H., Qian, Y.W., Nisenbaum, E.S., Tomita, S., and Bredt, D.S. (2010). Hippocampal AMPA receptor gating controlled by both TARP and cornichon proteins. Neuron **68,** 1082-1096.

Kimura, S., Laosinchai, W., Itoh, T., Cui, X., Linder, C.R., and Brown, R.M., Jr. (1999). Immunogold labeling of rosette terminal cellulose-synthesizing complexes in the vascular plant vigna angularis. Plant Cell **11,** 2075-2086.

Kubicki, J.D., Yang, H., Sawada, D., O'Neill, H., Oehme, D., and Cosgrove, D. (2018). The Shape of Native Plant Cellulose Microfibrils. Sci Rep **8,** 13983.

Kumar, M., and Turner, S. (2015). Plant cellulose synthesis: CESA proteins crossing kingdoms. Phytochemistry **112,** 91-99.

Kumar, S., Stecher, G., and Tamura, K. (2016). MEGA7: Molecular Evolutionary Genetics Analysis Version 7.0 for Bigger Datasets. Mol Biol Evol **33,** 1870-1874.

Lai-Kee-Him, J., Chanzy, H., Muller, M., Putaux, J.L., Imai, T., and Bulone, V. (2002). In vitro versus in vivo cellulose microfibrils from plant primary wall synthases: Structural differences. J Biol Chem **277,** 36931-36939.

Lane, D.R., Wiedemeier, A., Peng, L., Hofte, H., Vernhettes, S., Desprez, T., Hocart, C.H., Birch, R.J., Baskin, T.I., Burn, J.E., Arioli, T., Betzner, A.S., and Williamson, R.E. (2001). Temperature-sensitive alleles of RSW2 link the KORRIGAN endo-1,4-beta-glucanase to cellulose synthesis and cytokinesis in Arabidopsis. Plant Physiol **126,** 278-288.

Laura L. Kiefer, W.S.Y., Alan G. Darvill, Peter Albersheim. (1989). Xyloglucan isolated from suspension-cultured sycamore cell walls is O-acetylated. Phytochemistry **28,** 2105-2107.

Ledbetter, M.C., and Porter, K.R. (1963). A "Microtubule" in Plant Cell Fine Structure. J Cell Biol **19,** 239-250.

Lei, L., Li, S., and Gu, Y. (2012). Cellulose synthase complexes: composition and regulation. Frontiers in plant science **3,** 75.

Lei, L., Li, S.D., Du, J., Bashline, L., and Gu, Y. (2013). CELLULOSE SYNTHASE INTERACTIVE3 Regulates Cellulose Biosynthesis in Both a Microtubule-Dependent and Microtubule-Independent Manner in Arabidopsis. Plant Cell **25,** 4912-4923.

Lei, L., Zhang, T., Strasser, R., Lee, C.M., Gonneau, M., Mach, L., Vernhettes, S., Kim, S.H., D, J.C., Li, S., and Gu, Y. (2014). The jiaoyao1 Mutant Is an Allele of korrigan1 That Abolishes Endoglucanase Activity and Affects the Organization of Both Cellulose Microfibrils and Microtubules in Arabidopsis. Plant Cell **26,** 2601-2616.

Li, H., Pu, Y., Kumar, R., Ragauskas, A.J., and Wyman, C.E. (2014). Investigation of lignin deposition on cellulose during hydrothermal pretreatment, its effect on cellulose hydrolysis, and underlying mechanisms. Biotechnol Bioeng **111,** 485-492.

Li, S., Lei, L., Somerville, C.R., and Gu, Y. (2012). Cellulose synthase interactive protein 1 (CSI1) links microtubules and cellulose synthase complexes. Proc Natl Acad Sci U S A **109,** 185-190.

Liang, Y., Basu, D., Pattathil, S., Xu, W.L., Venetos, A., Martin, S.L., Faik, A., Hahn, M.G., and Showalter, A.M. (2013). Biochemical and physiological characterization of fut4 and fut6 mutants defective in arabinogalactan-protein fucosylation in Arabidopsis. J Exp Bot **64,** 5537-5551.

Liepman, A.H., Wilkerson, C.G., and Keegstra, K. (2005). Expression of cellulose synthase-like (Csl) genes in insect cells reveals that CslA family members encode mannan synthases. Proc. Natl. Acad. Sci. U. S. A. **102,** 2221-2226.

Liepman, A.H., Wightman, R., Geshi, N., Turner, S.R., and Scheller, H.V. (2010). Arabidopsis - a powerful model system for plant cell wall research. Plant J **61,** 1107-1121.

Lin, C., Choi, H.S., and Cho, H.T. (2011). Root hair-specific EXPANSIN A7 is required for root hair elongation in Arabidopsis. Mol Cells **31,** 393-397.

Little, A., Lahnstein, J., Jeffery, D.W., Khor, S.F., Schwerdt, J.G., Shirley, N.J., Hooi, M., Xing, X., Burton, R.A., and Bulone, V. (2019). A Novel (1,4)-beta-Linked Glucoxylan Is Synthesized by Members of the Cellulose Synthase-Like F Gene Family in Land Plants. ACS Cent Sci **5,** 73-84.

Little, A., Schwerdt, J.G., Shirley, N.J., Khor, S.F., Neumann, K., O'Donovan, L.A., Lahnstein, J., Collins, H.M., Henderson, M., Fincher, G.B., and Burton, R.A. (2018). Revised Phylogeny of the Cellulose Synthase Gene Superfamily: Insights into Cell Wall Evolution. Plant Physiol **177,** 1124-1141.

Liu, X.L., Liu, L., Niu, Q.K., Xia, C., Yang, K.Z., Li, R., Chen, L.Q., Zhang, X.Q., Zhou, Y., and Ye, D. (2011). Male gametophyte defective 4 encodes a rhamnogalacturonan II xylosyltransferase and is important for growth of pollen tubes and roots in Arabidopsis. Plant J **65,** 647-660.

Liu, Y.B., Lu, S.M., Zhang, J.F., Liu, S., and Lu, Y.T. (2007). A xyloglucan endotransglucosylase/hydrolase involves in growth of primary root and alters the deposition of cellulose in Arabidopsis. Planta **226,** 1547-1560.

Liu, Z., Schneider, R., Kesten, C., Zhang, Y., Somssich, M., Zhang, Y., Fernie, A.R., and Persson, S. (2016). Cellulose-Microtubule Uncoupling Proteins Prevent Lateral Displacement of Microtubules during Cellulose Synthesis in Arabidopsis. Dev Cell **38,** 305-315.

Liwanag, A.J., Ebert, B., Verhertbruggen, Y., Rennie, E.A., Rautengarten, C., Oikawa, A., Andersen, M.C., Clausen, M.H., and Scheller, H.V. (2012). Pectin biosynthesis: GALS1 in Arabidopsis thaliana is a beta-1,4-galactan beta-1,4-galactosyltransferase. Plant Cell **24,** 5024-5036.

MacKinnon, I.M., Sturcova, A., Sugimoto-Shirasu, K., His, I., McCann, M.C., and Jarvis, M.C. (2006). Cell-wall structure and anisotropy in procuste, a cellulose synthase mutant of Arabidopsis thaliana. Planta **224,** 438-448.

Madson, M., Dunand, C., Li, X., Verma, R., Vanzin, G.F., Caplan, J., Shoue, D.A., Carpita, N.C., and Reiter, W.D. (2003). The MUR3 gene of Arabidopsis encodes a xyloglucan galactosyltransferase that is evolutionarily related to animal exostosins. Plant Cell **15,** 1662-1670.

Majda, M., and Robert, S. (2018). The Role of Auxin in Cell Wall Expansion. Int J Mol Sci **19**.

Malinowski, R., and Filipecki, M. (2002). The role of cell wall in plant embryogenesis. Cell Mol Biol Lett **7,** 1137-1151.

Manabe, Y., Nafisi, M., Verhertbruggen, Y., Orfila, C., Gille, S., Rautengarten, C., Cherk, C., Marcus, S.E., Somerville, S., Pauly, M., Knox, J.P., Sakuragi, Y., and Scheller, H.V. (2011). Loss-of-function mutation of REDUCED WALL ACETYLATION2 in Arabidopsis leads to reduced cell wall acetylation and increased resistance to Botrytis cinerea. Plant Physiol **155,** 1068-1078.

Matsunaga, T., Ishii, T., Matsumoto, S., Higuchi, M., Darvill, A., Albersheim, P., and O'Neill, M.A. (2004). Occurrence of the primary cell wall polysaccharide rhamnogalacturonan II in pteridophytes, lycophytes, and bryophytes. Implications for the evolution of vascular plants. Plant Physiol **134,** 339-351.

McCaig, B.C., Meagher, R.B., and Dean, J.F. (2005). Gene structure and molecular analysis of the laccase-like multicopper oxidase (LMCO) gene family in Arabidopsis thaliana. Planta **221,** 619-636.

Meikle, P.J., Bonig, I., Hoogenraad, N.J., Clarke, A.E., and Stone, B.A. (1991). The Location of (1-]3)-Beta-Glucans in the Walls of Pollen Tubes of Nicotiana-Alata Using a (1-]3)-Beta-Glucan-Specific Monoclonal-Antibody. Planta **185,** 1-8.

Miart, F., Desprez, T., Biot, E., Morin, H., Belcram, K., Hofte, H., Gonneau, M., and Vernhettes, S. (2014). Spatio-temporal analysis of cellulose synthesis during cell plate formation in Arabidopsis. Plant J **77,** 71-84.

Mikkelsen, M.D., Harholt, J., Ulvskov, P., Johansen, I.E., Fangel, J.U., Doblin, M.S., Bacic, A., and Willats, W.G. (2014). Evidence for land plant cell wall biosynthetic mechanisms in charophyte green algae. Ann Bot **114,** 1217-1236.

Mohnen, D. (2008). Pectin structure and biosynthesis. Curr Opin Plant Biol **11,** 266-277.

Molendijk, A.J., Bischoff, F., Rajendrakumar, C.S., Friml, J., Braun, M., Gilroy, S., and Palme, K. (2001). Arabidopsis thaliana Rop GTPases are localized to tips of root hairs and control polar growth. EMBO J **20,** 2779-2788.

Morgan, J.L.W., Strumillo, J., and Zimmer, J. (2013). Crystallographic snapshot of cellulose synthesis and membrane translocation. Nature **493,** 181-U192.

Morgan, J.L.W., McNamara, J.T., Fischer, M., Rich, J., Chen, H.M., Withers, S.G., and Zimmer, J. (2016). Observing cellulose biosynthesis and membrane translocation in crystallo. Nature **531,** 329-+.

Newcomb, E.H., and Bonnett, H.T. (1965). Cytoplasmic Microtubule and Wall Microfibril Orientation in Root Hairs of Radish. J Cell Biol **27,** 575-589.

Nguema-Ona, E., Vicre-Gibouin, M., Gotte, M., Plancot, B., Lerouge, P., Bardor, M., and Driouich, A. (2014). Cell wall O-glycoproteins and N-glycoproteins: aspects of biosynthesis and function. Frontiers in plant science **5,** 499.

Nishikawa, S., Zinkl, G.M., Swanson, R.J., Maruyama, D., and Preuss, D. (2005). Callose (beta-1,3 glucan) is essential for Arabidopsis pollen wall patterning, but not tube growth. Bmc Plant Biol **5,** 22.

Nixon, B.T., Mansouri, K., Singh, A., Du, J., Davis, J.K., Lee, J.G., Slabaugh, E., Vandavasi, V.G., O'Neill, H., Roberts, E.M., Roberts, A.W., Yingling, Y.G., and Haigler, C.H. (2016). Comparative Structural and Computational Analysis Supports Eighteen Cellulose Synthases in the Plant Cellulose Synthesis Complex. Sci Rep-Uk **6**.

Obel, N., Erben, V., Schwarz, T., Kuhnel, S., Fodor, A., and Pauly, M. (2009). Microanalysis of plant cell wall polysaccharides. Mol Plant **2,** 922-932.

Ogawa-Ohnishi, M., Matsushita, W., and Matsubayashi, Y. (2013). Identification of three hydroxyproline O-arabinosyltransferases in Arabidopsis thaliana. Nat Chem Biol **9,** 726-730.

Omadjela, O., Narahari, A., Strumillo, J., Melida, H., Mazur, O., Bulone, V., and Zimmer, J. (2013). BcsA and BcsB form the catalytically active core of bacterial cellulose synthase sufficient for in vitro cellulose synthesis. Proc Natl Acad Sci U S A **110,** 17856-17861.

Paredez, A.R., Somerville, C.R., and Ehrhardt, D.W. (2006). Visualization of cellulose synthase demonstrates functional association with microtubules. Science **312,** 1491-1495.

Park, S., Szumlanski, A.L., Gu, F.W., Guo, F., and Nielsen, E. (2011). A role for CSLD3 during cell-wall synthesis in apical plasma membranes of tip-growing root-hair cells. Nat Cell Biol **13,** 973-U227.

Pauly, M., and Keegstra, K. (2008). Cell-wall carbohydrates and their modification as a resource for biofuels. Plant J **54,** 559-568.

Pena, M.J., Kong, Y., York, W.S., and O'Neill, M.A. (2012). A galacturonic acid-containing xyloglucan is involved in Arabidopsis root hair tip growth. Plant Cell **24,** 4511-4524.

Peng, L.C., Kawagoe, Y., Hogan, P., and Delmer, D. (2002). Sitosterol-beta-glucoside as primer for cellulose synthesis in plants. Science **295,** 147-150.

Persson, S., Paredez, A., Carroll, A., Palsdottir, H., Doblin, M., Poindexter, P., Khitrov, N., Auer, M., and Somerville, C.R. (2007). Genetic evidence for three unique components in primary cell-wall cellulose synthase complexes in Arabidopsis. Proc Natl Acad Sci U S A **104,** 15566-15571.

Purushotham, P., Cho, S.H., Diaz-Moreno, S.M., Kumar, M., Nixon, B.T., Bulone, V., and Zimmer, J. (2016). A single heterologously expressed plant cellulose synthase isoform is sufficient for cellulose microfibril formation in vitro. Proc. Natl. Acad. Sci. U. S. A. **113,** 11360-11365.

Qu, Y., Egelund, J., Gilson, P.R., Houghton, F., Gleeson, P.A., Schultz, C.J., and Bacic, A. (2008). Identification of a novel group of putative Arabidopsis thaliana beta-(1,3)-galactosyltransferases. Plant Mol Biol **68,** 43-59.

Reiss, H.D., Schnepf, E., and Herth, W. (1984). The Plasma-Membrane of the Funaria Caulonema Tip Cell - Morphology and Distribution of Particle Rosettes, and the Kinetics of Cellulose Synthesis. Planta **160,** 428-435.

Richmond, T.A., and Somerville, C.R. (2000). The cellulose synthase superfamily. Plant Physiol **124,** 495-498.

Richmond, T.A., and Somerville, C.R. (2001). Integrative approaches to determining Csl function. Plant Mol Biol **47,** 131-143.

Rippert, P., Puyaubert, J., Grisollet, D., Derrier, L., and Matringe, M. (2009). Tyrosine and phenylalanine are synthesized within the plastids in Arabidopsis. Plant Physiol **149,** 1251-1260.

Ro, D.K., Mah, N., Ellis, B.E., and Douglas, C.J. (2001). Functional characterization and subcellular localization of poplar (Populus trichocarpa x Populus deltoides) cinnamate 4-hydroxylase. Plant Physiol **126,** 317-329.

Roberts, A.W., and Bushoven, J.T. (2007). The cellulose synthase (CESA) gene superfamily of the moss Physcomitrella patens. Plant Mol Biol **63,** 207-219.

Rodriguez-Gacio Mdel, C., Iglesias-Fernandez, R., Carbonero, P., and Matilla, A.J. (2012). Softening-up mannan-rich cell walls. J Exp Bot **63,** 3976-3988.

Sampedro, J., and Cosgrove, D.J. (2005). The expansin superfamily. Genome Biol **6,** 242.

Samuels, A.L., Giddings, T.H., and Staehelin, L.A. (1995). Cytokinesis in Tobacco by-2 and Root-Tip Cells - a New Model of Cell Plate Formation in Higher-Plants. J Cell Biol **130,** 1345-1357.

Sanchez-Rodriguez, C., Rubio-Somoza, I., Sibout, R., and Persson, S. (2010). Phytohormones and the cell wall in Arabidopsis during seedling growth. Trends Plant Sci **15,** 291-301.

Sanchez-Rodriguez, C., Ketelaar, K., Schneider, R., Villalobos, J.A., Somerville, C.R., Persson, S., and Wallace, I.S. (2017). BRASSINOSTEROID INSENSITIVE2 negatively regulates cellulose synthesis in Arabidopsis by phosphorylating cellulose synthase 1. Proc Natl Acad Sci U S A **114,** 3533-3538.

Sato, S., Kato, T., Kakegawa, K., Ishii, T., Liu, Y.G., Awano, T., Takabe, K., Nishiyama, Y., Kuga, S., Sato, S., Nakamura, Y., Tabata, S., and Shibata, D. (2001). Role of the putative membrane-bound endo-1,4-beta-glucanase KORRIGAN in cell elongation and cellulose synthesis in Arabidopsis thaliana. Plant Cell Physiol **42,** 251-263.

Scavuzzo-Duggan, T.R., Chaves, A.M., Singh, A., Sethaphong, L., Slabaugh, E., Yingling, Y.G., Haigler, C.H., and Roberts, A.W. (2018). Cellulose synthase "class specific regions' are intrinsically disordered and functionally undifferentiated. J Integr Plant Biol **60,** 481-497.

Scheible, W.R., and Pauly, M. (2004). Glycosyltransferases and cell wall biosynthesis: novel players and insights. Curr Opin Plant Biol **7,** 285-295.

Scheible, W.R., Eshed, R., Richmond, T., Delmer, D., and Somerville, C. (2001). Modifications of cellulose synthase confer resistance to isoxaben and thiazolidinone herbicides in Arabidopsis Ixr1 mutants. Proc Natl Acad Sci U S A **98,** 10079-10084.

Scheller, H.V., and Ulvskov, P. (2010). Hemicelluloses. Annu Rev Plant Biol **61,** 263-289.

Schindelin, J., Arganda-Carreras, I., Frise, E., Kaynig, V., Longair, M., Pietzsch, T., Preibisch, S., Rueden, C., Saalfeld, S., Schmid, B., Tinevez, J.Y., White, D.J., Hartenstein, V., Eliceiri, K., Tomancak, P., and Cardona, A. (2012). Fiji: an open-source platform for biological-image analysis. Nat Methods **9,** 676-682.

Schultink, A., Cheng, K., Park, Y.B., Cosgrove, D.J., and Pauly, M. (2013). The identification of two arabinosyltransferases from tomato reveals functional equivalency of xyloglucan side chain substituents. Plant Physiol **163,** 86-94.

Sethaphong, L., Haigler, C.H., Kubicki, J.D., Zimmer, J., Bonetta, D., DeBolt, S., and Yingling, Y.G. (2013). Tertiary model of a plant cellulose synthase. Proc. Natl. Acad. Sci. U. S. A. **110,** 7512-7517.

Showalter, A.M. (1993). Structure and function of plant cell wall proteins. Plant Cell **5,** 9-23.

Showalter, A.M., Keppler, B., Lichtenberg, J., Gu, D., and Welch, L.R. (2010). A bioinformatics approach to the identification, classification, and analysis of hydroxyproline-rich glycoproteins. Plant Physiol **153,** 485-513.

Singh, S.K., Fischer, U., Singh, M., Grebe, M., and Marchant, A. (2008). Insight into the early steps of root hair formation revealed by the procuste1 cellulose synthase mutant of Arabidopsis thaliana. Bmc Plant Biol **8,** 57.

Slabaugh, E., Davis, J.K., Haigler, C.H., Yingling, Y.G., and Zimmer, J. (2014). Cellulose synthases: new insights from crystallography and modeling. Trends Plant Sci **19,** 99-106.

Smith, P.J., Wang, H.-T., York, W.S., Peña, M.J., and Urbanowicz, B.R. (2017). Designer biomass for next-generation biorefineries: leveraging recent insights into xylan structure and biosynthesis. Biotechnology for biofuels **10,** 286.

Somerville, C. (2006). Cellulose synthesis in higher plants. Annu Rev Cell Dev Biol **22,** 53-78.

Somerville, C., Bauer, S., Brininstool, G., Facette, M., Hamann, T., Milne, J., Osborne, E., Paredez, A., Persson, S., Raab, T., Vorwerk, S., and Youngs, H. (2004). Toward a systems approach to understanding plant cell walls. Science **306,** 2206-2211.

Sterling, J.D., Atmodjo, M.A., Inwood, S.E., Kumar Kolli, V.S., Quigley, H.F., Hahn, M.G., and Mohnen, D. (2006). Functional identification of an Arabidopsis pectin biosynthetic homogalacturonan galacturonosyltransferase. Proc Natl Acad Sci U S A **103,** 5236-5241.

Stone, B.A. (2006). Cell Walls of Cereal Grains. Cereal Foods World **51,** 62-65.

Stone, B.C., A. E. (Adrienne Elizabeth). (1992). Chemistry and biology of (1 --> 3)-[beta]-glucans. (La Trobe University Press).

Tan, L., Eberhard, S., Pattathil, S., Warder, C., Glushka, J., Yuan, C., Hao, Z., Zhu, X., Avci, U., Miller, J.S., Baldwin, D., Pham, C., Orlando, R., Darvill, A., Hahn, M.G.,

Kieliszewski, M.J., and Mohnen, D. (2013). An Arabidopsis cell wall proteoglycan consists of pectin and arabinoxylan covalently linked to an arabinogalactan protein. Plant Cell **25,** 270-287.

Taylor, N.G. (2007). Identification of cellulose synthase AtCesA7 (IRX3) in vivo phosphorylation sites--a potential role in regulating protein degradation. Plant Mol Biol **64,** 161-171.

Taylor, N.G., Laurie, S., and Turner, S.R. (2000). Multiple cellulose synthase catalytic subunits are required for cellulose synthesis in Arabidopsis. Plant Cell **12,** 2529-2540.

Taylor, N.G., Scheible, W.R., Cutler, S., Somerville, C.R., and Turner, S.R. (1999). The irregular xylem3 locus of Arabidopsis encodes a cellulose synthase required for secondary cell wall synthesis. Plant Cell **11,** 769-780.

Taylor, N.G., Howells, R.M., Huttly, A.K., Vickers, K., and Turner, S.R. (2003). Interactions among three distinct CesA proteins essential for cellulose synthesis. Proc Natl Acad Sci U S A **100,** 1450-1455.

Toller, A., Brownfield, L., Neu, C., Twell, D., and Schulze-Lefert, P. (2008). Dual function of Arabidopsis glucan synthase-like genes GSL8 and GSL10 in male gametophyte development and plant growth. Plant J **54,** 911-923.

Turner, S., Gallois, P., and Brown, D. (2007). Tracheary element differentiation. Annu Rev Plant Biol **58,** 407-433.

Ueda, T. (2014). Cellulase in Cellulose Synthase: A Cat among the Pigeons? Plant Physiol **165,** 1397-1398.

Vain, T., Crowell, E.F., Timpano, H., Biot, E., Desprez, T., Mansoori, N., Trindade, L.M., Pagant, S., Robert, S., Hofte, H., Gonneau, M., and Vernhettes, S. (2014). The

Cellulase KORRIGAN Is Part of the Cellulose Synthase Complex. Plant Physiol **165,** 1521-1532.

Van Bruaene, N., Joss, G., and Van Oostveldt, P. (2004). Reorganization and in vivo dynamics of microtubules during Arabidopsis root hair development. Plant Physiol **136,** 3905-3919.

Vandavasi, V.G., Putnam, D.K., Zhang, Q., Petridis, L., Heller, W.T., Nixon, B.T., Haigler, C.H., Kalluri, U., Coates, L., Langan, P., Smith, J.C., Meiler, J., and O'Neill, H. (2016). A Structural Study of CESA1 Catalytic Domain of Arabidopsis Cellulose Synthesis Complex: Evidence for CESA Trimers. Plant Physiol **170,** 123-135.

Vanholme, R., Demedts, B., Morreel, K., Ralph, J., and Boerjan, W. (2010). Lignin biosynthesis and structure. Plant Physiol **153,** 895-905.

Vanholme, R., Cesarino, I., Rataj, K., Xiao, Y., Sundin, L., Goeminne, G., Kim, H., Cross, J., Morreel, K., Araujo, P., Welsh, L., Haustraete, J., McClellan, C., Vanholme, B., Ralph, J., Simpson, G.G., Halpin, C., and Boerjan, W. (2013). Caffeoyl shikimate esterase (CSE) is an enzyme in the lignin biosynthetic pathway in Arabidopsis. Science **341,** 1103-1106.

Vaten, A., Dettmer, J., Wu, S., Stierhof, Y.D., Miyashima, S., Yadav, S.R., Roberts, C.J., Campilho, A., Bulone, V., Lichtenberger, R., Lehesranta, S., Mahonen, A.P., Kim, J.Y., Jokitalo, E., Sauer, N., Scheres, B., Nakajima, K., Carlsbecker, A., Gallagher, K.L., and Helariutta, Y. (2011). Callose biosynthesis regulates symplastic trafficking during root development. Dev Cell **21,** 1144-1155.

Velasquez, S.M., Ricardi, M.M., Dorosz, J.G., Fernandez, P.V., Nadra, A.D., Pol-Fachin, L., Egelund, J., Gille, S., Harholt, J., Ciancia, M., Verli, H., Pauly, M., Bacic, A.,

Olsen, C.E., Ulvskov, P., Petersen, B.L., Somerville, C., Iusem, N.D., and Estevez, J.M. (2011). O-glycosylated cell wall proteins are essential in root hair growth. Science **332,** 1401-1403.

Vergara, C.E., and Carpita, N.C. (2001). beta-D-Glycan synthases and the CesA gene family: lessons to be learned from the mixed-linkage (1 -> 3),(1 -> 4)beta-D-glucan synthase. Plant Mol Biol **47,** 145-160.

Verhertbruggen, Y., Yin, L., Oikawa, A., and Scheller, H.V. (2011). Mannan synthase activity in the CSLD family. Plant Signal Behav **6,** 1620-1623.

Verma, D.P., and Hong, Z. (2001). Plant callose synthase complexes. Plant Mol Biol **47,** 693-701.

Veytsman, B.A., and Cosgrove, D.J. (1998). A model of cell wall expansion based on thermodynamics of polymer networks. Biophys J **75,** 2240-2250.

Vorwerk, S., Somerville, S., and Somerville, C. (2004). The role of plant cell wall polysaccharide composition in disease resistance. Trends Plant Sci **9,** 203-209.

Wang, T., Zabotina, O., and Hong, M. (2012). Pectin-cellulose interactions in the Arabidopsis primary cell wall from two-dimensional magic-angle-spinning solid-state nuclear magnetic resonance. Biochemistry **51,** 9846-9856.

Wang, X., Cnops, G., Vanderhaeghen, R., De Block, S., Van Montagu, M., and Van Lijsebettens, M. (2001). AtCSLD3, a cellulose synthase-like gene important for root hair growth in Arabidopsis. Plant Physiol **126,** 575-586.

Watanabe, Y., Schneider, R., Barkwill, S., Gonzales-Vigil, E., Hill, J.L., Jr., Samuels, A.L., Persson, S., and Mansfield, S.D. (2018). Cellulose synthase complexes display distinct

dynamic behaviors during xylem transdifferentiation. Proc Natl Acad Sci U S A **115,** E6366-E6374.

Xie, B., Wang, X., Zhu, M., Zhang, Z., and Hong, Z. (2011). CalS7 encodes a callose synthase responsible for callose deposition in the phloem. Plant J **65,** 1-14.

Xu, P., Donaldson, L.A., Gergely, Z.R., and Staehelin, L.A. (2006). Dual-axis electron tomography: a new approach for investigating the spatial organization of wood cellulose microfibrils. Wood Science and Technology **41,** 101.

Xu, S.L., Rahman, A., Baskin, T.I., and Kieber, J.J. (2008). Two leucine-rich repeat receptor kinases mediate signaling, linking cell wall biosynthesis and ACC synthase in Arabidopsis. Plant Cell **20,** 3065-3079.

Yang, J., Bak, G., Burgin, T., Barnes, W.J., Mayes, H.B., Pena, M.J., Urbanowicz, B.R., and Nielsen, E. (2020). Biochemical and Genetic Analysis Identify CSLD3 as a beta-1,4-Glucan Synthase That Functions during Plant Cell Wall Synthesis. Plant Cell **32,** 1749-1767.

Yang, W.B., Schuster, C., Beahan, C.T., Charoensawan, V., Peaucelle, A., Bacic, A., Doblin, M.S., Wightman, R., and Meyerowitz, E.M. (2016). Regulation of Meristem Morphogenesis by Cell Wall Synthases in Arabidopsis. Curr Biol **26,** 1404-1415.

Yin, L., Verhertbruggen, Y., Oikawa, A., Manisseri, C., Knierim, B., Prak, L., Jensen, J.K., Knox, J.P., Auer, M., Willats, W.G.T., and Scheller, H.V. (2011). The Cooperative Activities of CSLD2, CSLD3, and CSLD5 Are Required for Normal Arabidopsis Development. Mol Plant **4,** 1024-1037.

Yoshikawa, T., Eiguchi, M., Hibara, K.I., Ito, J.I., and Nagato, Y. (2013). Rice SLENDER LEAF 1 gene encodes cellulose synthase-like D4 and is specifically expressed in M-phase cells to regulate cell proliferation. J Exp Bot **64,** 2049-2061.

Zabotina, O.A., Avci, U., Cavalier, D., Pattathil, S., Chou, Y.H., Eberhard, S., Danhof, L., Keegstra, K., and Hahn, M.G. (2012). Mutations in multiple XXT genes of Arabidopsis reveal the complexity of xyloglucan biosynthesis. Plant Physiol **159,** 1367-1384.

Zakzeski, J., Bruijnincx, P.C., Jongerius, A.L., and Weckhuysen, B.M. (2010). The catalytic valorization of lignin for the production of renewable chemicals. Chem Rev **110,** 3552-3599.

Zhang, X., Dominguez, P.G., Kumar, M., Bygdell, J., Miroshnichenko, S., Sundberg, B., Wingsle, G., and Niittyla, T. (2018). Cellulose Synthase Stoichiometry in Aspen Differs from Arabidopsis and Norway Spruce. Plant Physiol **177,** 1096-1107.

Zhang, Y., Nikolovski, N., Sorieul, M., Vellosillo, T., McFarlane, H.E., Dupree, R., Kesten, C., Schneider, R., Driemeier, C., Lathe, R., Lampugnani, E., Yu, X., Ivakov, A., Doblin, M.S., Mortimer, J.C., Brown, S.P., Persson, S., and Dupree, P. (2016). Golgi-localized STELLO proteins regulate the assembly and trafficking of cellulose synthase complexes in Arabidopsis. Nat Commun **7,** 11656.

Zhu, X., Li, S., Pan, S., Xin, X., and Gu, Y. (2018). CSI1, PATROL1, and exocyst complex cooperate in delivery of cellulose synthase complexes to the plasma membrane. Proc Natl Acad Sci U S A **115,** E3578-E3587.